Modeling the Inelastic Behavior of Heat Exchangers Accounting for Fluid-Structure Interactions

Dissertation
zur Erlangung des akademischen Grades

Doktoringenieur
(Dr.-Ing.)

von MSc Getachew Shunki Tibba

geb. am 21.11.1977 in Bedele, Äthiopie

genehmigt durch die Fakultat für Maschinenbau

der Otto-von-Guericke-Universität Magdeburg

Gutachter: Prof. Dr.-Ing. habil. Holm Altenbach
                  Prof. Dr.-Ing.habil Eckehard Specht

Promotionskolloquium am: 27.11.2013

Preface

Ethiopia is currently working hard with a goal of transforming its economy to join middle income nations in the next few years. To fulfill this goal, plenty of activities are being carried out. Among these are the capacity building activities of the higher education institutions through human resource development to enable the production of highly qualified graduates in large number as an input to the economic development activity needs. The sandwich PhD study program, which has been initiated and sponsored by the Engineering Education Capacity Building Program (EECBP) of the country, is one that contributes to the educational resource development.

Being one of the beneficiaries of the PhD program, I would like to use this opportunity to owe my deepest gratitude to the following bodies and individuals who played great role in successful completion of my study:

- The Engineering Education Capacity Building Program (EECBP) of Ethiopia for initiating and sponsoring the PhD program.

- Jimma University for giving me the opportunity to benefit from the scholarship.

- The German Academic Exchange Service (DAAD) for effectively administering the EECBP scholarship.

- Martin-Luther-Universität Halle-Wittenberg for giving me admission for the first six months period of the sandwich study time.

- Otto-von-Guericke Universität Magdeburg for giving me admission for the remaining duration of my study and providing me with a scholarship of six months.

- Prof. Dr.-Ing. Hab. Holm Altenbach for his previous and present collaboration with the Mechanical Engineering department of Jimma University, his willingness to be my PhD study supervisor and providing me with fast responses and solutions to all my questions providing me a scholarship extension for six months, to mention few.

- Prof. Venkata Ramayya for his willingness to be my supervisor on my PhD study, and providing me with very useful comments and suggestions. Prof. Venkata is an exceptional, devoted and inspirational person who has played an invaluable role in the successful journey of the Mechanical Engineering department of Jimma University.

Abstract

The energy need of human being is ever increasing. The naturally available energy resources are in a crude form and need conversion to a form which is readily available for end use. Power plants play the role of this conversion process. The conversion processes need to address two very important and current burning issues: highly efficient and environmental friendly operation. To fulfill these two needs, the majority of the conversion processes take place at severe conditions of very high temperature and high pressure. However, these severe conditions have great impact on the life and proper functioning of the power plant components involved in the energy conversion processes as a result of inelastic behavior like creep and fatigue exhibited by the materials of the components. Therefore, the design and life prediction of such components should take this inelastic behavior in to consideration.

This work focuses on modeling the inelastic behavior, which is exhibited as a response to the severe loading conditions, of heat exchanger materials. Specifically, inelastic constitutive model of T91 steel, which is commonly used for constructing power plant components, is developed. Material parameters have been identified and the model has been verified against experimental data from literature and good agreements between the data points and the model fit has been obtained. Finally, a material user-subroutine has been written to incorporate the model in to commercial software ABAQUS. The model has been used to simulate the creep behavior of a superheater tube made of T91 steel.

Kurzreferat

Der Energiebedarf der Menschen wird immer größer. Die natürlich vorhandenen Energieressourcen sind in roher Form in der Natur und müssen in eine Form umgewandelt werden, die für den Endverbraucher leicht zugänglich ist. In diesem Umwandlungsprozess spielen Kraftwerke eine entscheidende Rolle. Die Umwandlungsprozesse müssen zwei wichtige und aktuelle Probleme berücksichtigen - hocheffizienten und umweltfreundlichen Betrieb. Um diesen beiden Anforderungen gerecht zu werden, sind die Umwandlungsprozesse in der Regel mit sehr hohen Temperaturen und hohem Druck verbunden. Diese Bedingungen haben großen Einfluss auf Lebensdauer und sicheren Betrieb der Kraftwerkskomponenten in den Energieumwandlungsprozessen als Folge des inelastischen Materialverhaltens wie Kriechen und Ermüdung in den beteiligten Komponenten. Daher sollte die Lebensdauervorhersage dieser Komponenten das inelastischen Verhalten berücksichtigen.

Der Fokus dieser Arbeit liegt in der Modellierung des inelastischen Werkstoffverhaltens, das sich als Reaktion auf die Lastbedingungen einstellt. Beispielhaft wird dazu ein Wärmetauscher betrachtet. Insbesondere wird ein inelastisches Konstitutivgesetz für den Stahl T91 entwickelt, der üblicherweise für Kraftwerkskomponenten verwendet wird. Wichtige Parameter sind identifiziert und die Modellvorhersagen sind für einachsige experimentelle Daten aus der Literatur verifiziert worden. Eine gute Übereinstimmung zwischen den Messwerten und den Modellvorhersagen wurde erhalten. Schließlich wurde für das Materialmodell eine nutzerspezifische Materialroutine geschrieben, um das Modell in das kommerziellen Softwarepaket ABAQUS zu integrieren. Das Modell wurde eingesetzt, um das Kriechverhalten einer Rohrleitung aus T91 Stahl zu simulieren.

Contents

List of Figures

List of Tables

1

Introduction

Materials are utilized in all activities of producing commodities (goods and services) that are used in fulfilling the basic or better life needs of human being. These materials experience different kinds of loads when serving the activities. The loads may be high enough to the extent where the materials may not be able to withstand them anymore. If the materials fail while a process is underway, catastrophic disaster to lives and properties may occur. To avoid or minimize this, the strength and life of components made of these materials must be predicted considering all possible loading and operation conditions. A simple schematic representation of how prediction is important in design analysis is shown in Fig. 1.1. The fishing line was weaker and failed on the first attempt. This made the fisher unsuccessful in his fishing and the fish to suffer for the remaining time of its life due to the hook and long fishing line on its body. To avoid this the strength of the components should have been confirmed through property modeling considering all the possible dynamic loads that can be exerted by a fish before manufacturing the components.

For other processes with complicated loading and operation conditions, the disaster may be more sever, like the breaking in half of a merchant ship during the world war II [12]. This work focuses on modeling material properties of components used in energy conversion processes accounting for the working conditions of high temperature and pressure.
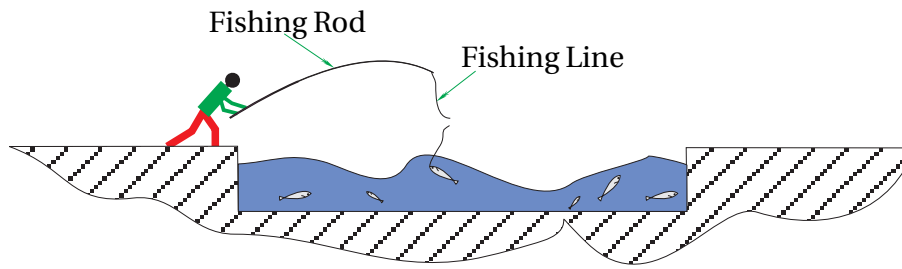
Figure 1.1   Fishing Failure due to Failure in Proper Prediction of Life of Components

1.1 Motivation

Energy is among the basic commodities that all human being need individually or from small household level to multinational companies and industries. Just like for the case of other commodities, the energy demand of human being is ever increasing [83, 69, 45]. What is special with this commodity is the challenge related to its conversion as will be explained in this section.

1.1.1 Energy Conversion Efficiency and the Environment

The naturally available energy resources are in a crude form and need conversion to a form which is readily available for end use. Power plants play the role of this conversion process. The components of power plants (boiler tubes, superheaters, reheaters, economizers, turbines, waste heat recovery systems etc., to mention few) involved in the conversion process face the following severe conditions:

- The majority of the conversion processes take place at very **high** temperature and very **high** pressure.

- As energy utilization is non-stopping, the conversion is also a **continuous** process.

- Moreover, the conversion processes take place in transient and turbulent environment and this results in **fluctuation** of pressure in fluid media, stress in solid media and temperature in both media. The start-up and shut-down operations of the power plants also result in fluctuation of loads in the components.

- The inner and outer surfaces of components like superheater tubes experience different temperatures (for example, 600°C on steam side

and 1400°C on flue gas side) over a small thickness (mostly less than 5 mm). This results in high **thermal gradient**.

Due to this nature (high temperature and pressure, continuous operation, fluctuation of pressure/stress and temperature, and high thermal gradient) of energy conversion processes, the materials of power plant components involved are expected to exhibit inelastic behavior like plasticity, creep and fatigue. The inelastic behavior has adverse effect on the life and proper functioning of these components and should be duly considered during design analysis.

Few of the most common energy conversion processes, where the severe situations explained above are expected to occur, are shown, in broad sense, in Fig. 1.2. As an example of areas where high temperature and high pressure processes occur in power plants, the steam turbine power plant, whose schematic view of simplified steam cycle is shown in Fig. 1.3, has been selected. In this power plant, the superheaters and reheaters are components which experience the most sever conditions as it can be seen from the corresponding Temperature-Entropy diagram in Fig. 1.4.

1.1.2 High Temperature Operations: Importance and Challenges

Why do we need high temperature operations in energy conversion technologies? The answer is something related to the efficiency of these technologies. Again we can consider the thermal power plants to see the importance of high temperature operations. For all thermal processes which operate between two different temperatures, their thermal efficiency [88] should satisfy the inequality given by (1.1)

$$\eta_{th} \le 1 - \frac{T_{Cold}}{T_{Hot}}, \tag{1.1}$$
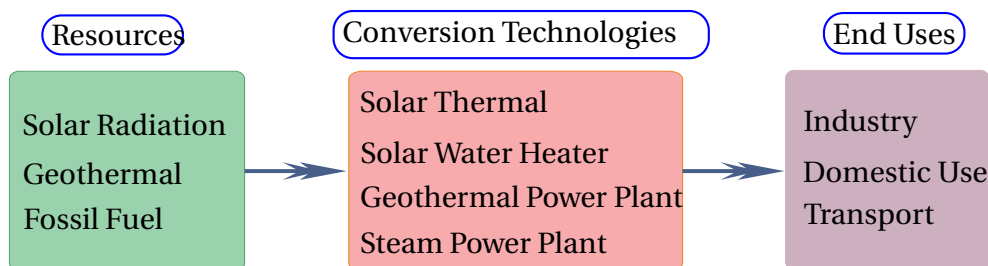
Figure 1.2 Examples of Energy Conversion Technologies
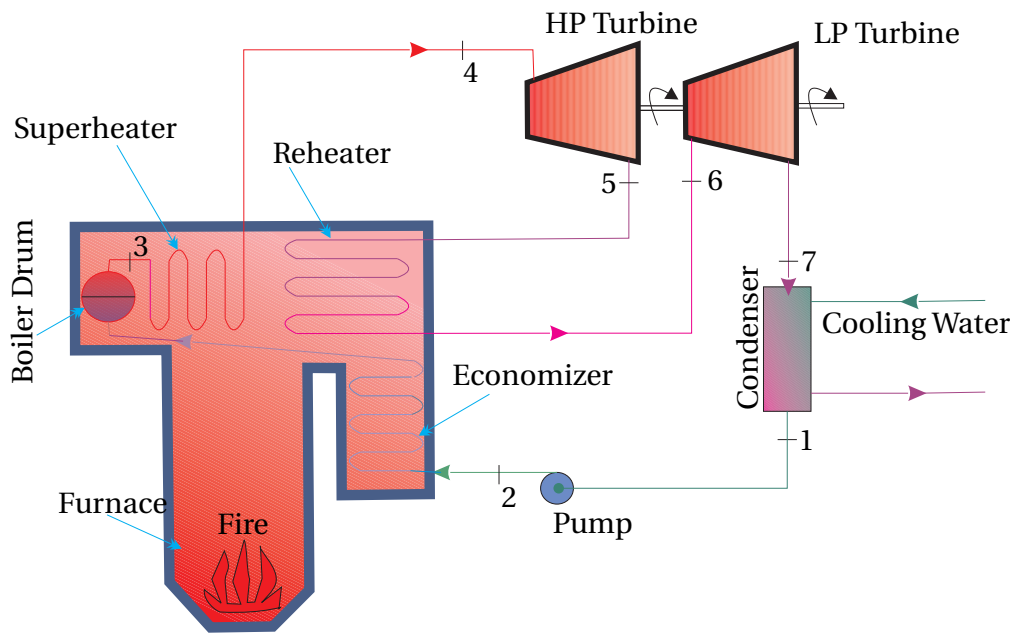
Figure 1.3 Schematic View of the Reheat Rankine Cycle in Steam Powerplant (after [37, 89])

where η_{th} is thermal efficiency, T_{Cold} and T_{Hot} are minimum and maximum temperatures in the power plant, respectively.

In (1.1), the equality holds for the ideal Carnot cycle and real cycles will have less efficiency. The thermal efficiency of power plants has to be increased for at least two reasons:

- to minimize plant operation cost - **Economic operation**,

- to reduce emission of CO_2 and other pollutant gases - **Environmental Issue** [69, 51, 1].

Referring to (1.1), the thermal efficiency can be increased either by increasing T_{Hot}, or by decreasing T_{Cold}. If the condenser is cooled by an open type cooling system, decreasing T_{Cold} is difficult since it is related to the temperature of the environment, which acts like a heat sink. Also from environmental protection point of view, these types of cooling systems are becoming under restriction and will not be incorporated in future power plants. On the other hand, if the condenser cooling water is a closed (circulating) type, reducing T_{Cold} is not economical [37] as it requires large investment on cooling towers and other components. Therefore, the only reasonable option of increasing the thermal efficiency is to increase T_{Hot}.
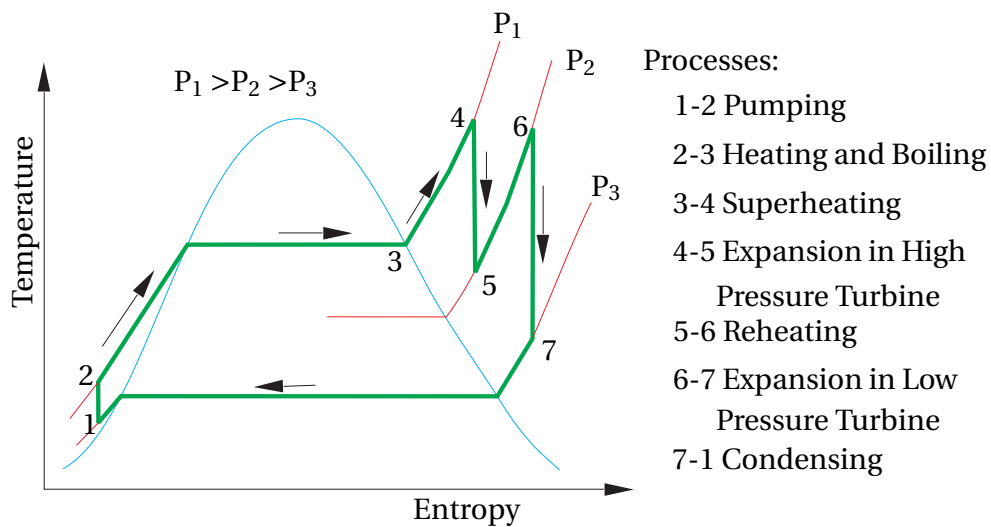
Figure 1.4   Temperature-Entropy Diagram of the Reheat Rankine Cycle (after [37, 89, 108])

The overall efficiency of the plant can also be measured in terms of the decrease in the net heat energy input

$$\frac{\Delta W_{net-in}}{W_{net-in}}$$

to the power plant. Increases in steam pressure and steam temperature increase the power plant overall efficiency by improving net heat consumption as shown in Fig. 1.5 (for a plant initially operating at steam temperature of 535°C and steam pressure of 18.5MPa) but an increase in temperature has a greater effect.

For the power plant presented in Fig. 1.5, several literature sources (example [101] among others) indicate that an increase in steam pressure from 18.5MPa to 30MPa improved the overall plant efficiency by 1.9% and an increase of steam temperature from 535°C to 650°C increased the overall plant efficiency by 5.7%. The combined increase of the two gives efficiency rise of more than 8%.

In addition to increasing the thermal efficiency of the plant, superheating helps in preventing early condensation of the steam in steam turbines. If steam condenses in the turbines, it will corrode the turbine blades and can result in early failure of the whole turbine. If superheating is not successful due to limitations of the materials to withstand the high temperature, all or part of the steam is extracted, reheated in the furnace and sent back to the turbine [39].
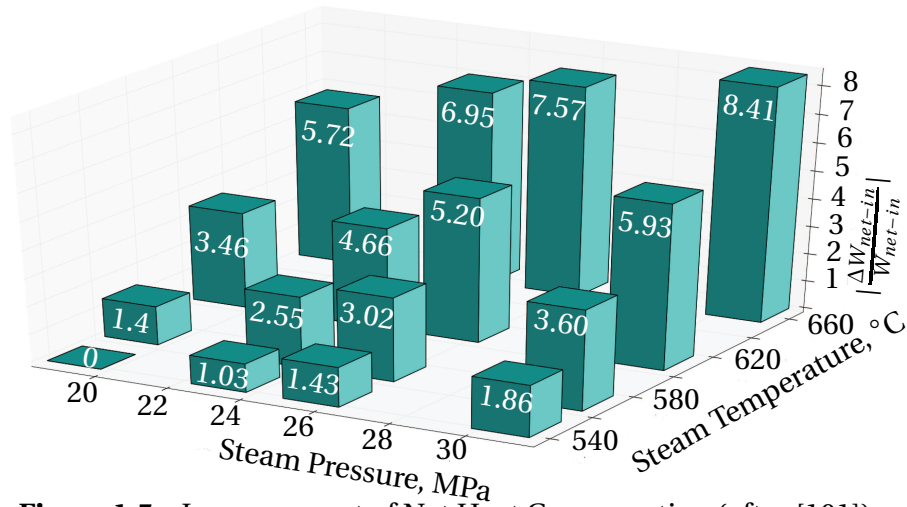
Figure 1.5   Improvement of Net Heat Consumption (after [101])

Table 1.1   Comparison of Present and Future Power Plants

Capacity and Operation Conditions	Subcritical	Supercritical	Ultra-Supercritical
Net Plant Output (MW)	500	500	500
Coal Use (10^6 tones/year)	1.548	1.378	1.221
CO_2 Emitted (10^6 tones/year)	3.47	3.09	2.74
Tempetature (°C)	538	538	600
Pressure (MPa)	16.55	24	30
Efficiency (%)	34.3	38.5	43.3

1.1.3   Future Fate of Power Plant Components

To meet high efficiency requirements of energy production, old power plants operating at subcritical conditions are being replaced by those which operate at supercritical and ultra-supercritical conditions [68, 92]. Table 1.1 shows a comparison of these three power plants which have the same capacity of producing 500MW of electric power [75]. The power plant that operates at ultra-supercritical conditions has best efficiency, less coal consumption and less CO_2 emission. On the other hand, it operates at highest pressure and highest temperature.

As the name implies, the heating process of water in the boilers of the super- and ultra-supercritical power plants passes above the critical point of water (21.8MPa and 374°C) as shown in Fig. 1.6. Therefore, future trend of
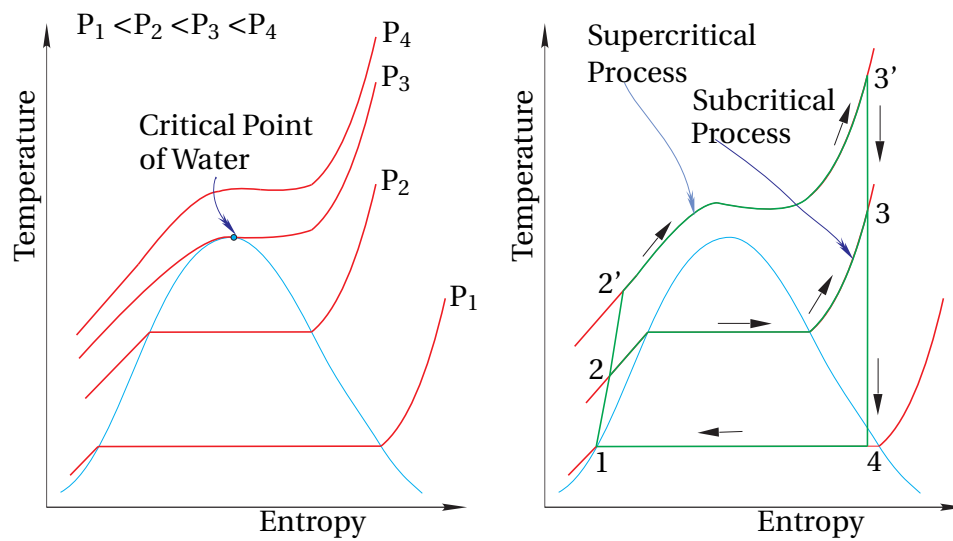
Figure 1.6 Temperature-Entropy Diagram of the Subcritical and Supercritical Processes (after [23, 78, 37])

the utilization of supercritical and ultra-supercritical operations indicate that components of power plants continue to operate at more and more severe conditions than the present ones. This, in turn, calls for strong material modeling activities in design and analysis of the components.

Another issue which makes use of heat exchangers inevitable is the future trend of renewable energy utilization. Due to environmental issues and future depletion threat of conventional energy resources, renewable energy utilization has become a global concern. Among renewable energy conversion technologies, solar-thermal power plants are the promising ones.

An example of solar-thermal power plants is schematically shown in Fig. 1.7. In this power plant there are a number of heat exchangers. For real plants, the number could even be more. As in the case of conventional power plants, the efficiency of these plants can be increased by using steam generation above the critical point of water. Again this is an indication of the possibility of heat exchangers in renewable energy resource power plants to face sever conditions of high temperatures and high pressure like those in the conventional power plants. Generally, be it in the conventional or in the renewable energy resource power plants the heat exchangers and other components like steam and gas turbines have the fate of working at severe conditions. This is the motivation of this work.
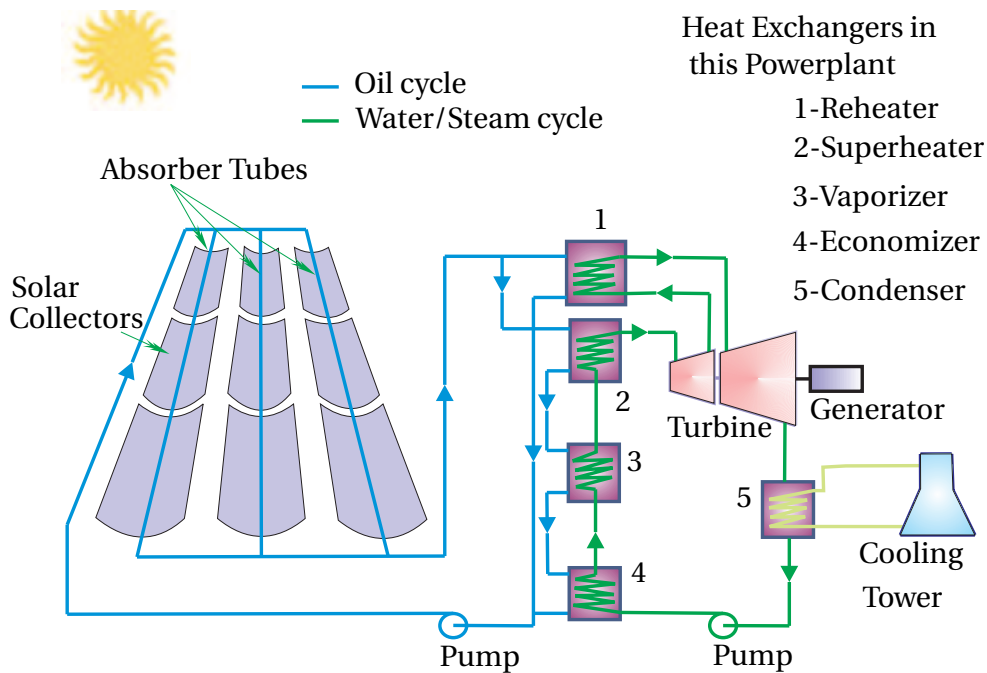
Figure 1.7   Heat Exchangers in Solar-Thermal Power Plant (after [87])

1.2   Confronting the Inelastic Behavior of Materials

It has been explained in the previous section that the materials of power plant components operating at severe conditions exhibit inelastic behavior which will eventually result in failures ranging from malfunctioning to catastrophic rupture of the components. To mitigate this problem, plenty of works (by individuals, research groups, research institutes, etc.) have been done from two directions:

1. **Material Science and Engineering point of view** is to design and manufacture new materials (like the 9-12% Chromium steels) which can more withstand the severe conditions mentioned above. This can be done by introducing new alloying elements, inducing new micro-structures or any other technique to enhance the properties of existing steels [3, 89]), and

2. **Engineering Mechanics point of view** is to model the inelastic behavior of the materials. This approach deals with development of constitutive models to simulate and analyze the responses of materials and predict the life of components made of these materials [80, 44] with the aim of

protecting any disaster that would otherwise result from failure of the components.

The work done in this thesis belongs to the second direction.

1.3   Thesis Objectives and Outline

The main objective of this thesis is to model the inelastic behavior of materials of heat exchangers used in power plants from continuum mechanics point of view.

The specific objectives include:

- Performing heat transfer and fluid flow modeling of a heat exchanger,

- Modeling constant– and cyclic loading creep behavior of the heat exchanger material,

- Developing material-user-subroutine for implementing the model in computational software for performing structural simulation,

- Performing full Fluid-Structure Interaction simulation of the heat exchanger by implementing the model.

To fulfill these objectives in a systematic manner, the thesis proceeds in a logical sequence as follows. It begins with an introductory chapter which mainly deals with explanation of the motivation of the study. Specifically, it focuses on the necessities of high temperature and high pressure operations in thermal power plants in order to get better efficiency. The negative consequence of operations to obtain higher efficiency on life and proper operation of components and how to deal with it is the key point of the chapter. It also tries to point out that this threat (i.e. the negative effect on component life and its operation) continues in the future even if there will be a shift from the conventional energy resources utilization to the renewable ones.

The second chapter deals with the general procedure of solving a fluid-structure interaction problem of a component used in thermal power plant. Apart from discussing the general fundamental equations and the constitutive equations relevant to the thesis, it indicates the specific challenges of dealing with fluid-structure interactions where large deformations are involved. The three main challenges indicated here are 1) the turbulent nature of fluid flow which results in fluctuation of loads on components, 2) the computational

challenge of coupling the loads from fluids with deformations of solids, and 3) the other computational challenge in dealing with largely distorted solid mesh elements. All these points are the hot issues of computational mechanics which need effort for better results. For these challenges, the chapter tries to indicate the current trends of solution directions. This chapter is the fundamental body of the thesis.

In chapter three, specific constitutive equation of inelastic behavior of materials relevant to the power plant components is presented. The inelastic constitutive equation, which is derived based on mixture of hard and soft constituents of a material, is utilized to model the behavior of T91 steel which is a material used for superheater construction. The modeling was first done for creep behavior resulting from constant stress and then for that resulting from fluctuating stress. The material constants in the model are calibrated through rigorous optimization work of creep data from literature. The model is then validated with different data sets from different experiments for the same material. The results are also compared with results from other models done by other researchers to see the accuracy of the model.

The fourth chapter is concerned with computational implementation of the model. Here a complete Fluid-Structure Interaction analysis of a superheater tube made from T91 steel is made. The thermal analysis was made using the finite volume method based software ANSYS FLUENT. The temperature distribution obtained from this analysis is then used as a thermal load for structural analysis. The structural analysis is made using the finite element method based software ABAQUS where the material model developed in chapter three is implemented. The implementation was done through the material user-subroutine called UMAT which is written in FORTRAN programming language.

Finally, the thesis is completed by drawing some conclusions, pointing out limitations of the work and mentioning future outlooks in the fifth chapter.

2

Fluid-Structure Interactions

On our planet, fluids and solids are always in contact and their motions are not independent [102, 15]. The interaction between the two is made through load transfer. The load can be large enough to result in deformation (motion) of the solid and/or result in flow (configuration change) of the fluid. Few examples are shown in Fig. 2.1. In the solar chimney power plant, the buoyancy driven flow of air drives a turbine located at the bottom of the chimney. The flow of wind between long buildings can result in a deflection and hence cracking of their walls. The energetic steam which receives energy from burning fuel and from pump drives a steam turbine. The hot and pressurized fluid flowing in heat exchangers can result in deformation of the tubes, etc. All these examples show that there are many applications where fluid-structure interactions are involved.

Some of these phenomena are natural like the flow of wind around buildings while majority of them are consequences of processes in converting of resources to commodities ready for use. All these phenomena need to be understood, mathematically modeled, and solved for the sake of safety reasons and/or high performance of the conversion processes.

This chapter deals with the fundamentals of fluid-structure interactions related to energy conversion processes. The main focus is on the balance laws, constitutive equations and computational solution techniques of related problems.

2.1 Introduction

In the introduction chapter of this thesis, it has been explained that fluids (steam, oil and flue gas) play great role in energy conversion processes in the two power plants considered (Figs. 1.3 and 1.7). All that these fluids do is receiving, transporting and transferring energy. In the case of steam turbine power plants, the flue gas receives energy from the burning fuel, transfers it to the boiler and other tubes. The boiler and tubes, in turn, transfer the energy to water/steam. Finally, the energetic steam rotates a steam turbine which drives an electricity generator. For the solar thermal power plants, the solar radiation is reflected on to the absorber-tubes which are located at the focal lines of the parabolic troughs. The absorber-tubes contain a fluid (usually oil, sky blue lines in Fig. 1.7) which is circulated with the help of a pump and is heated up by the solar energy (up 400°C). The circulating oil transfers its thermal energy to another circulating fluid (which is water/steam, green lines in Fig. 1.7) through the heat exchangers indicated [87]. Again the steam will drive a steam turbine to generate electricity. In both the sample power plants presented, the fluid-structure interaction takes place through thermal load (heat transfer) and mechanical load (pressure) transfer.

As can be observed from the above explanation, fluid-structure interaction is a multi-physics discipline which can include, at least, fluid mechanics, heat transfer and solid mechanics. In general, two major phenomena are expected to take place in fluid-structure interactions:

1. Fluid flow and heat transfer cause deformation or movement of structures as a result of load transfer, and

2. Motions or deformations of structures affect the flow or the configuration of fluids.

Based on the significance of the effect of the deformation of the solid structure on the configuration of the fluid, we have two approaches of modeling:

1. **One-way coupling** - deflection of the solid does not significantly affect fluid motion. In this case,

   - Computational fluid dynamics and computational solid dynamics solutions are running independently,

   - Loads are transferred in only one direction (normally, the computational fluid dynamics is performed first and its solutions are used
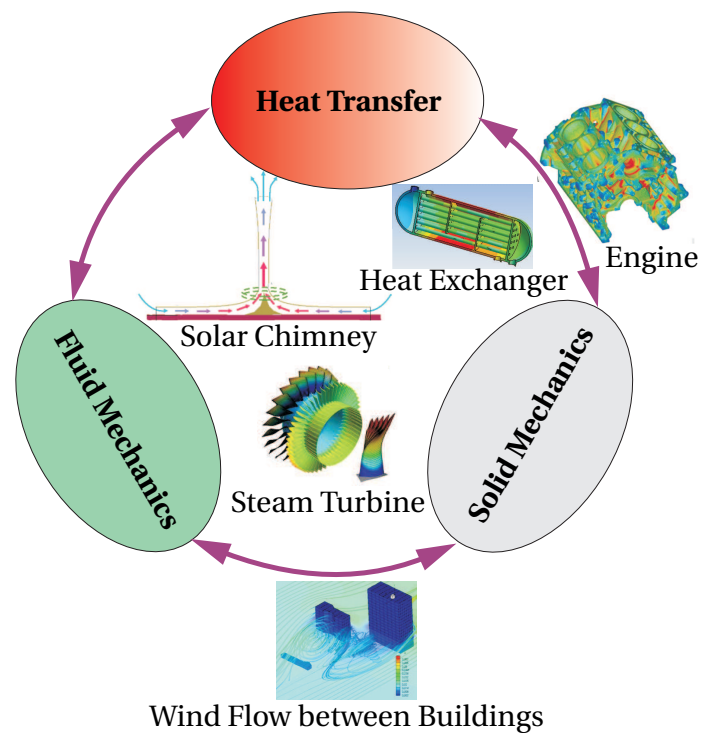
Figure 2.1   Fluid-Structure Interaction Examples (adapted from sources on internet)

as boundary conditions or predefined fields for the computational solid dynamics analysis).

As an example thermal stress analysis can be mentioned.

2. **Two-way coupling** - deflection of the solid affects fluid motion.

   - In this case the computational fluid dynamics and computational solid dynamics solutions are run simultaneously.

   - The solution of one is used as an input to the other during each and every iteration.

   - Much more iterations are involved.

   - More accurate solutions are obtained.

In both the coupling methods, the load transfer between the fluid and the structure takes place at **interfaces**. These loads include:

   - Pressure loads,

- Thermal loads (temperature, heat flux, convection coefficients, etc), and

- Displacements.

An example of fluid-structure interaction analysis made for shell-and-tube heat exchanger and the corresponding computational fluid dynamics and solid dynamics analyses results is shown in Fig. 2.2. Computational domains of the interacting media (fluid and solid) are shown in Fig. 2.2 a). Figure 2.2 b) shows the temperature distribution at interfaces which can be used as boundary conditions for computational solid dynamics (structural) analysis. The temperature distribution in the volume of a structure shown in Fig. 2.2 b) can also be used as a predefined temperature field for structural analysis. The deformed heat exchanger structure as a result of the temperature gradient and mechanical constraints is shown in Fig. 2.2 c). Mere understanding of physical phenomena is not sufficient for an engineer. The ultimate goal should be solving a practical problem by applying fundamental laws. Among the major solution steps is the description of the physical phenomena with mathematical models. This section introduces the universal physical laws, which apply to all media, and the constitutive laws, which are material dependent and supplement the physical laws, to get complete equations ready to be solved with some technique (either analytically or computationally).

a)

Fluid Domains

Solid Domain

b)

Temperature Distribution at Interfaces

to be used as boundary
conditionfor structural
analysis

Volume Temperature Distribution
to be used as Predefined Field
for Structural Analysis

c)

The wire frame shows the undeformed
structure position for comparison

Deformed Structure as a result of the load transfer
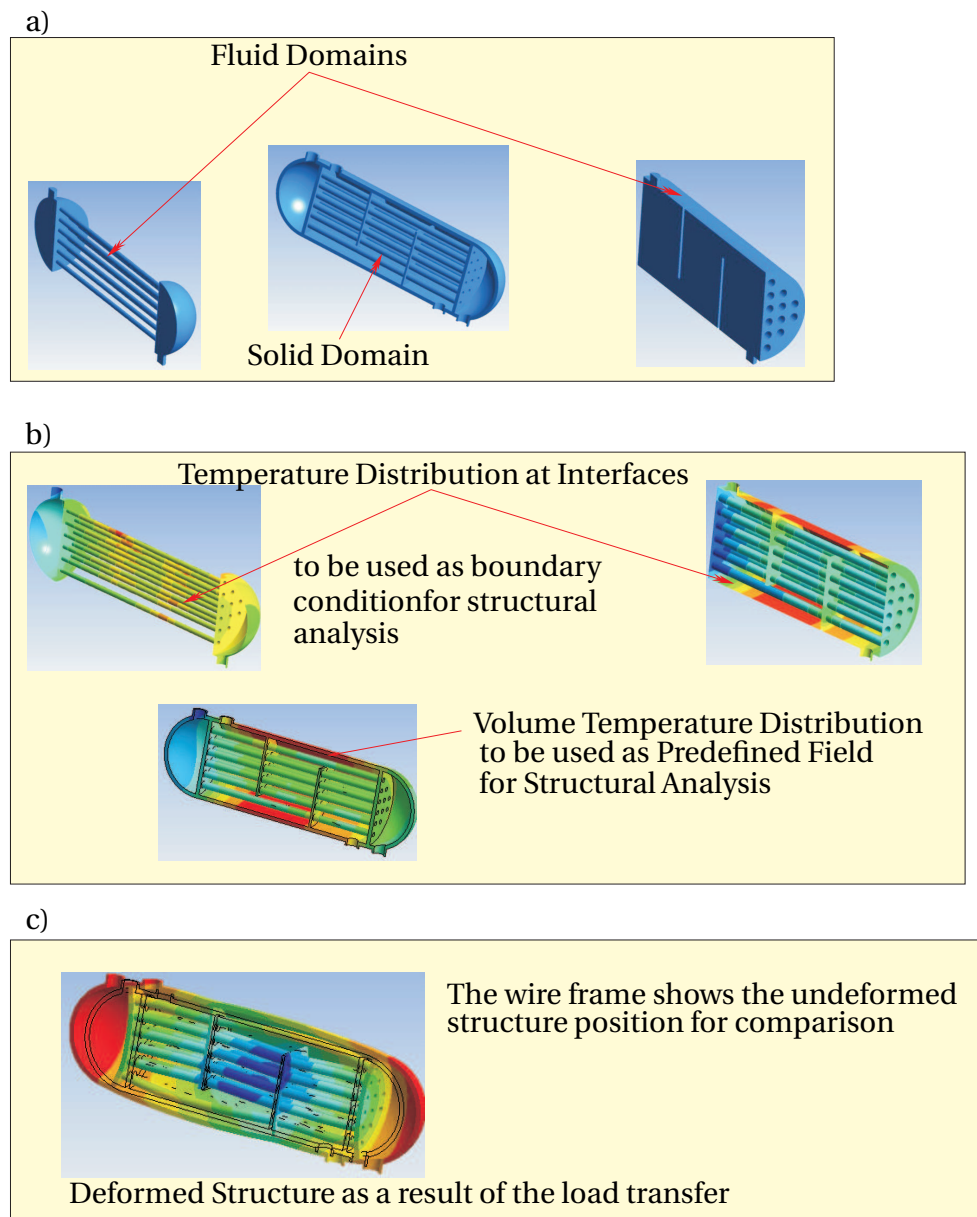
Figure 2.2   Interfaces and Volume for Thermal load transfer. a) Computa-
tional Domains, b) Computational Fluid Dynamics Results and c)
Computational Solid Dynamics Result

2.2   Balance Equations

The physical processes that take place in the material media (fluids and solids) involved in the fluid-structure interactions obey the fundamental laws of physics [91, 71, 104, 65, 72, 33]. These laws, also known as balance laws, are given by Eqs. (2.1) – (2.4).

- Conservation of Mass (Continuity Equation)

$$\frac{\partial \rho}{\partial t} + \mathbf{\nabla} \cdot (\rho \mathbf{v}) = 0 \tag{2.1}$$

- Linear Momentum Balance (Newtons Second Law of Motion)

$$\mathbf{\nabla} \cdot \boldsymbol{\sigma} + \rho \mathbf{b} = \rho \frac{D\mathbf{v}}{Dt} \tag{2.2}$$

- Angular Momentum Balance (symmetric nature of Cauchy stress, assuming no coupled-stresses or sources of angular momentum [8])

$$\boldsymbol{\sigma} = \boldsymbol{\sigma}^T \tag{2.3}$$

- Energy Balance (First Law of Thermodynamics)

$$\rho \frac{Du}{Dt} = \boldsymbol{\sigma} \cdot \cdot \mathbf{D} - \mathbf{\nabla} \cdot \mathbf{q} + \rho r \tag{2.4}$$

Where ρ is density, t is time, $\mathbf{v}$ is velocity vector, $\boldsymbol{\sigma}$ is stress tensor, $\boldsymbol{\sigma}^T$ is transpose of the stress tensor, $\mathbf{b}$ is body force vector, u is internal energy, $\mathbf{D}$ is rate of deformation tensor, $\mathbf{q}$ is heat flux vector, and r is body source including radiant heat constant and volumetric heat generation.

In Eqs. (2.1) – (2.4), we have eight independent scalar equations and seventeen unknown functions of time and space. The unknowns are the density, the three displacement (velocity) components, the nine stress tensor components, the three heat flux components and the internal energy [71].

For the set of these equations to be determinate, nine additional equations are needed. These equations are obtained from constitutive equations (from stress-strain(strain-rate) relations, heat equations and thermodynamic state equations).

The first law of thermodynamics shows us the possibility of transforming energy from one form to another. But it does not indicate whether all transformation directions are possible or not. In practical situations, the reverse of some energy conversion are not possible. A good example is the

conversion of kinetic energy to heat due to friction. The reverse process of converting heat generated due to friction to kinetic energy is impossible [35]. The possibility of a given energy conversion is governed by the second law of thermodynamics through the Clausius-Duhem inequality given by

$$\rho T \dot{s} - \rho \dot{u} + \boldsymbol{\sigma} \cdot \cdot \mathbf{D} - \frac{1}{T} \boldsymbol{\nabla} T \cdot \mathbf{q} \geq 0, \tag{2.5}$$

where *s* is specific entropy.

In (2.5) the equality holds for reversible processes where as the inequality for irreversible processes. The conclusion is that energy conversion processes proceed if they satisfy the Clausius-Duhem inequality [55, 26, 79].

2.3   Constitutive Equations

As mentioned in the previous section, the number of unknowns in the fundamental equations are more than the number of equations we have from the balance laws. At this moment, these equations can not be solved from mathematical point of view. Furthermore, the fundamental equations hold for all media and no information is known about the significance of a material from which the media is made. Therefore, additional equations, which are called constitutive equations (models), are required for the following two reasons:

1. **Closing the equations**. Constitutive models should come up with more equations so that the number of unknowns and the total number of equations (the fundamental equations plus the constitutive equations) will be equal. The set of equations can now be solved by applying appropriate boundary and/or initial conditions (well-posed problem).

2. **Reflecting the material behavior**. Constitutive models should predict how a specific material responds to loads applied on it.

There are a number of constitutive equations depending on the areas of application, but in this thesis only those from fluid mechanics, heat transfer and solid mechanics are briefly explained.

2.3.1   Fluid Flow and Heat Transfer Constitutive Equations

The constitutive models in fluid flow, generally, relate the shear stress to the velocity gradient (rate of deformation). Based on the types of fluids (flow),
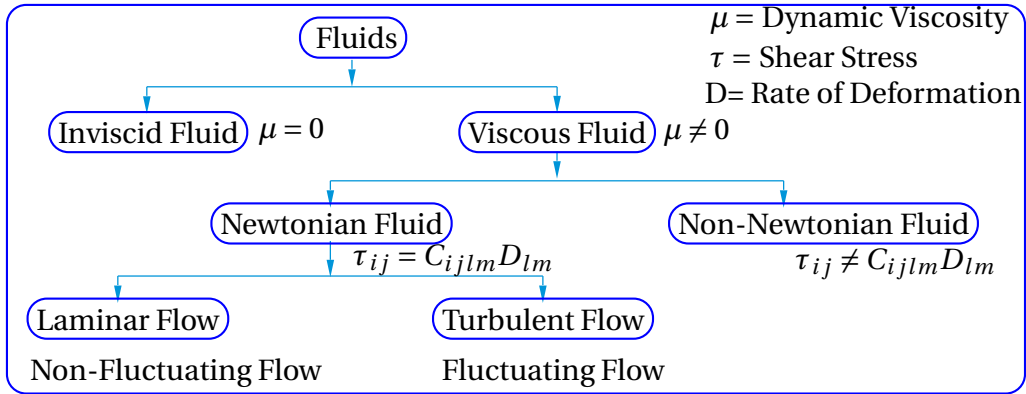
Figure 2.3 Fluid (Flow) Classification (after [102])

these relations can be different. Figure 2.3 depicts a common classification which helps in understanding the constitutive equations. Inviscid fluids are ideal fluids which are assumed to have zero or negligible viscosity. As a result, the shear stress in these fluids is zero and the total stress is equal to the pressure. In the viscous fluids, the viscosity is significant depending on the fluid type. Figure 2.4 shows the behavior of some viscous fluids as a response to applied shear stress [102].

The most common viscous fluids known as Newtonian Fluids, in which group we find water and air, show linear relation between shear stress τ and the rate of deformation **D**. The Non-Newtonian Fluid shows non-linear behavior. The Ideal Bingham Plastic Fluid requires high initial shear stress (equal to its yield strength) before it starts to flow. Figure 2.4 b) shows the thinning and thickening nature of Non-Newtonian Fluid with time. The Rheopectic Fluid becomes thicker with time and need more shear stress to make them flow at constant shear strain rate. The Thixotropic Fluid shows the opposite effect. The stress-strain-rate relation for Newtonian fluids is given by

$$\boldsymbol{\sigma} = -p\mathbf{I} + \mathbf{C}^{(4)} \cdot\cdot \mathbf{D}, \tag{2.6}$$

where p is static pressure and $\mathbf{C}^{(4)}$ is fourth order fluid viscosity coefficient tensor. For isotropic fluid, (2.6) reduces to

$$\boldsymbol{\sigma} = -p\mathbf{I} + \lambda\mathbf{I}\mathbf{D}\cdot\cdot\mathbf{I} + 2\mu\mathbf{D}, \tag{2.7}$$

where **I** is unit second order tensor, λ is the second coefficient of viscosity and μ is the dynamic viscosity.

Contraction of (2.7) gives us,

$$\boldsymbol{\sigma}\cdot\cdot\mathbf{I} = -3p + (3\lambda + 2\mu)\mathbf{D}\cdot\cdot\mathbf{I} = 3\sigma_m \tag{2.8}$$
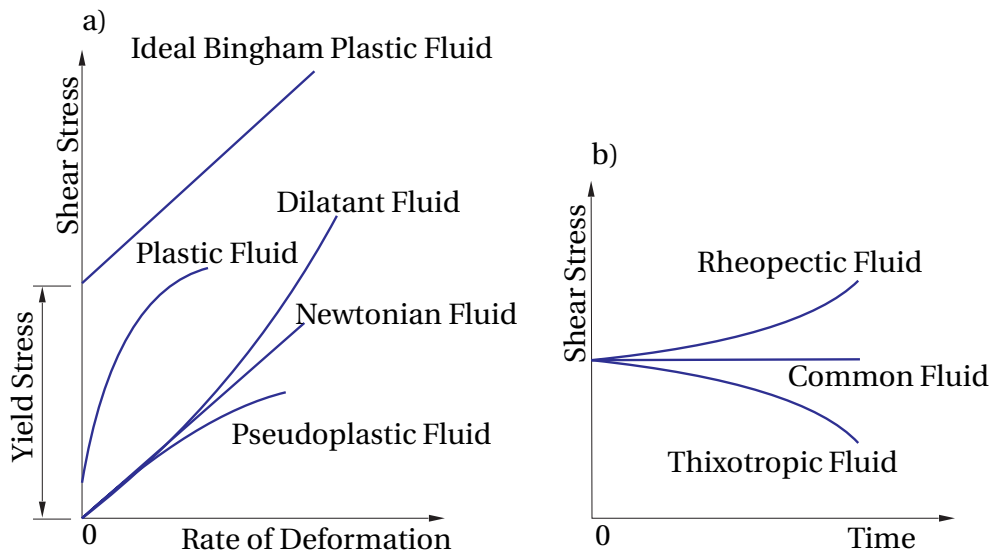
Figure 2.4 Schematic View of Fluid Constitutive Relations: a) Stress versus strain rate, b) Effect of time on applied stress at constant strain rate. (after [102])

According to George E. Stokes [41], the normal mean stress, σ_m, is assumed to be independent of the dilatation $\mathbf{D} \cdot \cdot \mathbf{I}$. This gives us the relation between the two viscosity coefficients (λ and μ), to be $\lambda = -\frac{2}{3}\mu$ [74]. The constitutive equation (2.7) now becomes,

$$\boldsymbol{\sigma} = -p\mathbf{I} - \frac{2}{3}\mu\mathbf{ID} \cdot \cdot \mathbf{I} + 2\mu\mathbf{D} \tag{2.9}$$

In majority of practical problems, the flow is turbulent where the velocity becomes extremely fluctuating. This fluctuation can result in variable loads on the structure with which the fluid is interacting. It also enhances the heat transfer between fluids and structure [10]. The study of turbulent phenomena is, therefore, very important in the design of machine components. However, turbulent flow is one of the unsolved problems so far [100, 86, 32]. The flow becomes time dependent even for steady boundary conditions as shown in Fig. 2.5. It is this fluctuation behavior which makes solution of turbulent flows very difficult. The current trend of solving turbulent flows is by numerical simulation or by modifying the governing equations. This modification of the governing equations results in more number of unknowns where turbulent models are needed to determine the unknowns from known quantities [11]. The approaches of solving turbulence flows so far available are categorized in to three [10, 32] as:

20
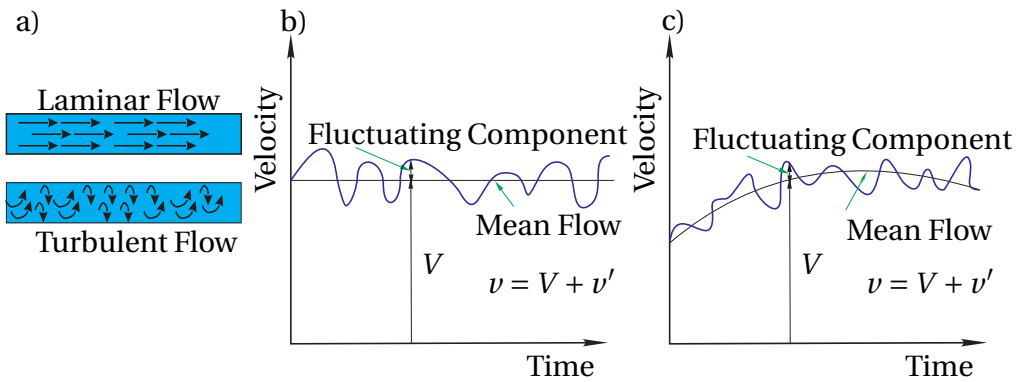
Figure 2.5 Turbulent Flow Phenomena: a) Visualized Flow, b) Steady Turbulent Flow, c) Transient Turbulent Flow. (after [103])

1. **Classical models** (also known as Reynolds Averaged Navier-Stokes Models): In this technique, the flow velocity is decomposed in to mean and fluctuating components, and inserted in to the fundamental equations. New terms will appear in the fundamental equations due to this process as will be discussed later in this section.

2. **Large Eddy Simulation (LES):** This technique decomposes the eddy formed in the flow in to small and large eddies by a technique known as filtering. Then large eddies will simulated and small eddies will be modeled. This technique is assumed to be more accurate and more expensive compared to the classical method.

3. **Direct Numerical Simulation (DNS):** This is a technique where all the eddies are numerically simulated. DNS is the most accurate and most expensive technique.

The classical $k - \epsilon$ model, which belongs to the classical models, will be briefly explained here because it will be used in this work for simulating a fluid-structure interaction problem. Compared to other models, this model is a validated one for wide range of problems [103]. It is based on the Reynolds averaging technique of decomposing the velocity in to mean and fluctuating components as in (2.10)

$$\mathbf{v} = \mathbf{V} + \mathbf{v}', \tag{2.10}$$

where **V** and **v'** are mean and fluctuating velocity component, respectively. The fluctuating velocity component results in turbulent kinetic energy, k, and energy dissipation rate, ϵ, which are defined according to (2.11) and (2.12),

respectively,

$$k = \frac{1}{2}\overline{\mathbf{v}' \cdot \mathbf{v}'}, \tag{2.11}$$

$$\epsilon = \nu\overline{\nabla\mathbf{v}' \cdot \cdot \nabla\mathbf{v}'}, \tag{2.12}$$

where ν is kinematic viscosity and the over bar indicates an average. Other scalar transport properties like temperature are also decomposed in a similar way as that of the velocity as in (2.13)

$$T = T_m + T', \tag{2.13}$$

where T' is fluctuating temperature. Inserting (2.10) in to the conservation equations (2.1) and (2.3), modified Eqns. (2.14) and (2.15) will be obtained:

- Modified Continuity Equation

$$\frac{\partial \rho}{\partial t} + \nabla \cdot (\rho\mathbf{V}) = 0 \tag{2.14}$$

- Modified Momentum Equation (Momentum Transport Equation)

$$\rho\frac{\partial \mathbf{V}}{\partial t} + \nabla \cdot (\rho\mathbf{V} \otimes \mathbf{V}) = -\nabla p + \nabla \cdot [\mu(\nabla\mathbf{V} + \nabla\mathbf{V}^T) - \rho\overline{\mathbf{v}' \otimes \mathbf{v}'}] + \mathbf{S}^u \tag{2.15}$$

The term $-\rho\overline{\mathbf{v}' \otimes \mathbf{v}'} = \boldsymbol{\tau}^t$ in (2.15) is called the Reynolds Stress Tensor. The energy equation also can be modified by making use of (2.13), Fourier's law of conduction ($\mathbf{q} = -k\nabla T$) [18, 50, 85] and state equations $u = c_v T$ and $h = c_p T$.

- Modified Energy Equation (Temperature Transport Equation)

$$\rho\frac{\partial T}{\partial t} + \nabla \cdot (\rho T\mathbf{V}) = \nabla \cdot (\frac{k}{c_p}\nabla T - \rho\overline{\mathbf{v}'T'}) + S^T, \tag{2.16}$$

where k is thermal conductivity, c_v and c_p are specific heat capacities at constant volume and constant pressure, respectively, $\mathbf{S}^u$ and $\mathbf{S}^T$ are momentum and thermal source terms, respectively, $\mathbf{h}$ is enthalpy and $\mathbf{u}$ is internal energy.

According to the classical turbulence modeling, $\boldsymbol{\tau}^t$ is modeled as

$$\boldsymbol{\tau}^t = \mu_t(\nabla\mathbf{V} + \nabla\mathbf{V}^T) - 2\rho k\mathbf{I}, \tag{2.17}$$

where μ_t is turbulent dynamic viscosity. The turbulent dynamic viscosity, μ_t, is given by

$$\mu_t = \rho C_\mu\frac{k^2}{\epsilon} \tag{2.18}$$

We have another new term $-\rho\overline{\mathbf{v}'T'}$ in (2.16) which is going to be modeled. This term can be modeled, like for the Reynold's stress case, according to

$$-\rho\overline{\mathbf{v}'T'} = -k_t\boldsymbol{\nabla}T_m \qquad (2.19)$$

k_t and μ_t are related by the so called Schmidt number, σ_t, as in [25, 99]

$$\sigma_t = \frac{\mu_t}{k_t}, \qquad (2.20)$$

where k_t is turbulent thermal conductivity and T_m is mean temperature. after some mathematical manipulations, transport equations for the turbulent kinetic energy, k, and its dissipation rate, ϵ, given in (2.21) and (2.22), respectively can be obtained [103]. These additional equations close the system of equations:

- k-Equation

$$\rho\frac{\partial k}{\partial t} + \rho\mathbf{V}\cdot\boldsymbol{\nabla}k = \boldsymbol{\tau}\cdot\cdot\boldsymbol{\nabla}\mathbf{V} - \rho\epsilon + \boldsymbol{\nabla}\cdot[(\mu+\frac{\mu_t}{\sigma_k})\boldsymbol{\nabla}k], \qquad (2.21)$$

- ϵ-Equation

$$\rho\frac{\partial\epsilon}{\partial t} + \rho\mathbf{V}\cdot\boldsymbol{\nabla}\epsilon = C_{\epsilon 1}\frac{\epsilon}{k}\boldsymbol{\tau}\cdot\cdot\boldsymbol{\nabla}\mathbf{V} - C_{\epsilon 2}\rho\epsilon^2 + \boldsymbol{\nabla}\cdot[(\mu+\frac{\mu_t}{\sigma_\epsilon})\boldsymbol{\nabla}\epsilon], \qquad (2.22)$$

where k is turbulent kinetic energy and ϵ is turbulent kinetic energy dissipation rate. The closure constants are $C_{\epsilon 1} = 1.44$, $C_{\epsilon 2} = 1.92$, $\sigma_k = 1.0$, and $\sigma_\epsilon = 1.3$, $C_\mu = 0.09$ as given in [11]. Equations (2.21) and (2.22) should be solved in addition to the conservation equations.

2.3.2 Thermomechanical Constitutive Equations

As it has been explained in the introduction chapter, the majority of the energy conversion processes operate at high temperatures. The externally applied loads come from thermal processes. Therefore, it is important to include the thermal influence in the constitutive equations of solid media. The development of constitutive equations for solid bodies usually begins with uni-axial tests [40, 35]. The instantaneous response of typical ductile materials for such tests is shown in Fig. 2.6. The stress, σ, and strain, ε, in
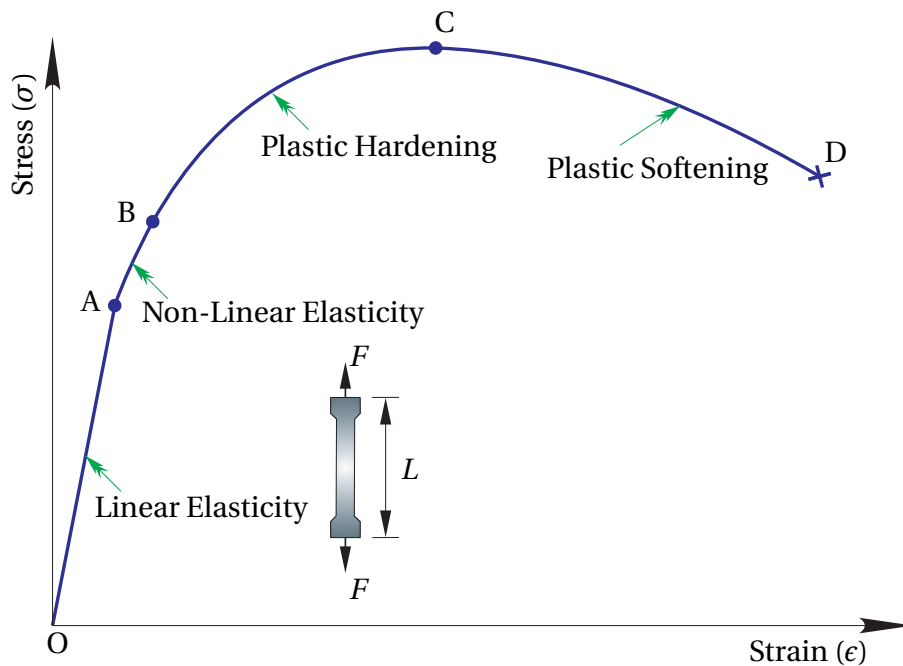
Figure 2.6   Typical Load-Elongation Curve (after [93, 73, 9])

the figure are related to the applied force, F, the initial length, L_0, and initial cross-sectional area, A_0, of the test specimen as

$$\sigma = \frac{F}{A_0}, \tag{2.23}$$

$$\varepsilon = \frac{\Delta L}{L_0}. \tag{2.24}$$

The first linear (0-A) and the next non-linear (A-B) parts of the curve (elastic regions) are fully recoverable when the load is removed, i.e. the specimen attains its original length after removal of the load. The remaining parts of the curve show inelastic behavior where the test specimen shows permanent deformation. The inelastic behavior has two parts. In the first part (B-C) the material becomes harder as the stress is increased till point C is attained where this hardening behavior ceases. After point C, the material becomes more and more soft as the force increase and finally fractures at point D. This nature of the response of materials to loads is dependent on the micro-structural changes that take place as more and more load is applied. Moreover, the curves obtained for the same material show different nature if the test is performed at different temperatures and at different loading rates.

From the nature of the curve, it can be observed that the development of constitutive relations for the whole region and specially for the inelastic

part is difficult. The nature of these curves is strongly material dependent. Even though, Fig. 2.6 shows typical and simplified curve that represents many materials, there are lots of materials with stress-strain curves having much different nature.

Based on the curve in Fig. 2.6 constitutive models developed can be grouped in two as,

1. Elastic Constitutive Models and

2. Inelastic Constitutive Models.

Linear Elasticity Constitutive Models

The elastic part of the curve shows relatively simple nature. The non-linear part of the curve is usually neglected. In general the relation between the stress, σ, and strain, ε, can be given as,

$$\sigma = E\varepsilon, \tag{2.25}$$

where σ is stress, ε is strain and E is the Young's modulus. The Young's modulus E is the slope of the linear elastic part of the curve. For high temperature operations (2.25) has to take the effect of thermal expansion as

$$\sigma = E[\varepsilon - \alpha(T - T_0)], \tag{2.26}$$

where α is thermal expansion coefficient of the material and T_0 is reference temperature. This represents a thermo-mechanical problem. Equations (2.25) and (2.26) hold for uni-directional test specimens. These relations can be extended to three dimensions as

$$\boldsymbol{\sigma} = \mathbf{C}_s^{(4)} \cdot\cdot \boldsymbol{\varepsilon}, \tag{2.27}$$

The fourth rank material property tensor $\mathbf{C}_s^{(4)}$ has $3^4 = 81$ components. Due to symmetric nature of stress and strain tensors (thanks to the balance of angular momentum, assuming no coupled stresses [8]) and due to symmetric nature of materials themselves (isotropic, orthotropic, ...), not all the components are independent [47]. In the case of isotropic materials, only two components are independent and majority of the components have zero values. In this case, $\mathbf{C}_s^{(4)}$ will have the form,

$$\mathbf{C}_s^{(4)} = \lambda_s \mathbf{I} \otimes \mathbf{I} + 2\mu_s \mathbf{I}^{(4)} \tag{2.28}$$

In terms of the Young's modulus, E, and Poisson's ration, v, Lamé modulus, λ_s, and shear modulus, μ_s, can be given, respectively, as in (2.29) and (2.30).

$$\lambda_s = \frac{Ev}{(1+v)(1-2v)} \tag{2.29}$$

$$\mu_s = \frac{E}{2(1+v)} \tag{2.30}$$

The thermo-mechanical stress-strain relation in three dimension for isotropic material becomes

$$\boldsymbol{\sigma} = \lambda_s \, tr(\boldsymbol{\varepsilon})\mathbf{I} + 2\mu_s\boldsymbol{\varepsilon} - \frac{E\alpha\Delta T}{1-2v}\mathbf{I} \tag{2.31}$$

This is the generalized Hooke's law that includes thermal effects [107]. The inverse relation of (2.31) is given by

$$\boldsymbol{\varepsilon} = -\frac{v}{E} \, tr(\boldsymbol{\sigma})\mathbf{I} + \frac{1+v}{E}\boldsymbol{\sigma} + \alpha\Delta T\mathbf{I} \tag{2.32}$$

Inelastic Constitutive Models

The inelastic behavior of materials can be categorized in to two types as,

1. Rate-Independent (Classical) Plasticity, and

2. Rate-Dependent Plasticity (Viscoplasticity), which includes creep and relaxation [35, 40, 52].

Both of these categories will be briefly explained beginning with facts from uni-axial tests and extending them to three dimensional problems as it has been done for elasticity problems.

Rate-Independent Plasticity   In developing constitutive models for classical plasticity problems, the yield criteria, flow rules and hardening laws are the three points to be considered [30, 16]. These will be briefly discussed here based on Fig. 2.7.

1. **Yield Criteria**,
   When load greater than the initial yield strength of materials (Y_0 on Fig. 2.7) is applied on uni-axial test specimens, subsequent yielding of the materials is observed. When load is removed, the unloading curve follows a straight line approximately parallel to the initial elastic loading line as shown in Fig. 2.7. Based on this fact, the following relation can be obtained.

   $$\sigma = E(\varepsilon - \varepsilon^p) = E\varepsilon^e, \tag{2.33}$$

   where ε^p is plastic strain. After the unloading is completed ($\sigma = 0$), the material will have a permanent strain equal to ε^p and the recovered
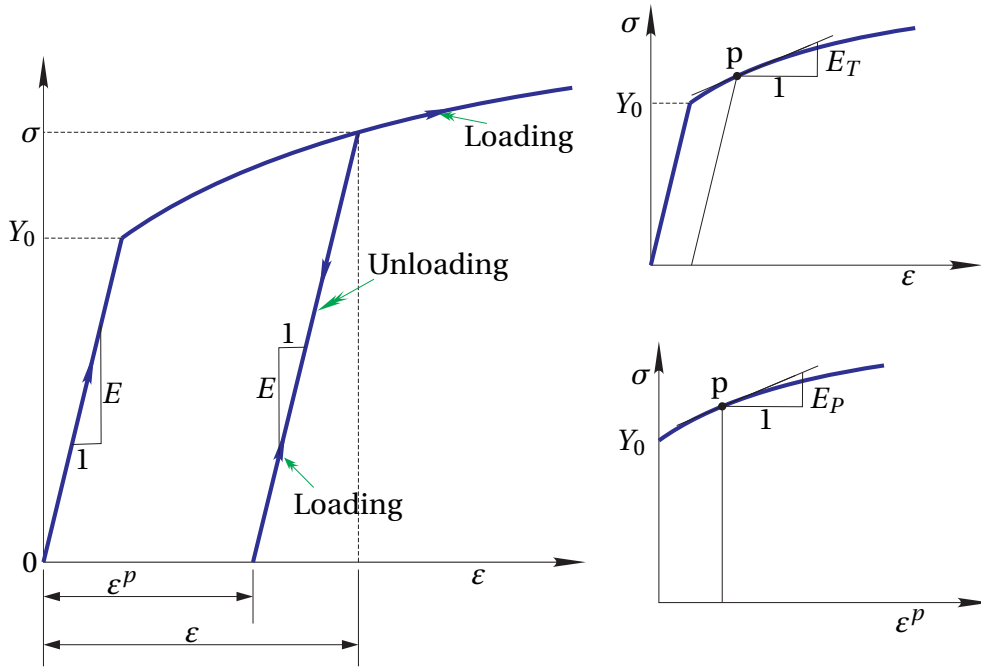
Figure 2.7 Stress-Strain Curve for Classical Plasticity (after [31, 9])

strain will be the elastic strain $\varepsilon^e = \varepsilon - \varepsilon^p$. This leads to the split of the total strain in to elastic and plastic parts, which also helps in determining the relation between the young's modulus, E, the tangent modulus, E_T and the plastic modulus E_P.

$$\varepsilon \quad = \varepsilon^e + \varepsilon^p \tag{2.34}$$

$$\Rightarrow \frac{\sigma}{E_T} \quad = \frac{\sigma}{E} + \frac{\sigma}{E_P}$$

$$\Rightarrow \frac{1}{E_T} \quad = \frac{1}{E} + \frac{1}{E_P} \tag{2.35}$$

At any point on the plastic curve of Fig. 2.7, the stress, σ, is equal to the new yield strength of the material, Y, that is $\sigma = Y$ or $\sigma - Y = 0$. This is a yield function, f [22], usually defined as

$$f = \sigma - Y = 0 \tag{2.36}$$

The figure depicts that the yield strength is a function of the plastic strain, and the yield function can be written as $f = f(\sigma, \varepsilon^p, K)$, where K represents additional internal state variables of the material on which yielding depends. This function helps in determining the
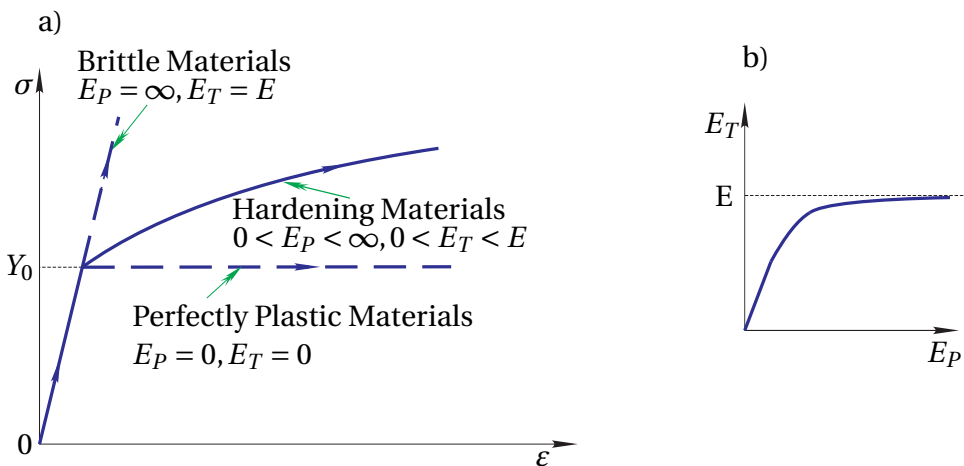
Figure 2.8   Ductility of Materials: a) Comparison of Brittle and Perfectly Plastic Materials, b) Tangent Modulus versus Plastic Modulus. (after [31])

loading/unloading conditions as follows [40],

$$
\left.\begin{array}{l}
\dfrac{\partial f}{\partial \sigma} d\sigma < 0 \text{ and } f = 0 \Longrightarrow \text{Unloading} \\[2mm]
\dfrac{\partial f}{\partial \sigma} d\sigma = 0 \text{ and } f = 0 \Longrightarrow \text{Neutral Loading} \\[2mm]
\dfrac{\partial f}{\partial \sigma} d\sigma > 0 \text{ and } f = 0 \Longrightarrow \text{Loading}
\end{array}\right\}
\qquad (2.37)
$$

Figure 2.9 shows the variation of stress, yield strength and yield function with strain during elastic loading, plastic loading and elastic unloading for uni-axial test. The loading/unloading conditions is also depicted in the magnified view. In three dimensional problems, the stress state is a point in a nine-dimensional stress space. This space has origin where all the components of the stress tensor are zero. The boundary of the space is the yield surface. Interior of the space is the elastic region. For perfectly-plastic materials, the yield surface is fixed while for hardening materials it is expanding, translating or combination of the two. Due to symmetric nature of stress and strain tensors, the dimension of the space will be reduced to six. For isotropic materials further simplifications can be made:

- the yield surface is independent of the directions of the stress tensor components. Then the yield function is function of only the stress tensor invariants.
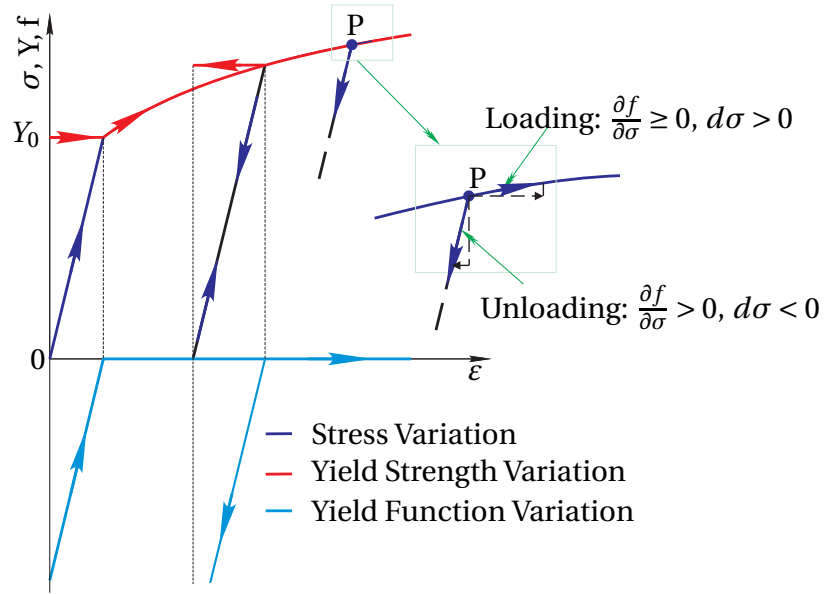
Figure 2.9 Variation of Yield Function (after [31])

- the yield surface is independent of the hydrostatic stress. Then the yield function will be function of the invariants of the deviatoric stress tensor.

Now for isotropic materials we have a yield function dependent on the invariants, J_2 and J_3, of the deviatoric stress, **S**,

$$f = f(J_2, J_3) \tag{2.38}$$

The deviatoric stress is defined as,

$$\mathbf{S} = \boldsymbol{\sigma} - \sigma_m \mathbf{I} \tag{2.39}$$

The invariants are

$$J_2 = \frac{1}{2}\mathbf{S} \cdot \cdot \mathbf{S}, \tag{2.40}$$

$$J_3 = det(\mathbf{S}), \tag{2.41}$$

where $\sigma_m = \frac{1}{3}\boldsymbol{\sigma} \cdot \cdot \mathbf{I}$ is mean or hydrostatic stress, J_2 and J_3 are second and third invariants, respectively, of the deviatorc stress. According to von-Mises yield criteria the yield function has the form,

$$f = J_2 - K^2 = 0, \tag{2.42}$$
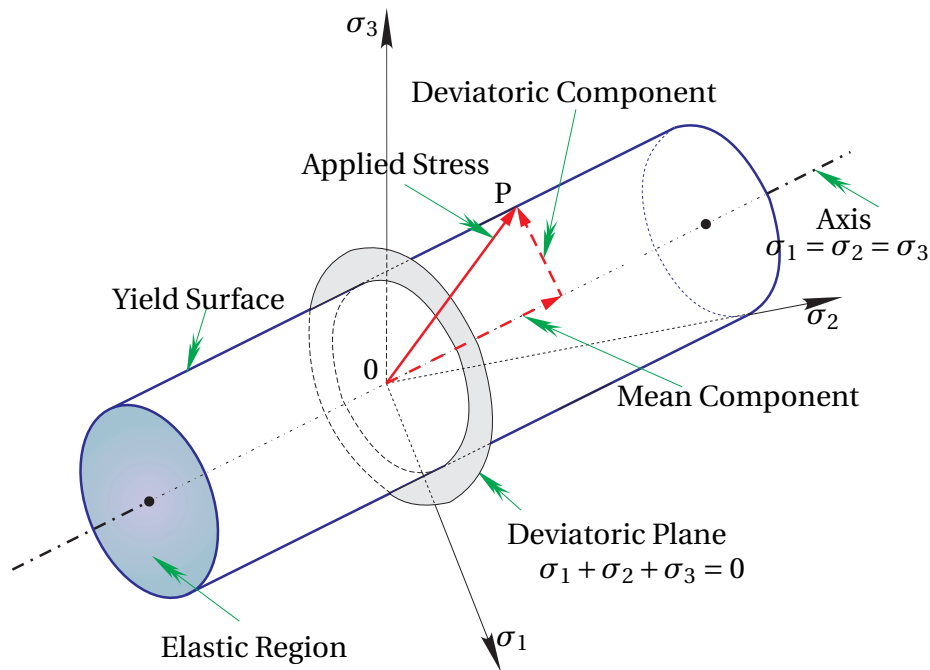
Figure 2.10 von-Mises Yield Surface (after [30, 36, 107])

where Y is the yield strength obtained from uni-axial test. In (2.42), $K = \frac{1}{\sqrt{3}}Y$. Then the yield function becomes,

$$f = \frac{1}{2}\mathbf{S}\cdot\cdot\mathbf{S} - \frac{1}{3}Y^2 = 0 \tag{2.43}$$

In general, the yield surface forms a right cylinder in principal stress space for isotropic materials for which the hydrostatic stress has no effect on plastic deformation [30]. For the von-Mises yield criteria, the yield surface forms a circular cylinder as shown in Fig. 2.10. The axis of the cylinder is the line where $\sigma_1 = \sigma_2 = \sigma_3$. Any applied stress on the yield surface can be projected to this axis to give the mean (hydrostatic) component. The component perpendicular to the axis will be the deviatoric component.

2. **Flow Rule**,

The yield criteria discussed above sets conditions for plastic deformation to occur. The total strain was found to be the sum of the elastic and the plastic parts. The elastic component is determined by the generalized Hooke's law given by (2.32). The purpose of this section is to set some rules how to determine the plastic strain through what is known as the flow rule.
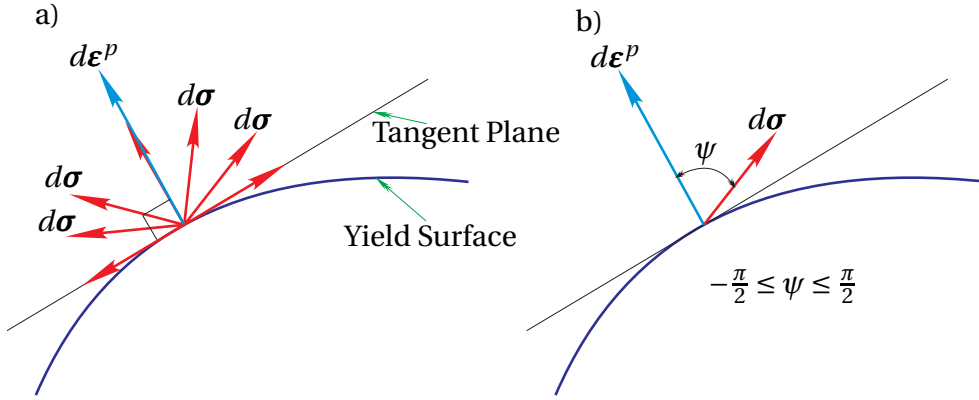
Figure 2.11   Drucker's Hypothesis on Yield Surface: a) $d\boldsymbol{\varepsilon}^p$ and all possible directions of $d\boldsymbol{\sigma}$ during loading, b) Angle between $d\boldsymbol{\sigma}$ and $d\boldsymbol{\varepsilon}^p$. (after [30])

The yield surface of hardening materials expands and/or translates as the applied stress increases and there are three hypotheses in relation to this, according to the work of Drucker [40]:

- The yield surface must be convex.

- The plastic strain increment is normal to the yield surface.

- The rate of change of plastic strain is a linear function of the rate of change of strain.

The other work of Drucker, which is basis for the derivation of the above three hypotheses, is that the work done during plastic increment, $d\boldsymbol{\varepsilon}^p$, due to the stress increment, $d\boldsymbol{\sigma}$, is always non-negative. That is

$$d\boldsymbol{\sigma} \cdot\cdot d\boldsymbol{\varepsilon}^p \geq 0, \tag{2.44}$$

where the equality holds for perfectly plastic material. Equation (2.44) is the dot product between the plastic strain increment vector and stress increment vector. This implies that the angle, ψ, Fig. 2.11 b) between the two vectors should be,

$$-\frac{\pi}{2} \leq \psi \leq \frac{\pi}{2} \tag{2.45}$$

The rate of change of the yield function $f(\boldsymbol{\sigma}, \boldsymbol{\varepsilon}^p, K) = 0$, assuming $K = K(\boldsymbol{\varepsilon}^p)$, is

$$\dot{f} = \frac{\partial f}{\partial \boldsymbol{\sigma}}\dot{\boldsymbol{\sigma}} + \frac{\partial f}{\partial \boldsymbol{\varepsilon}^p}\dot{\boldsymbol{\varepsilon}}^p + \frac{\partial f}{\partial K}\frac{\partial K}{\partial \boldsymbol{\varepsilon}^p}\dot{\boldsymbol{\varepsilon}}^p = 0 \tag{2.46}$$

Rearranging (2.46) gives us

$$\dot{\boldsymbol{\varepsilon}}^p = \left(\frac{-\frac{\partial f}{\partial \boldsymbol{\sigma}}}{\frac{\partial f}{\partial \boldsymbol{\varepsilon}^p} + \frac{\partial f}{\partial K} \frac{\partial K}{\partial \boldsymbol{\varepsilon}^p}} \right) \dot{\boldsymbol{\sigma}} \qquad (2.47)$$

Equation (2.47) is the same as Drucker's third hypothesis above. Now the relation between the rate of change of plastic strain and rate of change of stress has been obtained. Determination of the term in parenthesis in (2.47) follows from the hardening law, which will be explained next.

3. **Hardening Law**,

   Materials, mainly metals, become harder when loaded plastically. Higher load is required to cause plastic deformation or, in other words, the yield strength of the material increases because of accumulation of plastic strain [38]. Based on this fact, we have three modes of hardening:

   a) Isotropic Hardening,

   b) Kinematic Hardening, and

   c) Mixed Hardening.

   Isotropic Hardening. If the material is loaded in tension, the increase in yield strength in tension may result in an increase of yield strength in compression also. This is known as isotropic hardening, Fig. 2.12 a). For three dimensional loading, isotropic hardening results in expansion of the yield surface, Fig. 2.12 c), with the center of the surface remaining unchanged. The von-Mises yield function for isotropic hardening has the form,

   $$f(\sigma^{eq}, \varepsilon^p) = \sigma^{eq} - Y(\varepsilon^p) = 0, \qquad (2.48)$$

   where ε^p is accumulated plastic strain and σ^e is effective or equivalent stress. The von-Mises equivalent stress is given by

   $$\sigma^e = \left(\frac{3}{2} \mathbf{S} \cdot \cdot \mathbf{S} \right)^{\frac{1}{2}} \qquad (2.49)$$

   The accumulated plastic strain is given by,

   $$\varepsilon^p = \int \left(\frac{2}{3} \dot{\boldsymbol{\varepsilon}}^p \cdot \cdot \dot{\boldsymbol{\varepsilon}}^p \right)^{\frac{1}{2}} dt \qquad (2.50)$$

Kinematic Hardening. In case of kinematic hardening, an increase in tensile yield strength will result in reduction in compressive yield strength or vice versa, Fig. 2.12 b). This phenomena is known as the Bauschinger effect. For loading in three dimension, kinematic hardening brings about a translation of the yield surface with no change to the radius of the surface, Fig. 2.12 d).

In kinematic hardening, the yield function has a slight modification from that of the isotropic hardening to account for the translation of the yield surface and the fixed radius.

$$f(\mathbf{S}, \boldsymbol{\alpha}) = \left(\frac{3}{2}(\mathbf{S} - \boldsymbol{\alpha}) \cdot \cdot (\mathbf{S} - \boldsymbol{\alpha})\right)^{\frac{1}{2}} - Y_0 = 0, \qquad (2.51)$$

where $\boldsymbol{\alpha}$ is kinematic hardening variable also called back stress tensor and Y_0 is initial yield strength.

Mixed Hardening. The third mode of hardening is the mixed hardening, which combines the effects of both isotropic and kinematic hardening, Fig. 2.13. This model is the most accurate compared to the above two. In three-dimensional loading, the yield surface undergoes both expansion and translation as shown in Fig. 2.13 b) for mixed hardening.

The yield function for the mixed hardening will be obtained by combining the respective equations of the isotropic and kinematic hardening as

$$f(\mathbf{S}, \boldsymbol{\alpha}, \varepsilon^p) = \left(\frac{3}{2}(\mathbf{S} - \boldsymbol{\alpha}) \cdot \cdot (\mathbf{S} - \boldsymbol{\alpha})\right)^{\frac{1}{2}} - Y(\varepsilon^p) = 0 \qquad (2.52)$$

Rate-Dependent Plasticity

The rate-independent plasticity discussed in the previous section deals with the instantaneous response of a material to applied loads. But in practical applications there are cases where the loads developed in components become rate-dependent. Some case are explained below.

a) If loads are applied at different rates as shown in Fig. 2.14 a), different stress-strain relations can be obtained in the plastic range. This is called viscoplasticity. As shown in Fig. 2.15, the classical (rate-independent)
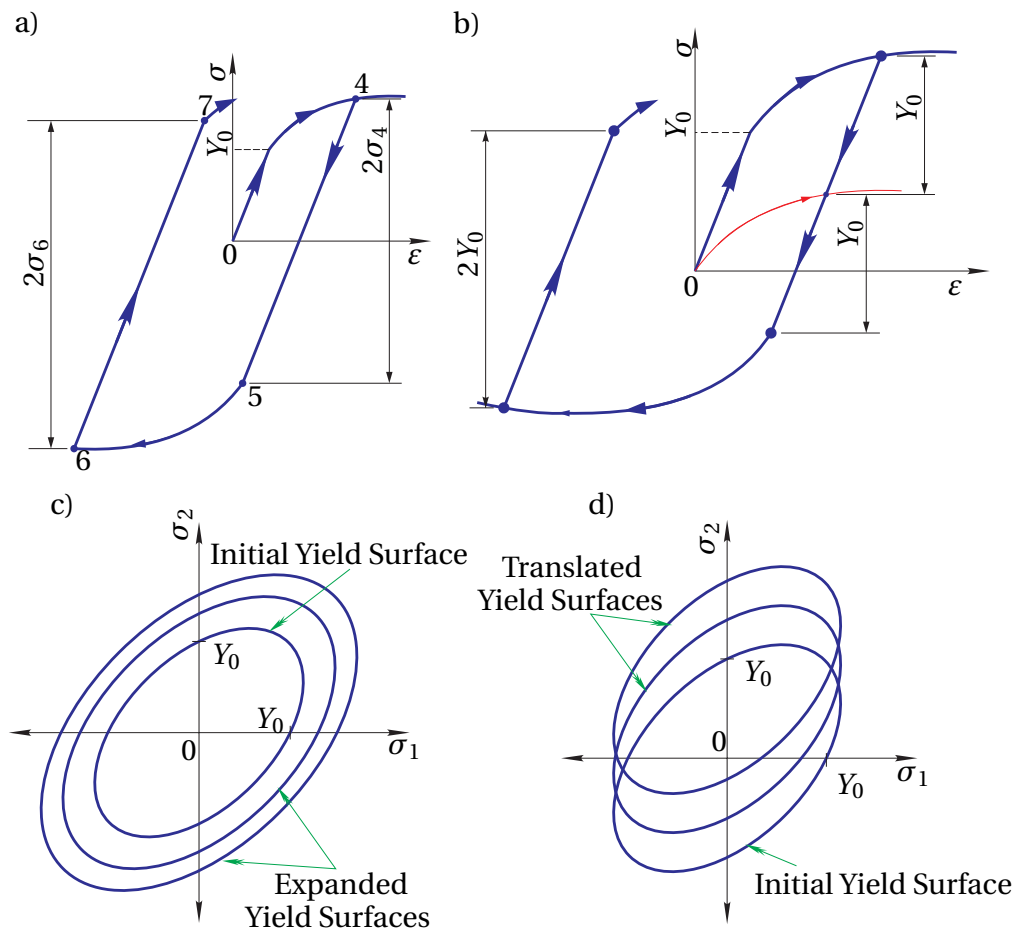
Figure 2.12 Plastic Hardening Models: a) Isotropic Hardening, b) Kinematic Hardening, c) Subsequent Yielding in Isotropic Hardening, d) Subsequent Yielding in Kinematic Hardening. (after [30])

plasticity stress-strain curve can be modified due to additional rate-dependent stress known as viscous stress.

There are two commonly known approaches of modeling this phenomena, namely the Over-Stress (Perzyna) model and the Consistency model [49].

In both cases, the total strain is split into elastic and viscoplastic parts, as in (2.53) below, like in the case of the classical plasticity modeling.

$$\boldsymbol{\varepsilon} = \boldsymbol{\varepsilon}^{el} + \boldsymbol{\varepsilon}^{vp} \tag{2.53}$$

and the stress is related to the recovered elastic strain as

$$\boldsymbol{\sigma} = \mathbf{C}_s^{(4)} \cdot \cdot \boldsymbol{\varepsilon}^{el} \tag{2.54}$$
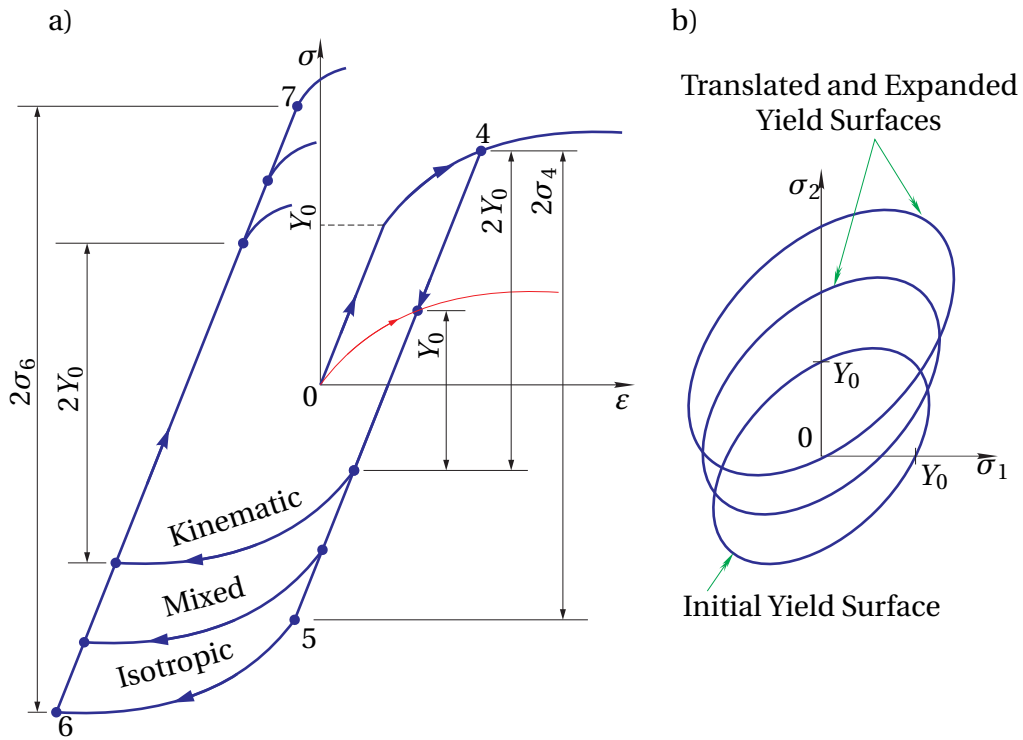
Figure 2.13 Mixed Hardening: a) Comparison with Other Hardening Models, b) Yield Surfaces during Subsequent Mixed Hardening. ([31])

In the case of the Perzyna model, the yield function becomes greater than zero during loading unlike the classical plasticity case. The viscous stress lies outside the yield surface. The name Over-Stress is given to this model based on this fact. The viscoplastic strain rate is given by

$$\dot{\boldsymbol{\varepsilon}}^{vp} = \gamma \langle \phi(f,K) \rangle \frac{\partial g}{\partial \boldsymbol{\sigma}} = \dot{\Lambda} \frac{\partial g}{\partial \boldsymbol{\sigma}}, \tag{2.55}$$

where ϕ is over stress function, g is viscoplastic potential function, Λ is consistency parameter and γ is fluidity parameter. The evolution of the internal variable, K, is usually given by,

$$\dot{K} = \sqrt{\frac{2}{3}\dot{\boldsymbol{\varepsilon}}^{vp} \cdot \dot{\boldsymbol{\varepsilon}}^{vp}} = \dot{\Lambda} \tag{2.56}$$

The consistency model incorporates rate dependency into the classical yield function. The rate dependent yield function is equal to zero like in the classical plasticity case [49], and is given by

$$f_{rd} = f_{rd}(\boldsymbol{\sigma}, \boldsymbol{\alpha}, \dot{\boldsymbol{\alpha}}) = 0 \tag{2.57}$$

b) The instantaneously applied constant loads may continue to be applied for long period of time as in Fig. 2.14 b). This results in different strain-time relations. This is a phenomena known as creep.

The stress is usually less than the yield strength of the material (or less than the static design stress) but usually applied at higher temperatures, $T = (0.3 - 0.5) T_{melt}$ [80]. Where T_{melt} is melting temperature of the material. Again, the first step in modeling creep is, like in the case of classical plasticity and viscoplasticity, splitting the total strain in to elastic and creep parts as

$$\boldsymbol{\varepsilon} = \boldsymbol{\varepsilon}^{el} + \boldsymbol{\varepsilon}^{cr} \tag{2.58}$$

Here also the stress is related to the recoverable elastic strain as

$$\boldsymbol{\sigma} = \mathbf{C}_s^{(4)} \cdot\cdot \boldsymbol{\varepsilon}^{el} \tag{2.59}$$

The creep curves are assumed to be stress, temperature and time dependent in an explicit way as in (2.60).

$$\boldsymbol{\varepsilon}^{cr} = f_1(\boldsymbol{\sigma}) f_2(T) f_3(t) \tag{2.60}$$

or alternatively, creep strain rates can be given as functions of stress, strain and temperature

$$\dot{\boldsymbol{\varepsilon}}^{cr} = f_1(\boldsymbol{\sigma}) f_2(\boldsymbol{\varepsilon}^{cr}) f_3(T) \tag{2.61}$$

The functions f_1, f_2 and f_3 are determined from optimization of experimental data of uni-axial tests and extended to multi-axial cases by making use of norm dependent quantities like equivalent creep strain rate.

c) The other case is the stress relaxation where the instantaneously obtained deformations may remain fixed for long time as shown in Fig. 2.14 c) resulting in gradual decrease of stress. The rate of change of the total strain will be,

$$\left.\begin{array}{l} \dot{\boldsymbol{\varepsilon}} = \dot{\boldsymbol{\varepsilon}}^{el} + \dot{\boldsymbol{\varepsilon}}^{cr} = 0 \\ \Rightarrow \mathbf{D}_s^{(4)} \cdot\cdot \dot{\boldsymbol{\sigma}} + \dot{\boldsymbol{\varepsilon}}^{cr} = 0 \end{array}\right\} \tag{2.62}$$

where $\mathbf{D}_s^{(4)}$ is fourth order elasticity compliance tensor. Equation (2.62) indicates that an increase in creep strain results in decreasing of stress as can also be seen from the uni-axial case in Fig. 2.14 c). The constitutive equations of creep and stress relaxation are the same and that developed for one should work for the other.
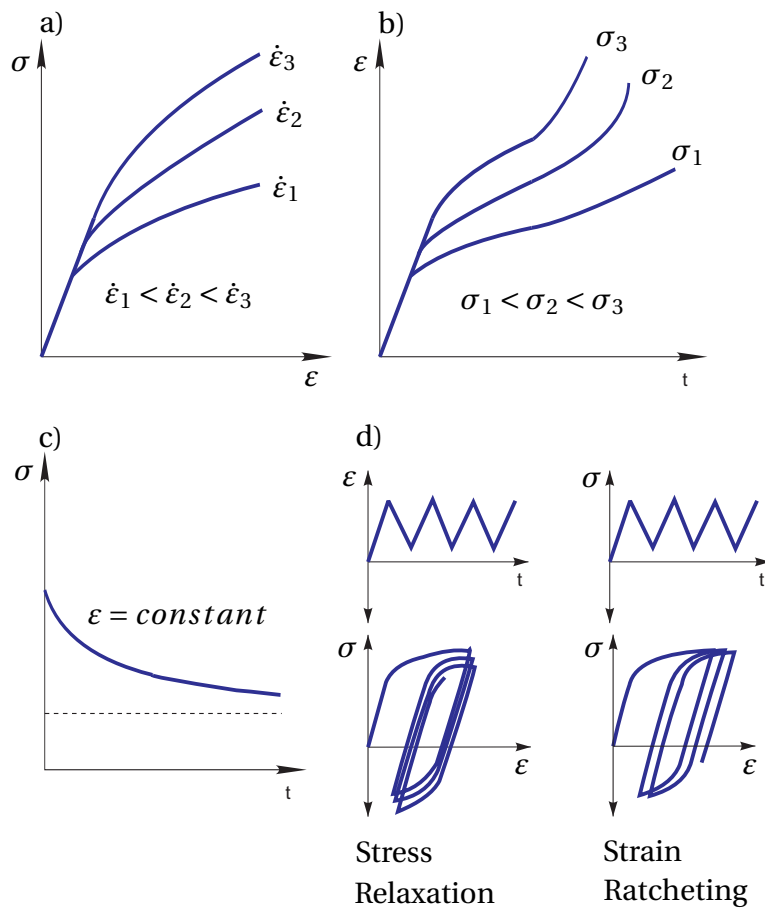
Figure 2.14 Rate Dependent Plasticity: a) Viscoplasticity, b) Creep, c) Relaxation, d) Strain and Stress Controlled Cyclic Loading. (after [28, 30, 80, 104, 29])

d) The last rate dependent inelastic phenomena is related to the response of materials to loads which vary with time as in Fig. 2.14 d). The input loads can be variable stresses or variable strains. In the case of variable strain input, the stress developed in the material varies in such a way that the mean stress gradually reduces. This is known as mean stress relaxation. If the input is a variable stress, the mean strain continues to increase, a phenomena called strain ratcheting.
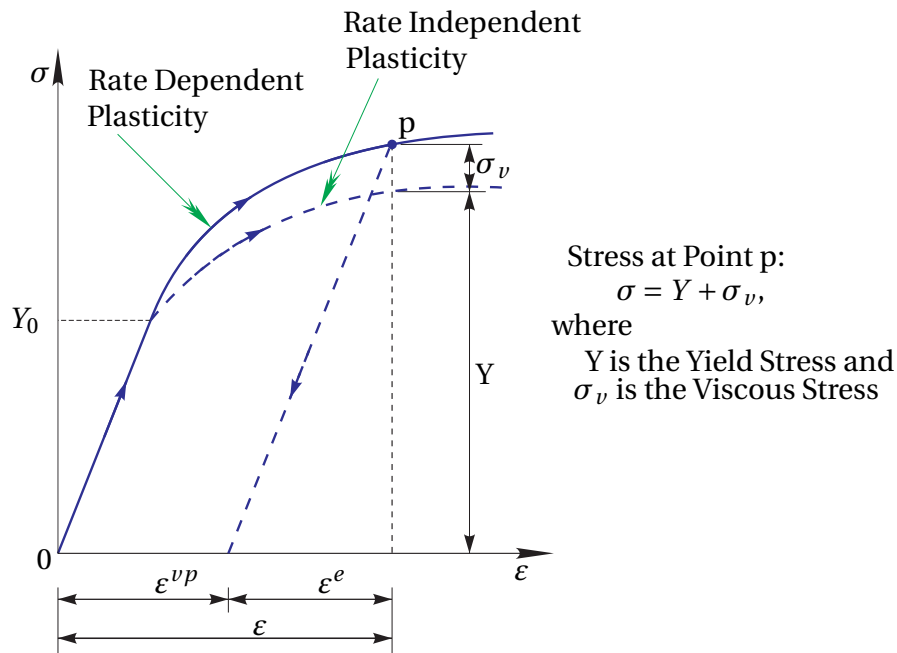
Figure 2.15 Viscoplasticity Model (after [104, 62])

2.4   Computational Solution Formulation

In the previous sections, governing equations and constitutive equations of major fluid-structure interaction phenomena were introduced. Once we have these equations at hand, the next step is to solve them with the objective of determining the distributions of stresses, strains, temperatures, etc., in the material under consideration. The solution can be done either analytically or computationally. Analytical solution is possible only for very simplified problems and it is of no practical interest. The computational solution is almost the only option of solving complicated equations with complex geometry and boundary and/or initial conditions.

In Fluid-Structure Interaction problems where inelastic behavior is expected, we have two problems which should be duly considered during kinematic motion/deformation formulation.

1. The load from the fluid deforms the solid structure and as a result the configuration of the fluid also changes.

2. The inelastic deformation of solids may be very large and result in distorted meshes. The computational results from distorted meshes were found to be less accurate [95].

These two points force us to use the Arbitrary-Lagrangian-Eulerian (ALE) formulation of the problem. The ALE formulation combines the two separate formulations, the Lagrangian formulation and the Eulerian formulation, which are normally used to model solid and fluid media, respectively. The difference between the two formulations lies on the nature of fluid flow and solid deformation problems. This difference in nature has an effect mainly on the mesh generation step as follows.

- In modeling ordinary flow problems where deformation of solid structure in/on which the fluid flows is negligible, fluid particles flow through a fixed volume. The interest in modeling is not concerned with individual fluid particles but rather with the effect of the flow in the volume. During computational analysis, this fixed volume will be meshed with mesh size and shape remaining unchanged, Fig. 2.16 c). It is the properties like temperature, pressure, fluid velocity, etc., which will have variation in the volume. With fixed boundaries of the fluid, pure Eulerian formulation can be used.

- In the case of solid body deformation modeling, the interest is on all material particles. The mesh is attached to material points and it will have new shape and new position during and after the body is deformed. The Lagrangian formulation will be used with no problem if the deformation is relatively small. If the deformation is very large, the change in shape of the mesh will create a problem (distorted mesh problem) and Lagrangian formulation may not be successful.

- In the case of Fluid-Structure Interaction with significant deformation of solid, the solid deforms to a new position and the fluid region also moves with the solid to attain a new configuration as in Fig. 2.16 b). In this case, none of the two formulations can handle the problem. The Eulerian formulation can not account for the shift in fluid configuration and the Lagrangian formulation may not be convenient to deal with the mesh independent fluid flow (convection effect).

  Therefore, a formulation that takes the advantages of both formulations and avoids their drawbacks is needed. Currently, the ALE formulation fulfills this need.

Now mathematical description of the ALE formulation is introduced here. The configurations shown in Fig. 2.17 can help in this aspect. In the ALE formulation a third configuration, in addition to the material and spatial
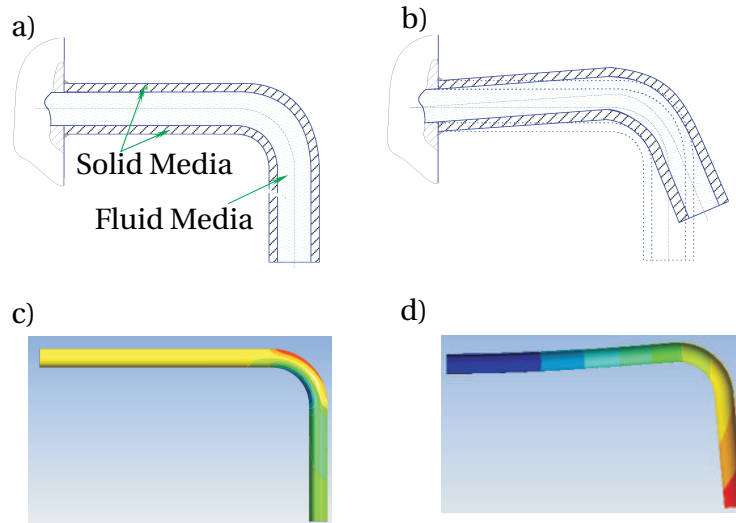
Figure 2.16 An Illustration for the need of ALE Formulation: a) Undeformed Body, b) Deformed Body (Fluid and Solid assume new position), c) Fluid Configuration unaffected after Simulation using Eulerian Formulation, d) Deformed Solid after Simulation using Lagrangian Formulation. (after [95])

configurations, which represents the mesh motion is needed. This third configuration is called reference configuration.

The mesh motion is independent of material motion and there will be a relative motion between the two [95]

$$\mathbf{v}_{rel} = \mathbf{v} - \mathbf{v}_{mesh}, \tag{2.63}$$

where $\mathbf{v}_{rel}$ and $\mathbf{v}_{msh}$ are relative and mesh velocities, respectively. Then the conservation equations which are usually given in Eulerian formulation are modified by introducing the relative velocity in (2.63) to get their corresponding ALE form. The Eulerian equations (2.64) and the corresponding ALE equations (2.65) are given below for comparison.

$$\left.\begin{array}{l} \text{Mass Balance:} \\ \dfrac{\partial \rho}{\partial t}\Big|_x + \mathbf{v}\cdot\nabla\rho + \rho\nabla\cdot\mathbf{v} = 0 \\ \text{Momentum Balance:} \\ \rho\left(\dfrac{\partial \mathbf{v}}{\partial t}\Big|_x + (\mathbf{v}\cdot\nabla)\mathbf{v}\right) - \nabla\cdot\sigma - \rho\mathbf{b} = 0 \\ \text{Energy Balance:} \\ \rho\left(\dfrac{\partial E}{\partial t}\Big|_x + \mathbf{v}\cdot\nabla E\right) - \nabla\cdot(\boldsymbol{\sigma}\cdot\mathbf{v}) - \mathbf{v}\cdot\rho\mathbf{b} = 0 \end{array}\right\} Euler \tag{2.64}$$
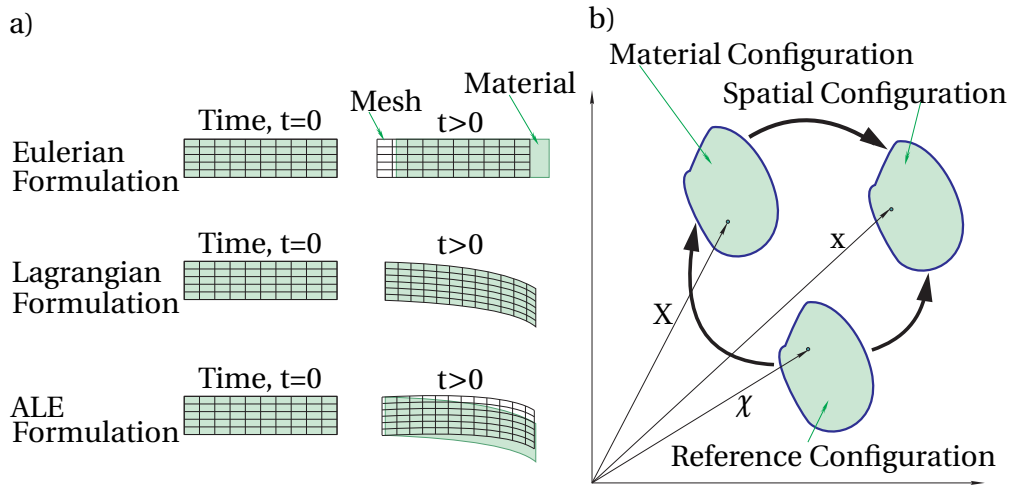
Figure 2.17 ALE Formulation Principle: a) Comparison of ALE formulation with others, b) Mapping among Material, Spatial and Reference Configurations in ALE Formulation. (after [95, 63])

$$\left.\begin{array}{l} \text{Mass balance:} \\ \dfrac{\partial \rho}{\partial t}|_\chi + \mathbf{v}_{rel} \cdot \nabla \rho + \rho \nabla \cdot \mathbf{v} = 0 \\ \text{Momentum Balance:} \\ \rho \left(\dfrac{\partial \mathbf{v}}{\partial t}|_\chi + (\mathbf{v}_{rel} \cdot \nabla)\mathbf{v} \right) - \nabla \cdot \boldsymbol{\sigma} - \rho \mathbf{b} = 0 \\ \text{Energy balance:} \\ \rho \left(\dfrac{\partial E}{\partial t}|_\chi + \mathbf{v}_{rel} \cdot \nabla E \right) - \nabla \cdot (\boldsymbol{\sigma} \cdot \mathbf{v}) - \mathbf{v} \cdot \rho \mathbf{b} = 0 \end{array}\right\} ALE \qquad (2.65)$$

Where x and χ are spatial and mesh positions, respectively. The Eulerian and Lagrangian equations are special forms of the ALE equations (2.65). $\mathbf{v}_{rel} = \mathbf{v}$ corresponds to Eulerian equations where as $\mathbf{v}_{rel} = 0$ corresponds to Lagrangian equations.

The necessity of the ALE formulation is its ability of allowing mesh motion and avoiding/minimizing mesh distortion. To bring about these effects, ALE computational formulation consists of two important steps: Mesh adaption and mesh regularization. This nature makes ALE formulation to be further applicable in handling problems with moving boundaries like free fluid surfaces [95].

The drawback of the ALE formulation is the need for more mathematical efforts both in problem formulation and computation, and this makes the formulation to be open for intensive research work towards its further simplification and accuracy.

This chapter has dealt with the fundamentals of mechanics applicable in thermal energy conversion. In the solution processes of thermal energy conversion processes where fluids are involved, there are three challenges pointed in this chapter:

1. the turbulent nature of fluids,

2. the inelastic behavior of solids, and

3. the computational challenges in handling fluid-structure interaction problems and modeling the inelastic behavior of solids.

The second challenge (modeling the inelastic behavior of solids) is the concern of this thesis and will be considered in more detail in the next chapter. Specifically, the next chapter deals with the modeling of creep (due to both constant and cyclic loading), which is most commonly observed in power plant components.

3 Modeling Inelastic Behavior of Materials

In Chapter one, it has been explained that the power plant components experience loads that are mainly exerted on their surfaces by the flow of fluids. These loads, which are commonly in the range of 100 to 200MPa, are quite low as compared to the yield strength of the components' materials and may not result in immediate failure of the components. Fig. 3.1 shows the dependence of strength of T91 steel (one of the Advanced steels used for power plant
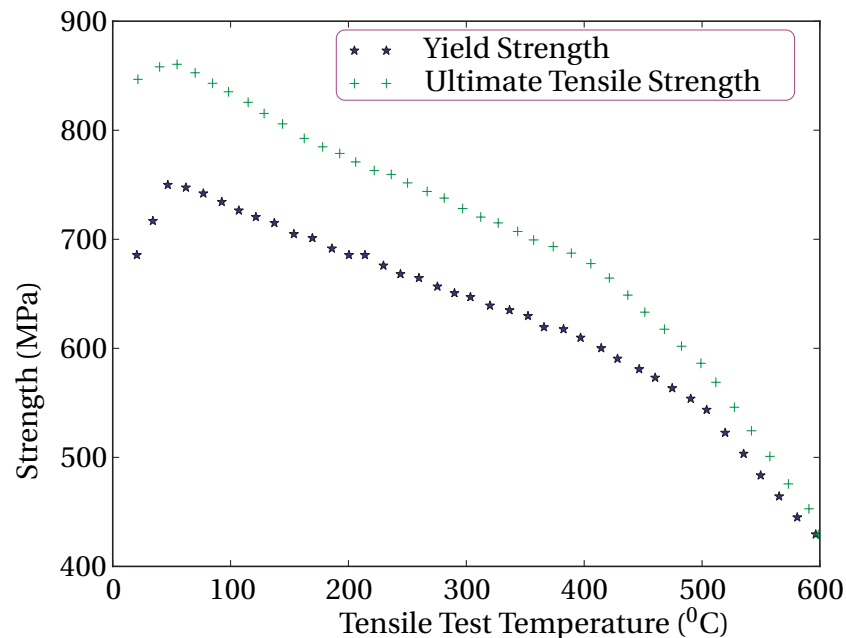

Figure 3.1 Strength of T91 Steel (after [70])

components construction) on temperature. The stresses developed in the components due to the loads from fluid flow are quite less than the strengths of the components. But what is special with these loads is that they

- act for a long period of time,

- are fluctuating in nature, and

- are accompanied by high temperature conditions.

This nature of the loads forces the components to exhibit time dependent inelastic behavior like creep and fatigue.

In this chapter, this inelastic behavior will be modeled based on the idea of mixture (fraction) modeling given in [81]. But to have a background on which the modeling will be founded, the phenomenology of the inelastic behavior (creep and fatigue) will be briefly discussed in the next section.

3.1 Creep and Fatigue Phenomenology

The time dependence of loads acting on power plant components is a reason for evolution of inelastic behavior of materials of these components. Due to nature of thermal energy conversion processes, mainly to attain high thermal efficiency, loads are accompanied by high temperature operation conditions. The inelastic behavior of a material exhibited as a result of constant load and high temperature is called creep while that results from fluctuating loads acting for a long period of time is called fatigue. These two phenomena simultaneously occur in thermal power plants and result in creep-fatigue interaction. In this section, brief explanation about the two phenomena will be made.

3.1.1 Creep

Creep is slow and permanent deformation of structures under the influence of stress. It is more dominant in relatively high temperature operations, $T > 0.3 T_m$, where T_m is the melting point temperature of the material [80]. Creep curves of many materials have three regions as shown in Fig. 3.2. The primary creep region shows hardening of the material as time progresses. Eventually, the material starts to soften and the softening and hardening balance each other in the secondary region . This region is almost a straight line compared to other regions. In the third region, softening highly dominates and near the

$$\varepsilon = \varepsilon^{el} + \varepsilon^{cr}$$
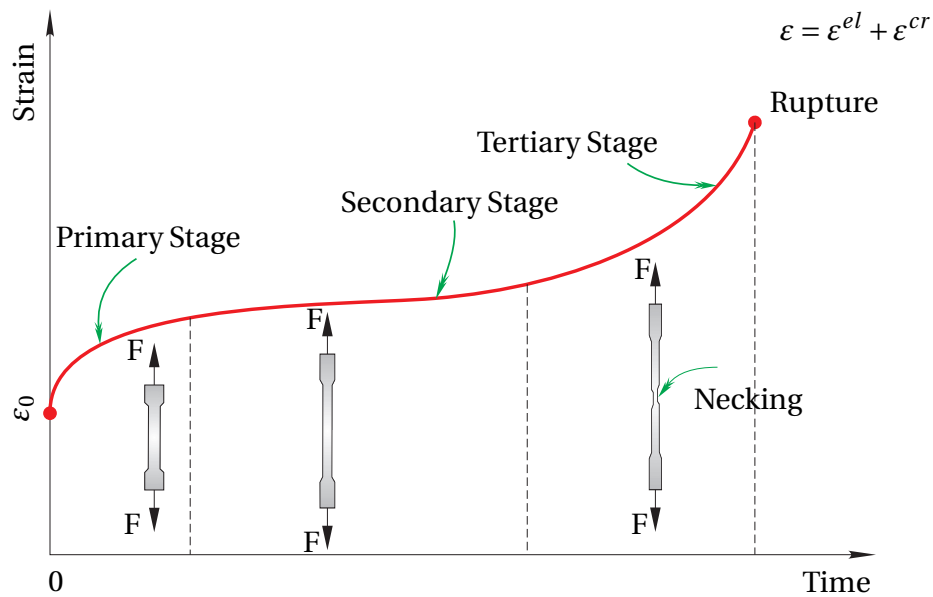
Figure 3.2   Typical Creep Curve from Uni-Axial Test (after [80, 21, 54, 82])
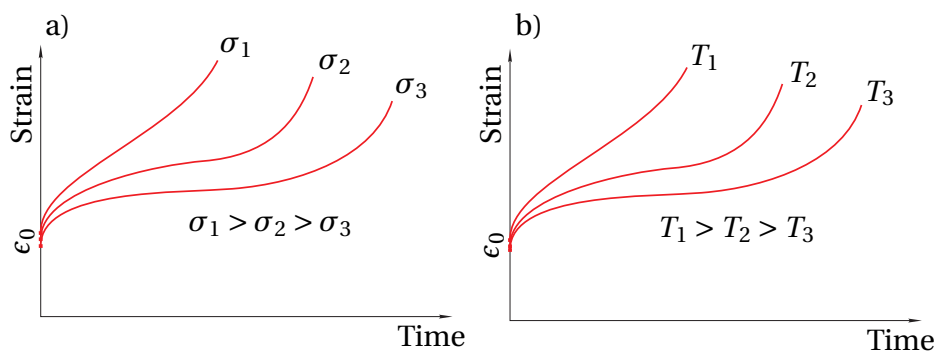
Figure 3.3   Effect of Stress and Temperature on Creep Curves: a) Effect of Stress, b) Effect of Temperature. (after [80])

end of the region damage propagation will result in failure of the component. Stress and temperature have effects of increasing creep strain rate. As stress and/or temperature increase, the creep strain increases faster as shown in Fig. 3.3. Failure due to creep does not necessarily mean physical rupture of a component. Fig. 3.4 shows typical areas of failure of components due to creep [44, 80, 13].

- In turbomachines like steam or gas turbines, the turbine blades can excessively elongate and may result in blocking of the fluid flow or
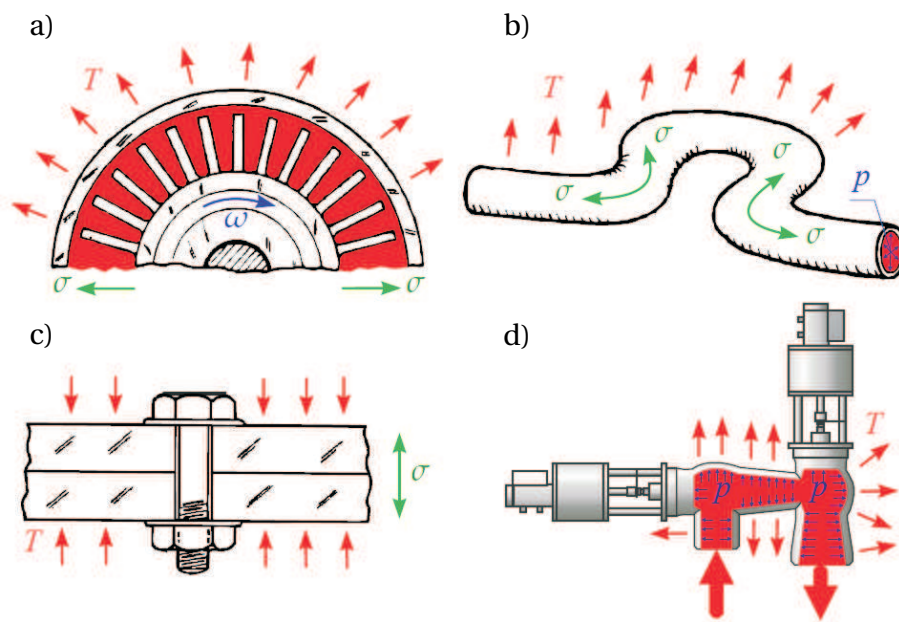
Figure 3.4 Failure Areas where Creep has to be Considered: a) Excess displacement, b) Buckling through time, c) Relaxation of tight containers, d) Continuous fracture. (after [44])

the blades may come in contact with the stators and may result in catastrophic failure. Fig. 3.4 a).

- In tubes containing hot fluids, buckling may occur which may result in malfunctioning of the component. Fig. 3.4 b).

- In bolted connections like in the case of pressure vessels, creeping of the bolts may result in leakage of the gas in the vessel. Fig. 3.4 c).

- In highly pressurized components, creep may result in to a sudden fracture. Fig. 3.4 d).

3.1.2 Creep from Microstructure Point of View

The inelastic behavior observed at macroscopic level is attributed to phenomena that take place at microstructure level. Few deformation mechanisms related to this will be discussed here. A material shows different creep deformation mechanisms depending on stress and temperature. Main mechanisms include:

- diffusion creep controlled by:
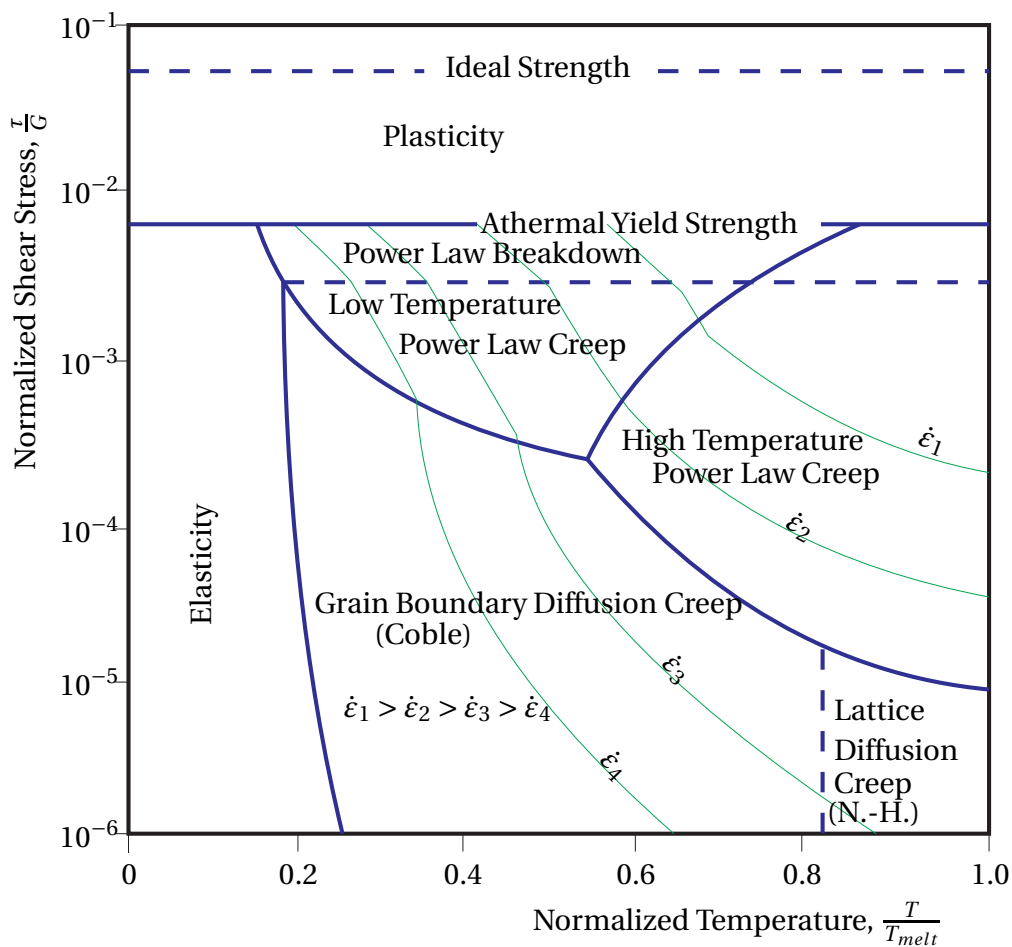
Figure 3.5 Deformation Mechanism map (after [13])

- – volume (lattice) diffusion (Nabarro-Herring creep) or

- – grain boundary diffusion (Coble creep),

- dislocation[1] creep controlled by

   - – high temperature power law creep, or

   - – low temperature power law creep [76].

These mechanisms are usually represented by deformation mechanism maps [3] as shown in Fig. 3.5 to have an information about which mode is dominant under a given creep condition.

Few points worth mentioning regarding the deformation mechanism map:

---

[1]Dislocation is a line defect in a material.

- Nabarro-Herring creep and high temperatures power law creep operate at higher temperatures owing to their higher activation energy for creep.

- Creep rates of both dislocation creep mechanisms are independent of grain size, but those of the diffusion creep mechanisms increase with decreasing grain size.

- In engineering steels, dislocation creep is the most relevant deformation mechanism.

- Below the athermal yield strength[2], the material first deforms elastically and then creep follows while above athermal yield strength rate-independent plasticity first occurs and creep (viscoplasticity) follows.

3.1.3 Fatigue

The loads applied on power plant components are not always of constant magnitude. The reasons for the variability of the loads can be due to start-up and shut-down conditions, fluid flow turbulence, cavitation etc. When variable loading process are takes place for long time, a different kind of failure which may result in catastrophic fracture may result even if the amplitude of the load is small. The response (degradation of strength) of materials to variable loading is called fatigue. Like in the case of creep, fatigue can occur at loads of magnitude much less than the strength of the material. In moving components it is estimated that about 90% of failures are attributed to fatigue [77]. In the case of power plants where there are few moving components, fatigue has still a significant effect.

Fatigue has the following characteristics which make its prediction a bit complicated:

- Even if there are ideally no initial discontinuities in the material, fatigue can result in dislocation movements which eventually result in nucleation of cracks.

- Stress concentration areas are the preferred locations for starting the fatigue process [84].

- Measured data of fatigue experiments show considerable scatter even in controlled environments.

---

[2]Athermal yield strength is temperature and strain rate independent yield strength of a material.
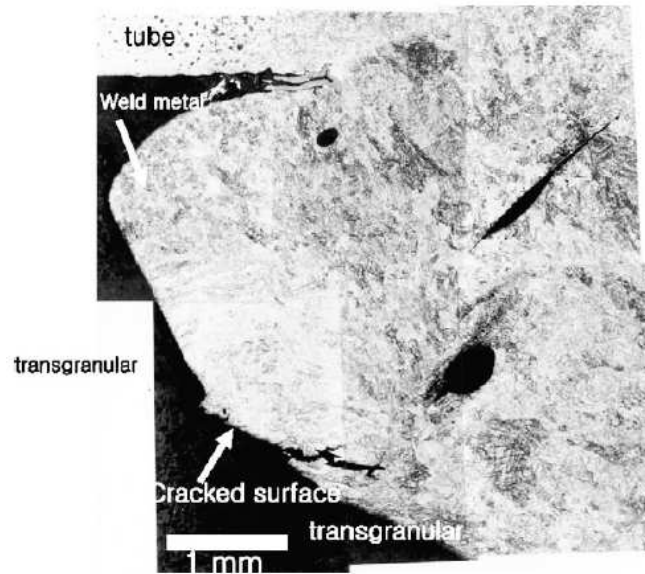
Figure 3.6 An Example of Failure where Fatigue was Predominant (Source: [56])

- Critical locations in a component face the possible maximum and minimum loads in an alternating manner. The possible combinations of these maximum/minimum loads can be tensile/tensile, tensile/compressive or compressive/compressive. These locations are susceptible for crack initiation in the component.

- High cycle (about 10^3 to 10^8 cycles) fatigue and low cycle (typically less than 10^3 cycles) fatigue need to be treated differently. The high cycle fatigue strength can be described by stress-based parameters while a strain-based parameter should be used for low cycle fatigue life prediction in metals and alloys.

Fatigue failure can also occur with other failure modes like corrosion. There are plenty of documents and research papers which are evident for this statement, example is shown in Fig. 3.6.

3.2 Modeling Procedure

Since the early observations of the inelastic behavior of materials, there are a number of works done to mathematically model this behavior. Few of the works include the first investigation by Andrade (1910), Norton's potential law
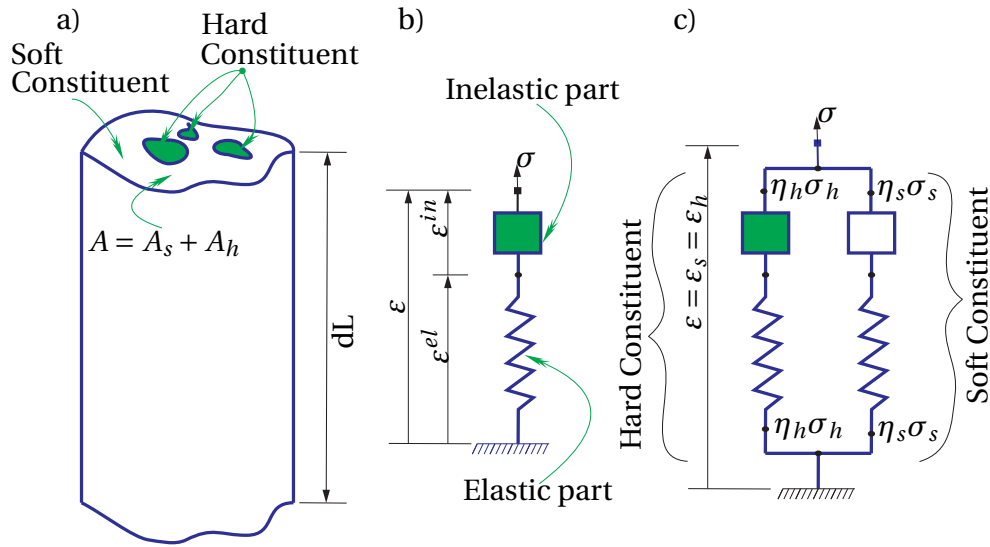
Figure 3.7 Material Hard and Soft Constituent Assumption Model: a) Conceptual Physical Model for Uni-Directional Test, b) Maxwell-Type Elastic-Inelastic Soft Constituent Model, c) Iso-Strain Connection of Creep-Soft and Creep-Hard Constituents.

(1929), practical usage in Gas Turbines by Stodola (1933) and in Polymers by Rabotnov (1948), etc. More recent works include investigation of anisotropy, stress effects by Altenbach et al. (1996) and creep damage analysis by Naumenko (1996), Altenbach et al. (1997).

The mixture constitutive model in [81, 20] will be used in this thesis. The starting point of the mixture modeling is the assumption that a material consists of hard and soft constituents. The volumes of these constituents are not constant but evolve with stress and strain. Figure 3.7 depicts this idea. The following are the main key elements of the modeling assumption [81].

- The deformation of the constituents is iso-strain type. That is both the soft and hard constituents will have the same strain. In rheological modeling approach, they can be connected in parallel as shown in Fig. 3.7 c).

- Both constituents show elastic and inelastic behavior as in Fig. 3.7 b). The elastic properties of the two constituents are assumed to be similar.

- There is non-uniform distribution of forces and, hence, non-uniform distribution of stresses in the two constituents. That is to say we

are going to have different stresses σ_s and σ_h in the soft and hard constituents, respectively.

- As deformation progresses, the volume fraction of the hard constituent is assumed to decrease to a certain saturation value due to the physical phenomena that take place in the material.

The total stress acting in the material can be written in terms of stresses developed in the constituents as in (3.1)

$$F = F_s + F_h \Rightarrow \sigma A = \sigma_s A_s + \sigma_h A_h \Rightarrow \sigma = \sigma_s \frac{A_s}{A} + \sigma_h \frac{A_h}{A}$$
$$\Rightarrow \sigma = \sigma_s (1 - \eta_h) + \sigma_h \eta_h \tag{3.1}$$

where F is the total force on some infinitesimal area, F_s and F_h are forces on areas (A_s and A_h) of soft and hard constituents, respectively, σ is total stress, σ_s and σ_h are stresses developed in soft and hard constituents, respectively, η_s and η_h are the volume fractions of the soft and hard constituents, respectively.

The variations of the strains in the constituents for uni-axial stress state are assumed to be governed by (3.2) as given in [81]

$$\dot{\varepsilon}_s = \frac{\dot{\sigma}}{9K} + \frac{\dot{\sigma}_s}{3G} + f(|\sigma_s|) \frac{\sigma_s}{|\sigma_s|}, \dot{\varepsilon}_h = \frac{\dot{\sigma}}{9K} + \frac{\dot{\sigma}_h}{3G} + \frac{\sigma_h - \sigma}{\sigma_{h_*} - \sigma} |\dot{\varepsilon}^c| \tag{3.2}$$

K and G are the bulk and shear modulus of the material, respectively, $\dot{\varepsilon}^c$ is the average creep rate of the mixture and σ_{h_*} is the saturation value of the stress in the hard-constituent.

To incorporate the physical phenomena in the development of the model, it is necessary to consider the nature of the creep curves given in Fig. 3.2. The main phenomena are hardening, softening and damage.

1. **Hardening** is the characteristic of the primary stage. It mainly arises due to an increase in dislocation density and formation of dislocation substructure. High Chromium steels contain high initial dislocation density introduced during martensitic transformation [3].

2. At high temperatures, dislocations can climb and annihilate themselves with other dislocations. This results in **softening** in the material. During steady state creep, there is a dynamic balance between multiplication and annihilation of dislocation. But in the tertiary stage annihilation of dislocation and hence, softening becomes more dominant.
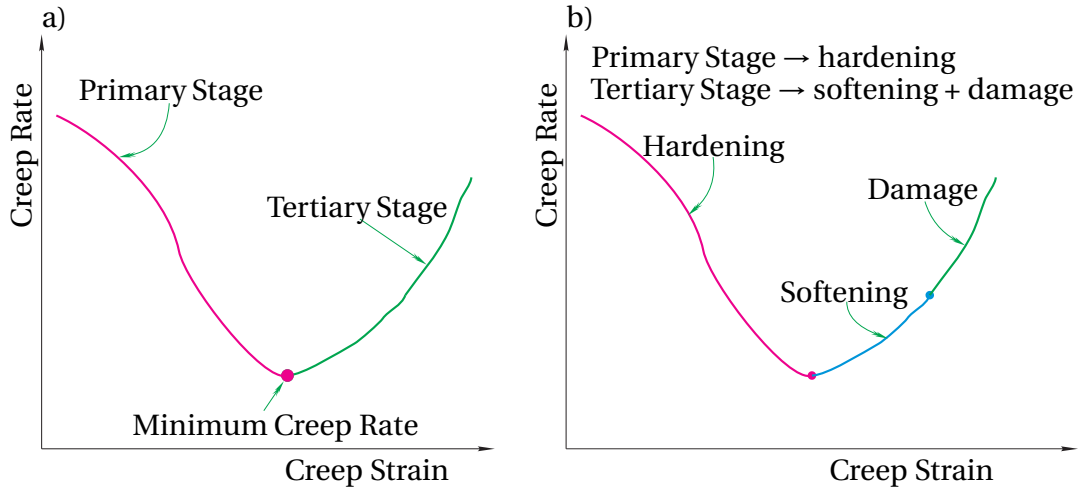
Figure 3.8 Nature of Creep Curves of 9-12% Cr Steels: a) Creep Stages, b) Corresponding Physical Processes-Evolution. (Based on idea from [81])

3. **Damage** is the creation of discontinuity in a material. Damage and softening aid each other at the end of the tertiary stage and bring about a fast increase in creep strain.

For materials that exhibit long secondary creep stages, hardening and softening balance each other during this stage.

The creep curves of 9-12% Cr steels, which are the main focus of this thesis, consist of only the primary and tertiary stages. The secondary stage is a single point usually identified by the minimum creep rate as shown in Fig. 3.8 a). The total strain is split into elastic and inelastic parts in the usual way as

$$\dot{\varepsilon} = \frac{\dot{\sigma}}{E} + \dot{\varepsilon}^c \tag{3.3}$$

Combining (3.1) through (3.3) and incorporating the three evolution variables representing the physical phenomena (hardening, softening and damage), the general constitutive equation that governs the inelastic behavior of the material can be given by (3.4)

$$\dot{\varepsilon}^c = f\left(\frac{|\sigma - \beta\Gamma|}{1 - \omega}\right)\frac{\sigma - \beta\Gamma}{|\sigma - \beta\Gamma|}, \tag{3.4}$$

where f is a function, β, Γ and ω are the evolution variables that govern the hardening, softening and damage processes, respectively, of the material.

The expected variations of the evolution parameters with strain are given in Fig. 3.9. The hardening variable β, also known as back stress, is zero at
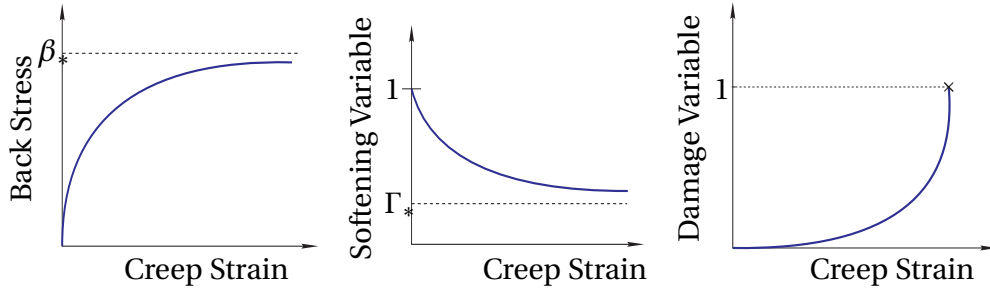
Figure 3.9   Expected Variation of Evolution Variables

zero strain and monotonically increases to some saturation value β_*. β_* is dependent on some reference value of the volume fraction η_{h_0} of the hard-constituent, the saturation stress in the hard constituent σ_{h_*} and the total stress σ, as given in (3.5)

$$\beta_* = \frac{\eta_{h_0}}{1 - \eta_{h_0}}(\sigma_{h_*} - \sigma) \tag{3.5}$$

The softening variable Γ which acts on the hardening variable is assumed to decrease, starting from unity, to some saturation value Γ_* which is, in turn, dependent on the volume fraction properties of the hard constituent as in (3.6).

$$\Gamma_* = \frac{\eta_{h_*}}{1 - \eta_{h_*}}\frac{1 - \eta_{h_0}}{\eta_{h_0}}, \tag{3.6}$$

where η_{h_*} is the saturation volume fraction of the hard-constituent.

The damage variable, which is not part of the mixture model assumption, is assumed to increase monotonically from zero (undamaged material) to a value of unity at a point where the material ruptures [5]. This assumption holds true only for tensile loading case. Compressive loading is assumed to be damage free [81]. The physical definition of the damage variable is related to discontinuities like voids and cracks developed in the material. It is the surface density of micro-cracks and intersection of micro-voids lying on a plane cutting the representative volume element (a volume in which all properties are represented by homogeneous variable, from continuum mechanics point of view) of cross-sectional area dA shown in Fig. 3.10, as given in (3.7). Detailed physical based derivation of the damage variable can be obtained from [66] and the interpretation of damage equations from [58]

$$\omega = \frac{dA_w}{dA} \tag{3.7}$$

Based on the assumptions of the variations of the evolution variables with strain given in Fig. 3.9, equations of the variables can be given below:
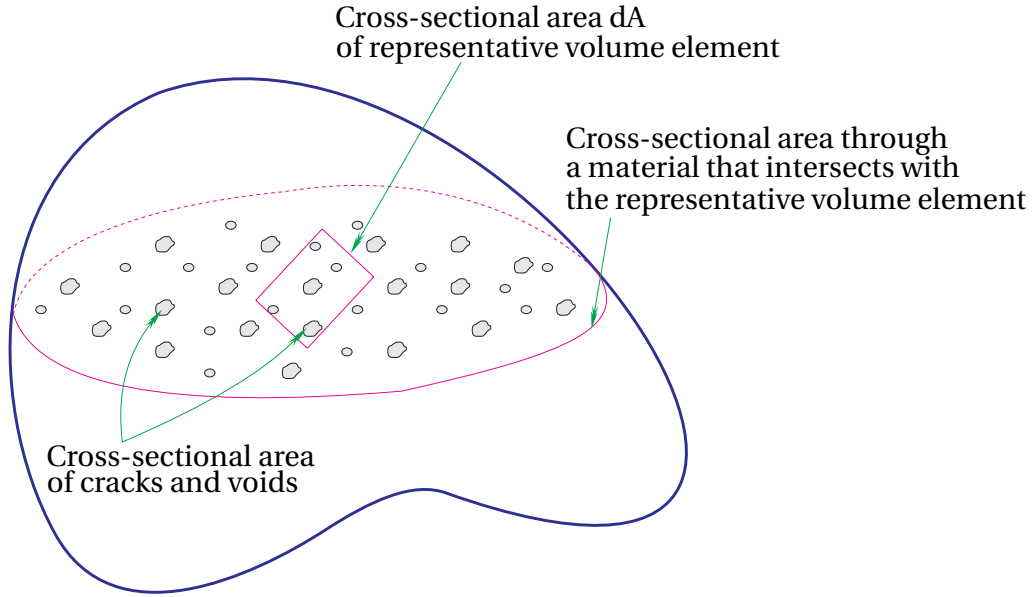
Figure 3.10 Damage Modeling Concept, (after [66, 109])

1. Evolution equation of Hardening Variable:

$$\dot{\beta} = \frac{3G}{c_h}(\dot{\varepsilon}^{cr} - |\dot{\varepsilon}^{cr}|\frac{\beta}{\beta_*}), \tag{3.8}$$

   where c_h is material parameter dependent on reference value of the volume fraction of the hard constituent.

2. Evolution equation of Softening Variable:

$$\dot{\Gamma} = A_s(\Gamma_* - \Gamma)|\dot{\varepsilon}^{cr}|, \tag{3.9}$$

   where A_s is a constant material parameter.

3. Evolution equation of Damage Variable:

$$\dot{\omega} = \left(\frac{\sigma + |\sigma|}{2\sigma}\right)\frac{m\omega^{\frac{m-1}{m}}}{\varepsilon_*}|\dot{\varepsilon}^{cr}|, \tag{3.10}$$

   where m and ε_* are material parameters. m is a constant while ε_* is stress dependent.

3.2.1   Creep Modeling

The modeling procedure begins with finding an appropriate function f to be used in (3.4). A function which is most suitable for modeling the variation of
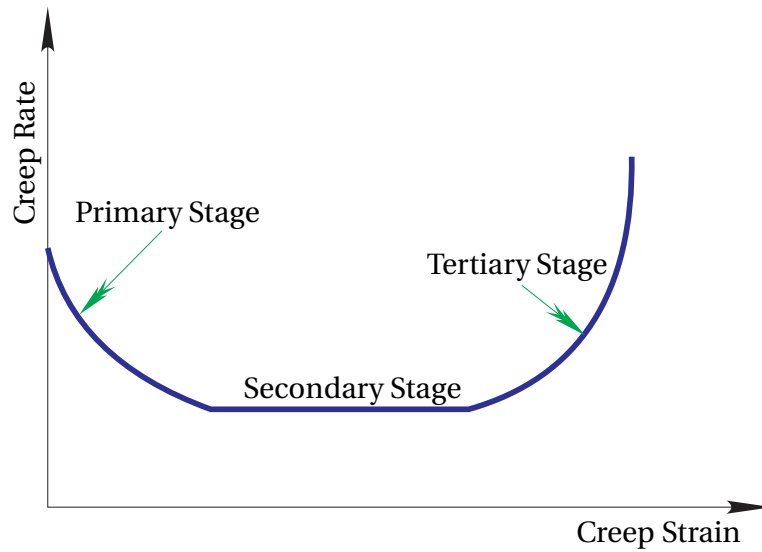
Figure 3.11 Creep Strain Independence of the Steady State Creep Rate

the minimum creep rate (steady state creep rate) with stress can be utilized. The steady state creep rate is dependent only on temperature and stress while the creep rate depends additionally on creep strain and other evolution variables as shown in Fig. 3.11. The Generalized Garofalo model has been found to fit better for T91 steel experimental data of minimum creep rate vs stress as shown in Fig. 3.12. The model is of the form given in (3.11).

$$\dot{\varepsilon}_{min}^{cr} = f(T, \sigma) = A(T)\sinh(B\sigma)^n, \tag{3.11}$$

$$A(T) = A_0 \exp\left(\frac{-\gamma}{T}\right), \tag{3.12}$$

where A_0, γ, B and n are material parameters to be determined here from curve fitting of the data. T is absolute temperature. The normalized minimum creep rate fit is shown in Fig. 3.13. In this figure, the experimental data coincide with a single line proving the possibility of writing the creep rate as separate functions of temperature and stress which has a great role in simplifying the creep rate equations [62].

As there are many material parameters in the evolution equations it is sometimes difficult to determine at a time all parameters that best fit the model. The following steps were found to be effective in this work in minimizing this difficulty.

- Starting fitting with only hardening part. The creep rate equation will

Figure 3.12 Varation of Minimum Creep Rate with Stress-Generalized Garofalo (Data source: [27, 59, 48, 97, 42])

Figure 3.13 Normalized Minimum Creep Rate

have the form

$$\dot{\varepsilon}^c = f\left(T, |\sigma - \beta|\right) \frac{\sigma - \beta}{|\sigma - \beta|}, \tag{3.13}$$

and the parameters of hardening evolution variable, c_h and β_* in (3.8) are determined here.

- Including the softening part with the creep rate equation now having the form,

$$\dot{\varepsilon}^c = f\left(T, |\sigma - \beta\Gamma|\right) \frac{\sigma - \beta\Gamma}{|\sigma - \beta\Gamma|} \tag{3.14}$$
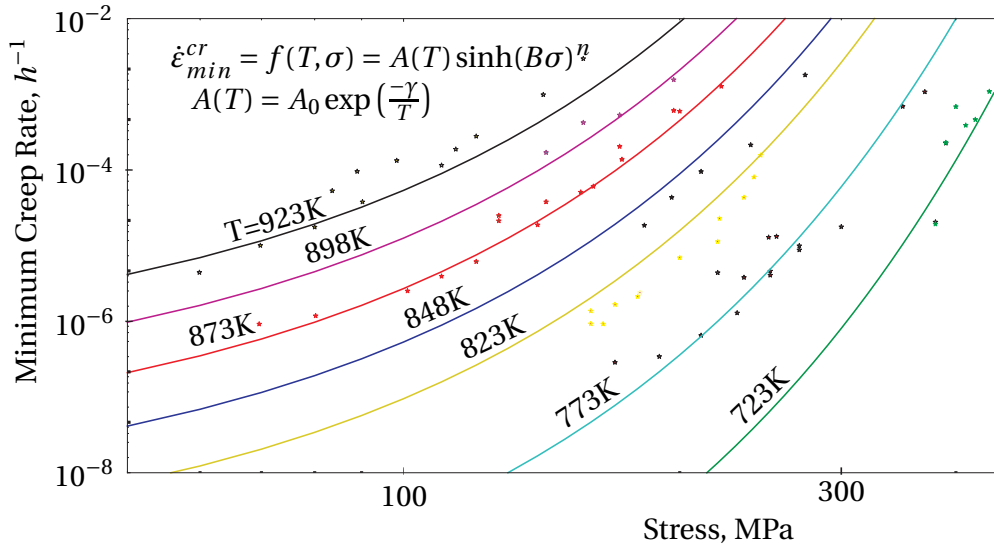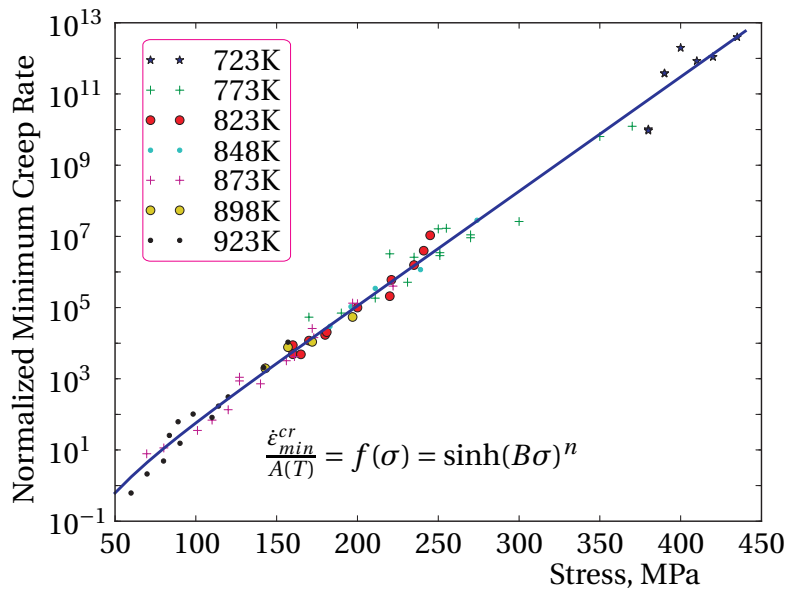
The softening parameters A_s and Γ_* in (3.9) are determined here. The hardening evolution variable parameters, c_h and β_* obtained in the previous step will be used as initial guess here and then updated.

- Finally including the damage variable in the way done in [6, 7, 4, 106], with the creep rate equation now becoming

$$\dot{\varepsilon}^c = f\left(T, \frac{|\sigma - \beta\Gamma|}{1 - \omega}\right) \frac{\sigma - \beta\Gamma}{|\sigma - \beta\Gamma|} \tag{3.15}$$

Here determining the parameters m and ε_* in (3.10) and updating the previously obtained softening and hardening parameters will be done.

The initial guess of the parameters has a big effect on the final values of the parameters, for obtaining fast and realistic solution. The results obtained should be examined for parameters which have a physical meaning. Parameters which are supposed to represent some physical phenomena may be expected to be non-negative or to lie in some range, but the optimization can give a value which violates this. If this happens, it is better to look for another initial guess for the parameter(s). It should be kept in mind that the set of parameters that give good fit are, mostly, not unique.

The fit for hardening part is shown in Fig. 3.14 and the final model for all separate stresses incorporating all evolution equations in Fig. 3.15. The next step is to identify parameters which depend on stress and write them as functions of stress to get a single model equation that works over a wide stress range. Fig. 3.16 shows a single equation fit result and its comparison with data. Once accepted accuracy of a constitutive model has been achieved, it has to be validated with data of different tests for the same material. Figures 3.17 and 3.18 show the validation of the model against experimental data, at 600°C, of creep strain with time and creep rate with time, respectively. The very good fit observed indicates the accuracy and appropriateness of the mixture model for modeling creep.
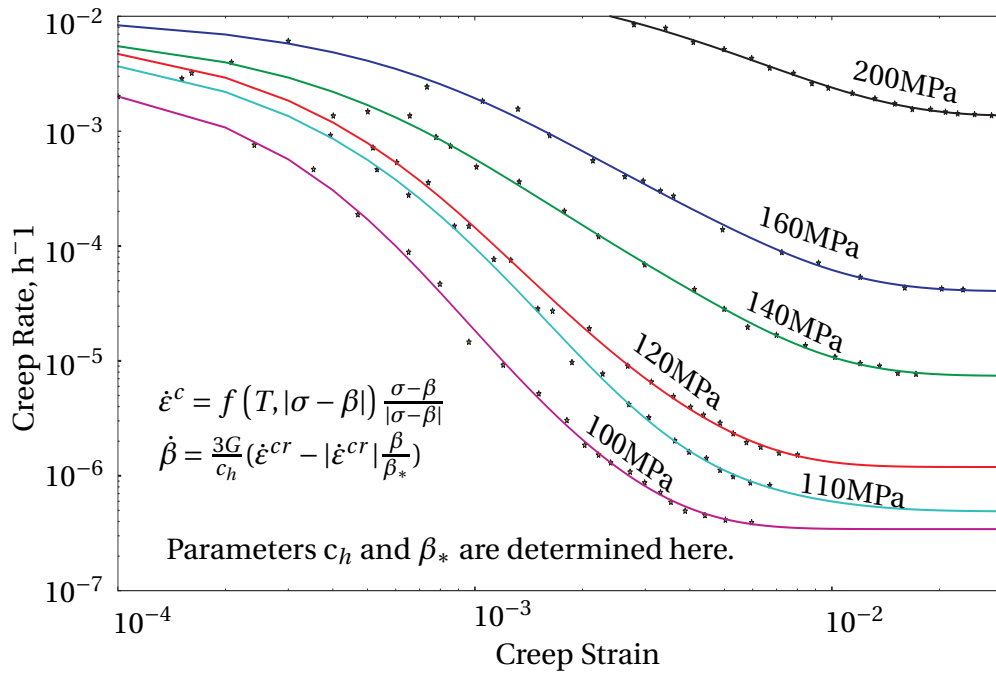
Figure 3.14 Variation of Creep Rate with Creep Strain at 600°C - Hardening (Data source: [59])

Figure 3.15 Variation of Creep Rate with Creep Strain at 600°C - Separate Equations (Data source: [59])
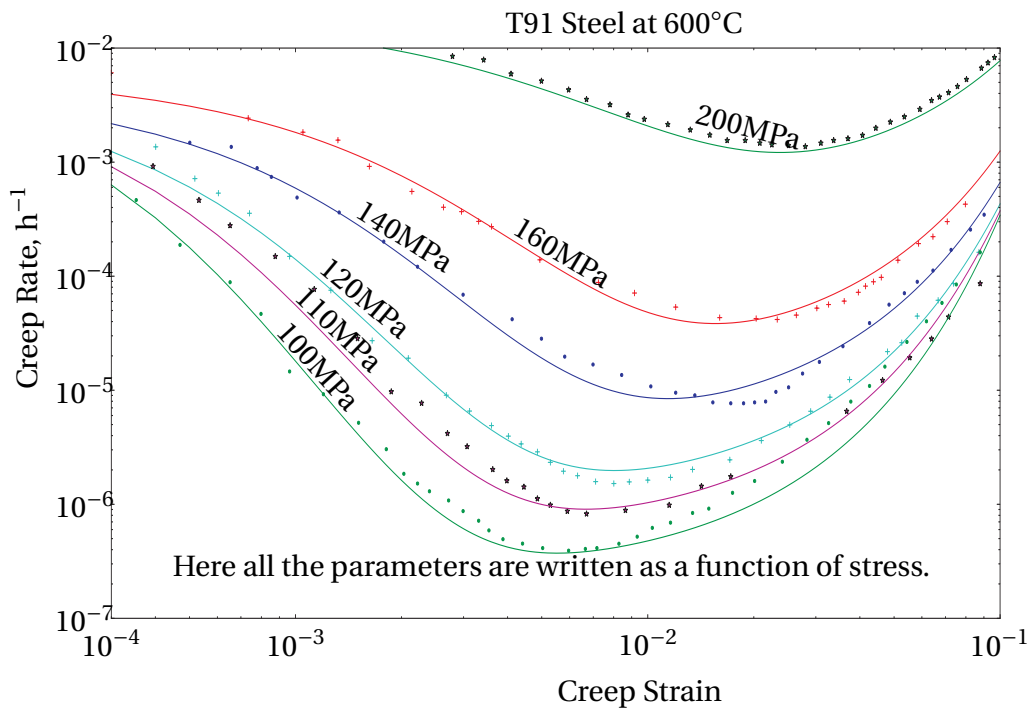
Figure 3.16 Variation of Creep Rate with Creep Strain at 600°C - Single Equation
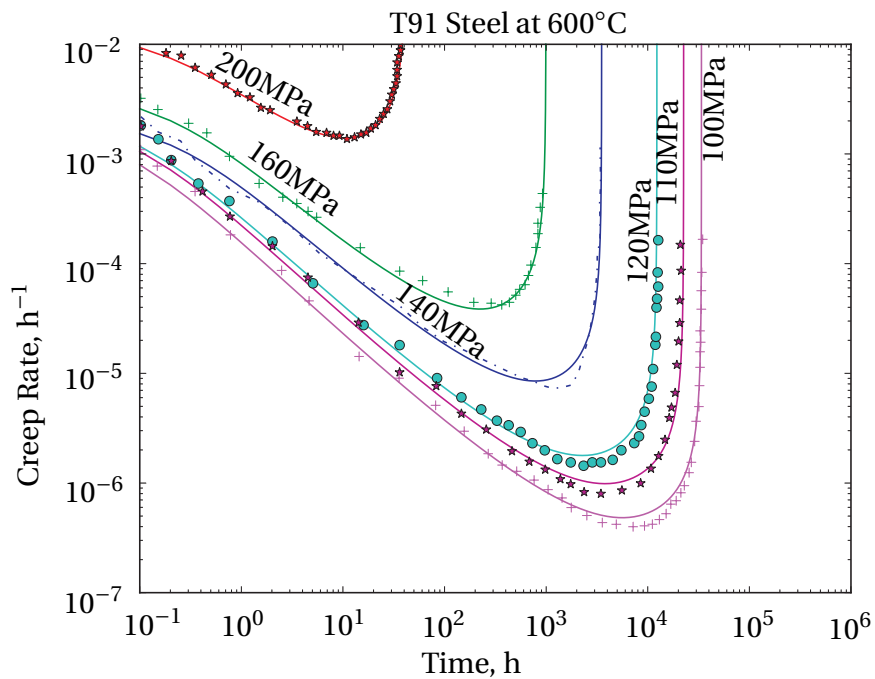
Figure 3.17 Variation of Creep Rate with Time at 600°C - Validation (Data source: [59])
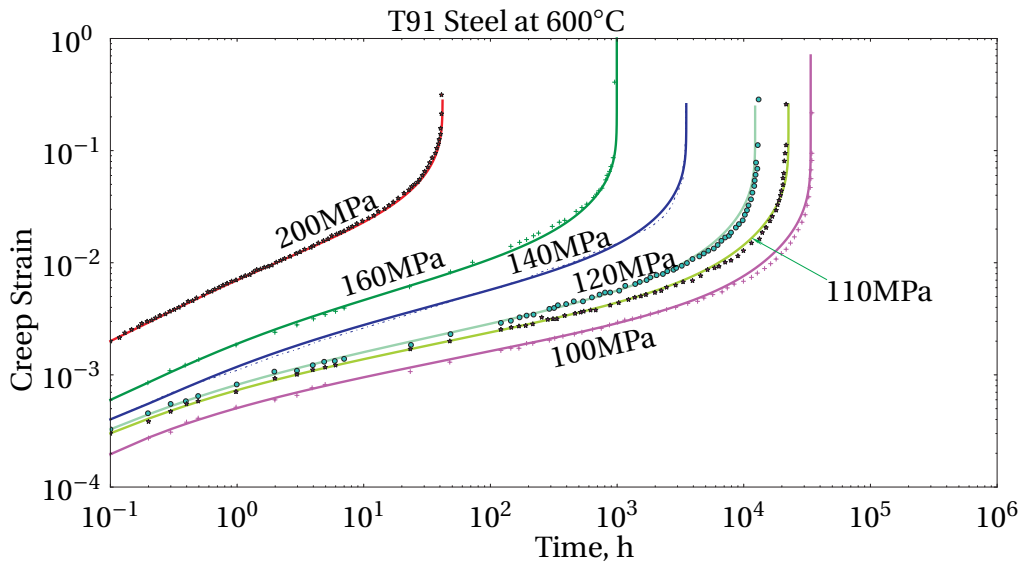
Figure 3.18   Variation of Creep Strain with Time at 600°C - Validation (Data
source: [59])

Still the material parameters obtained so far work for a single temperature
of 600°C. To get a model that works over a wide range of temperature,
the curve fitting process has to be done for data obtained at different
temperatures. Data and corresponding curve-fit at 550°C has been shown in
Fig. 3.19.

Figures 3.15 and 3.19 show that components loaded at low stresses
experience long softening and damage period. The creep rates show rapid
increase in the tertiary stage for low stress loading compared to high stress
loading case as indicated by crossing of curves. The surface plot given in
Fig. 3.20 makes clear the crossing nature of the curves. The justification for
this phenomena is that at high stresses, the tertiary creep stage is shorter
and there is no enough time for evolution of damage and other internal
variables. Consequently, the model is more accurate for high stress loading.
This indicates that more internal variables need to be included in the model
to improve its accuracy. The variation of the evolution variables with strain,
Fig. 3.21 , are in close agreement with the expected ones, Fig. 3.9. The damage
variable in Fig. 3.21 c) shows a kind of exponential growth instead of the
expected exponential rise. As it can be witnessed by the curve-fits shown, the
model has very high accuracy compared to other models so far used for the
same purpose. A comparison can be made with similar result shown in Fig.
3.22 from the work of M. Yaguchi and Y. Takahashi 1999 [105]. The result can

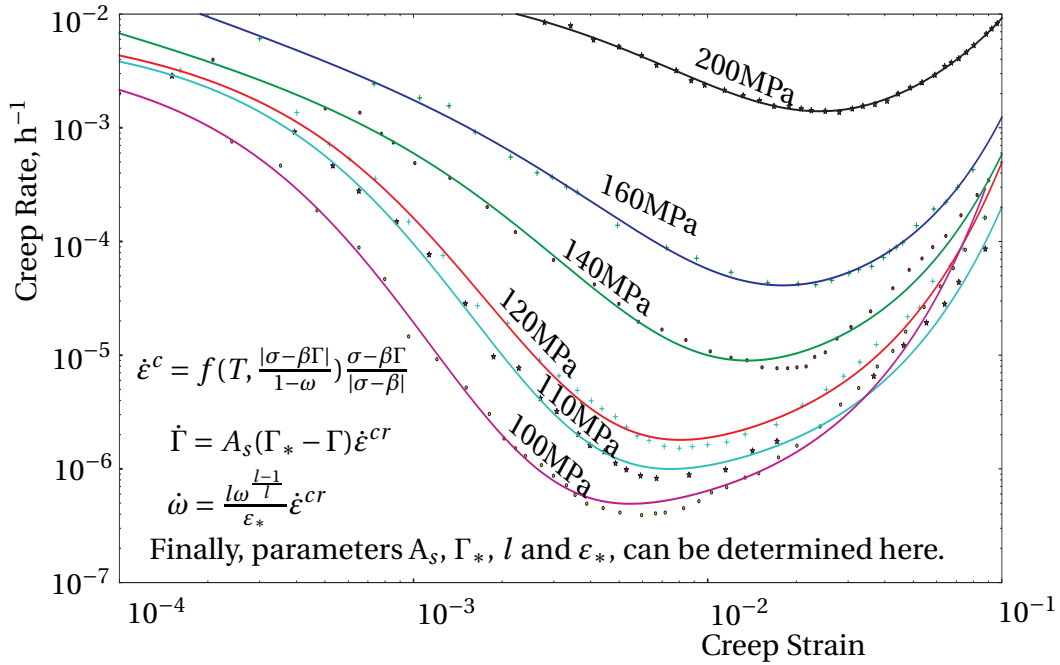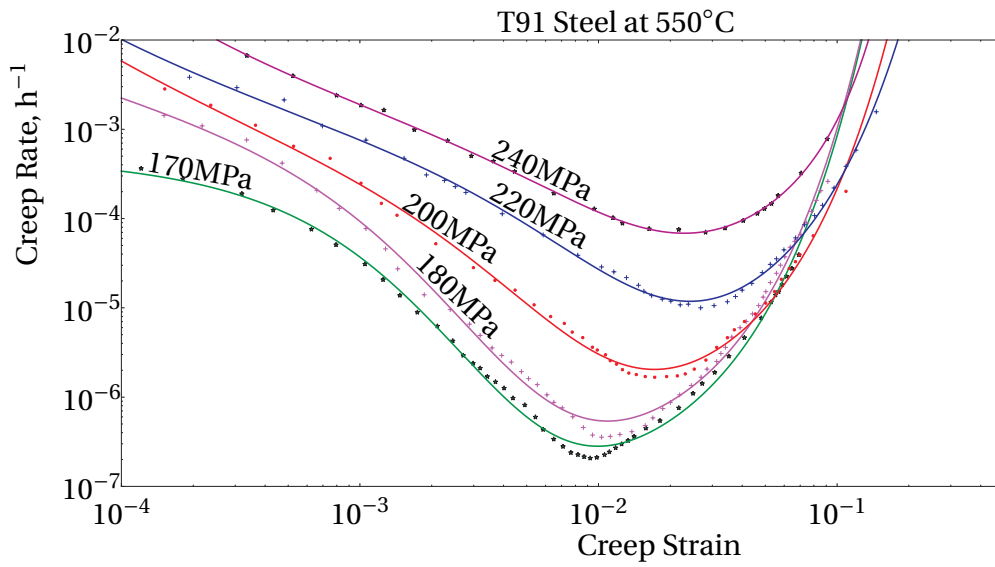**Figure 3.19** Variation of Creep Rate with Creep Strain at 550°C (Data source: [60])
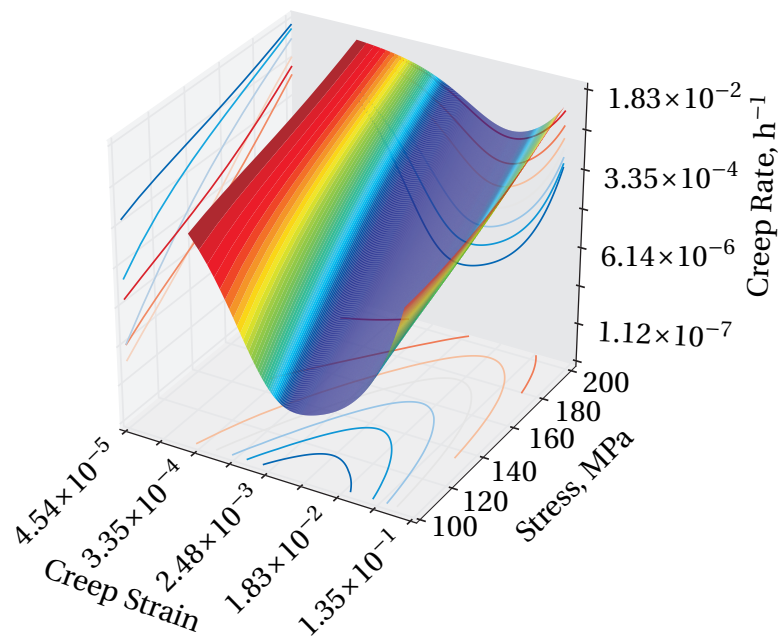
Figure 3.20 Variation of Creep Rate with Creep Strain and Stress at 600°C

a)

b)

c)
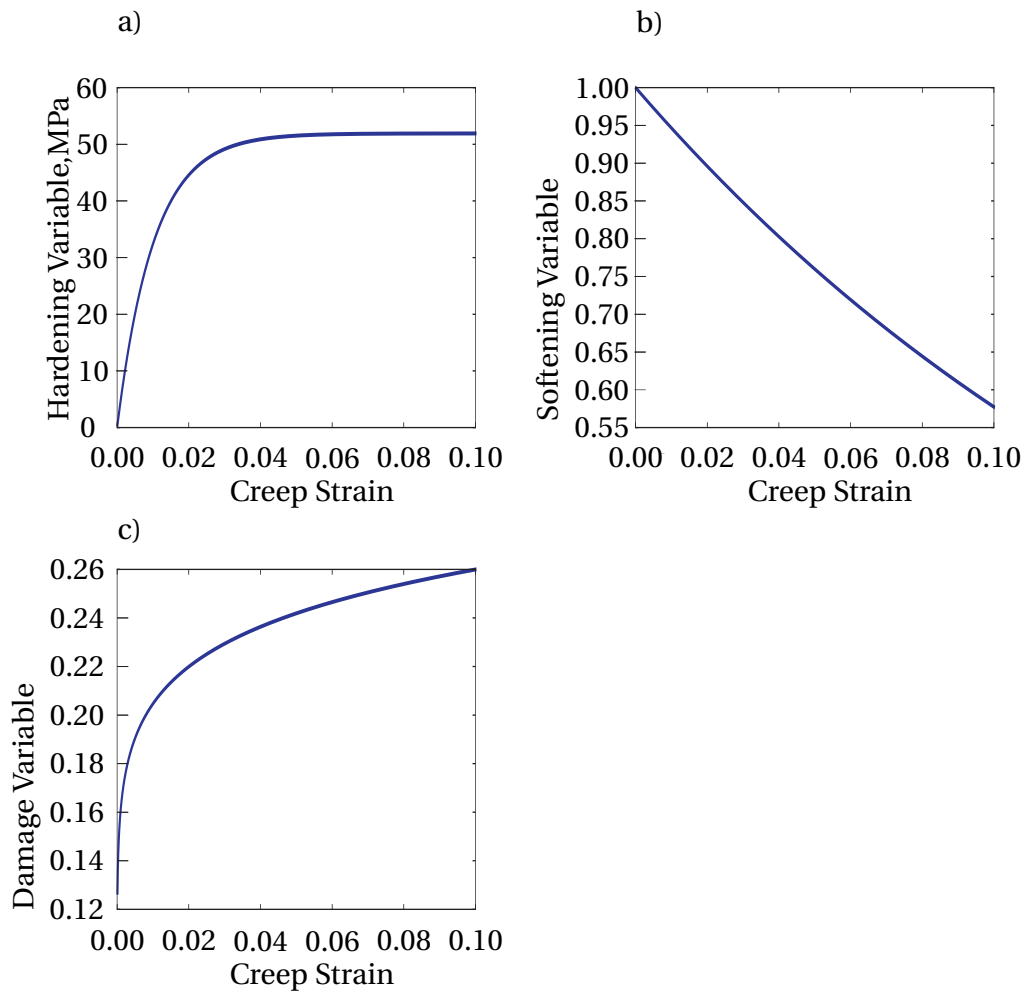
Figure 3.21   Variation of Evolution Variables with Creep Strain at 200MPa: a) Hardening Variable vs Creep Strain, b) Softening Variable vs Creep Strain, c) Damage Variable vs Creep Strain.

also be compared with works in [97]. Especially, the softening and damage phenomena are more accurately addressed by the mixture model used here.

3.2.2   Modeling Fatigue (Cyclic Loading)

The physical phenomena of hardening, softening and damage observed in constant stress induced creep are also there for cyclic loading case [64] as shown in Fig. 3.23. But the cyclic loading degrades the hardening strength of metals in a very short period of time. That is the primary (hardening) stage of cyclic creep curve is very short compared to that of creep curve obtained from constant loading.
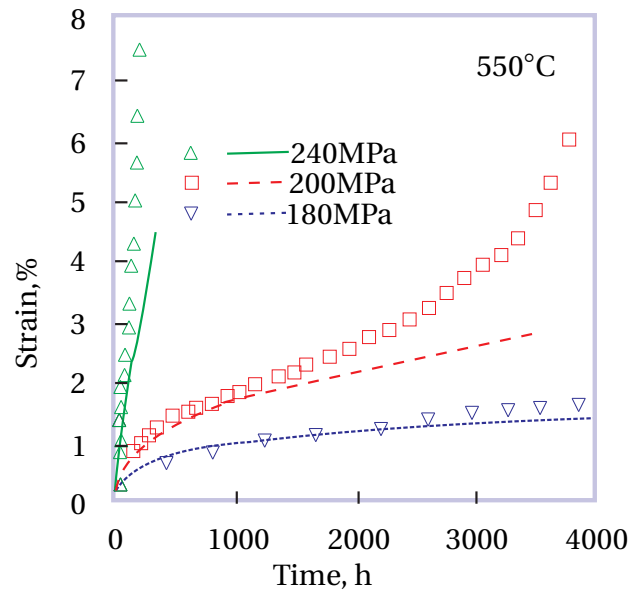
Figure 3.22   Model developed by M. Yaguchi and Y. Takahashi [105] shown
here for Comparison Purpose

There are some parameters which are important in modeling cyclic loads,
shown in Fig. 3.24. Eventhough the natural loads exerted on components do
not show clearly defined cyclic nature, it is a good practice to identify these
parameters for systematic study and experimentation.

- The stress range, $\Delta\sigma$, is the difference between the maximum and
  minimum stresses.

- The average of the maximum and minimum stresses gives us the mean
  stress, σ_m.

- Half of the stress change gives us the stress amplitude (also called
  alternating stress), σ_a.

The number of cycles N, the loading frequency f, and the total time t are
related by (3.16).

$$t = \frac{N}{f} \tag{3.16}$$

An increase in the mean stress has no effect on the nature of the cyclic creep
curve but it increases the amplitude of the plastic strain. There is no cyclic
saturation behavior for T/P91 steel, that is as the number of cycles increases
both the plastic strain amplitude and cyclic creep strain continue to increase.
The mixture assumption model used for modeling constant load creep has
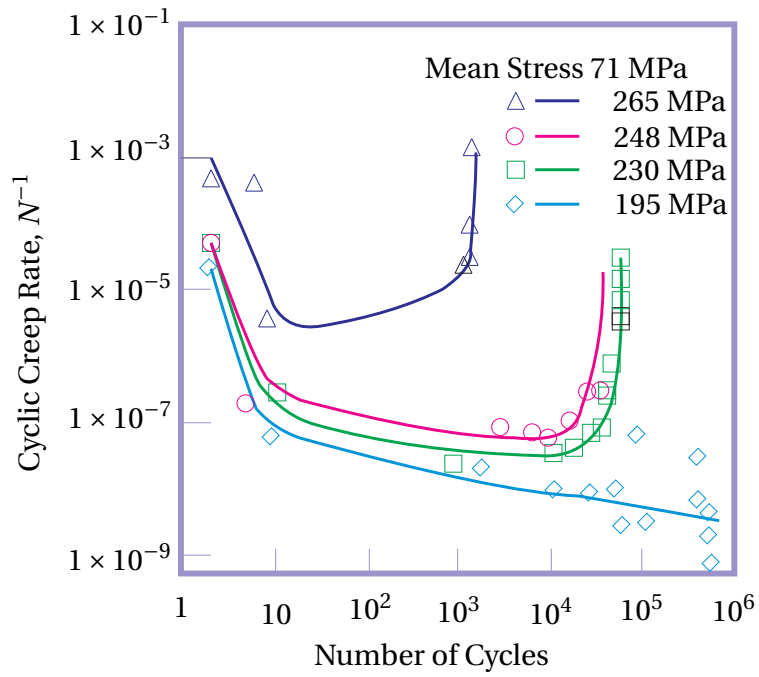
Figure 3.23 Nature of Cyclic Creep (after [64])
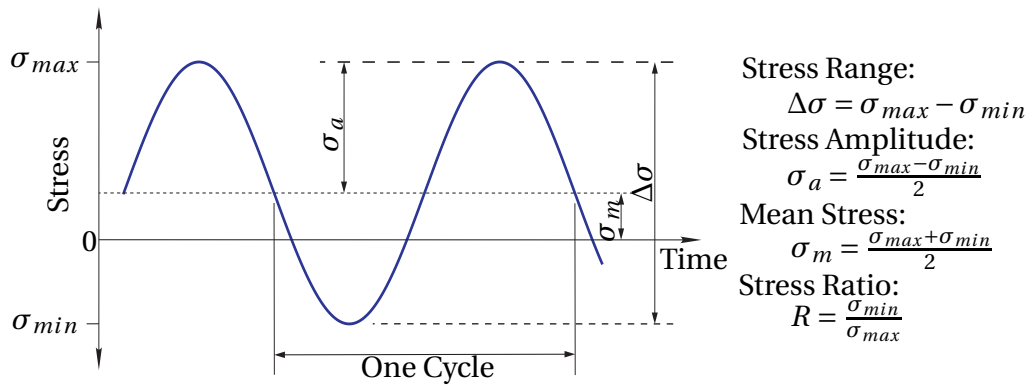
Figure 3.24 Cyclic Load Parameters (after [24])

Stress Range:
$$\Delta\sigma = \sigma_{max} - \sigma_{min}$$
Stress Amplitude:
$$\sigma_a = \frac{\sigma_{max} - \sigma_{min}}{2}$$
Mean Stress:
$$\sigma_m = \frac{\sigma_{max} + \sigma_{min}}{2}$$
Stress Ratio:
$$R = \frac{\sigma_{min}}{\sigma_{max}}$$
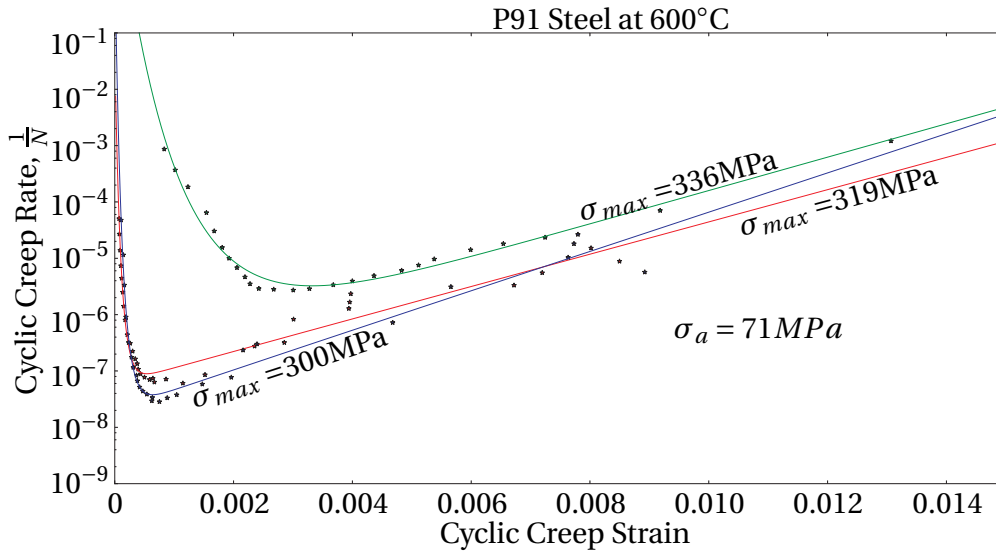
Figure 3.25 Cyclic Creep Rate versus Cyclic Creep Strain at 600°C

been also used here to get a fit between cyclic creep rate and cyclic creep strain. The results for P91 steel at 600°C are shown in Fig. 3.25. Experimental data used here is taken from [64] with some interpolations due to limited number of data points.

The curve-fitted figures shown in this chapter as a result of model optimization for both constant loading and cyclic loading induced creep show that the mixture model is much accurate in modeling inelastic behavior where hardening, softening and damage are expected to evolve over time in the P/T91 steel. This model has also been used for modeling the inelastic behavior of X20CrMoV12-1 steel with a good accuracy in reference [81]

3.2.3 Extension of the Model to Three dimensional Loading Case

The data used for determining material parameters in the constitutive model are obtained from uni-axial tests. But as loads in practical problems have multidimensional nature, the model has to be extended to account for this situation. Here the usual effective (equivalent) stress approach will be adopted as in reference [81].

The constitutive equation in multidimensional loading case will be,

$$\dot{\boldsymbol{\varepsilon}}^c = \frac{3}{2} f\left(\frac{\overline{\sigma}_{vM}}{1-\omega}\right) \frac{\overline{\mathbf{s}}}{\overline{\sigma}_{vM}} \tag{3.17}$$

Where $\dot{\boldsymbol{\varepsilon}}^c$ is the average creep rate tensor, $\mathbf{s}$ is the stress deviator tensor, $\overline{\mathbf{s}} = \mathbf{s} - \Gamma\boldsymbol{\beta}$, $\boldsymbol{\beta}$ is the back stress tensor, Γ is the softening variable (scalar), ω is the damage variable (scalar) and $\overline{\sigma}_{vM} = \sqrt{\frac{3}{2}\overline{\mathbf{s}}\cdot\cdot\overline{\mathbf{s}}}$. The corresponding evolution variables are given by the following equations.

$$\dot{\boldsymbol{\beta}} = A_h \left(\frac{2}{3}\dot{\boldsymbol{\varepsilon}}^c - \dot{\varepsilon}_{vM}\frac{\boldsymbol{\beta}}{\beta_*(\sigma_{vM})} \right), \tag{3.18}$$

$$\dot{\Gamma} = A_s \left[\Gamma_*(\sigma_{vM}) - \Gamma \right] \dot{\varepsilon}_{vM}, \tag{3.19}$$

$$\dot{\omega} = \left(\frac{\sigma_I + |\sigma_I|}{2\sigma_{vM}} \right) \frac{m\omega^{\frac{m-1}{m}}}{\varepsilon_*(\sigma_{vM})}\dot{\varepsilon}_{vM}, \tag{3.20}$$

where σ_I is the first principal stress and $\dot{\varepsilon}_{vM} = \sqrt{\frac{2}{3}\dot{\boldsymbol{\varepsilon}}^c\cdot\cdot\dot{\boldsymbol{\varepsilon}}^c}$.

In general, the main objective of the thesis has been met in this chapter. It has been possible to model the creep behavior of one of the advanced steels (T/P91 steel) as a response to static and cyclic loading. The constitutive equation based on the mixture model has given an extremely accurate fit to experimental data as can be seen from the optimization results shown in previous figures. The accuracy of the work and the model has also been proved by comparing the result with works of other researchers. The only limitation in fulfilling the objective is the lack of experimental data over a wide range of stress and temperature, especially for cyclic loading case.

The three dimensional constitutive equation (3.17) will be used for simulating creep in a practical problem of flow in a super heater tube in the next chapter as a computational implementation of the model.

4

Computational Implementation: Creep of a Superheater Tube

The ultimate goal of any constitutive model development is to predict the material response to applied loads as a tool for predicting life time of components. The distribution of the load inside a component under consideration can be determined by making use of commercially available computational softwares. But constitutive models already implemented in these software are usually of simple nature and thus can not accurately predict the response of the material. But a good feature of many computational software codes is that they allow users to implement their own constitutive models through user defined material subroutines.

In this work, fluid-structure interaction analysis of a superheater tube has been made with the main aim of implementing the constitutive model developed in the previous chapter into a computational software to more accurately predict the life time of the component. The fluid flow and heat transfer analysis has been made by making use of the computational software ANSYS FLUENT with the purpose of determining the temperature distribution in the component. The same model has been developed in ABAQUS and the temperature distribution from FLUENT result has been imported to be used as a predefined temperature load. Then the constitutive model developed in the previous chapter has been implemented in ABAQUS through the user material subroutine UMAT.

4.1 Problem Statement

Superheaters are among the main important components of a power plant. They increase the temperature of the steam from saturation temperature of the steam pressure to the maximum allowable by their material. As pointed out in chapter one, the superheating has to be done at highest possible temperature to insure the high efficiency requirements. But a small increase in efficiency requires large temperature rise. As an example, for steam pressure of 12MPa an increase of efficiency by 1% requires a temperature rise of about 20°C [90]. This temperature rise is experienced by superheaters and they are components with highest probability to fail due to creep. At higher temperatures, their metallurgical issues are very important. They experience the highest possible temperature in the boiler because they are located either inside or immediately after the furnace and their cooling medium is steam (not water) with less cooling effect. Therefore, they are critical components whose life determines the life of other components and need considerable attention in the design of power plants.

Creep life of the superheater shown in Fig. 4.1 will be estimated by imposing the conditions indicated. In the design of super heaters the steam pressure drops are required to be as minimum as possible ($\approx$ 8%) to reduce large pumping requirement [90]. Therefore, for the small portion used here for simulation purpose, uniform pressure distribution can be assumed.

Steam Inlet

T_i=723K
P=12MPa
v=24.4$\frac{m}{s}$

End constraints $\Rightarrow$ symmetry

Tube Inner Diameter=33.5mm
Tube Thickness=3.25mm

Flue Gas Condition
h_∞=64$\frac{W}{m^2 K}$
T_∞=1300K

FSI analysis $\Rightarrow$ ANSYS & ABAQUS

Thermal Analysis $\Rightarrow$ ANSYS FLUENT
Structural Analysis $\Rightarrow$ ABAQUS

Steam Outlet
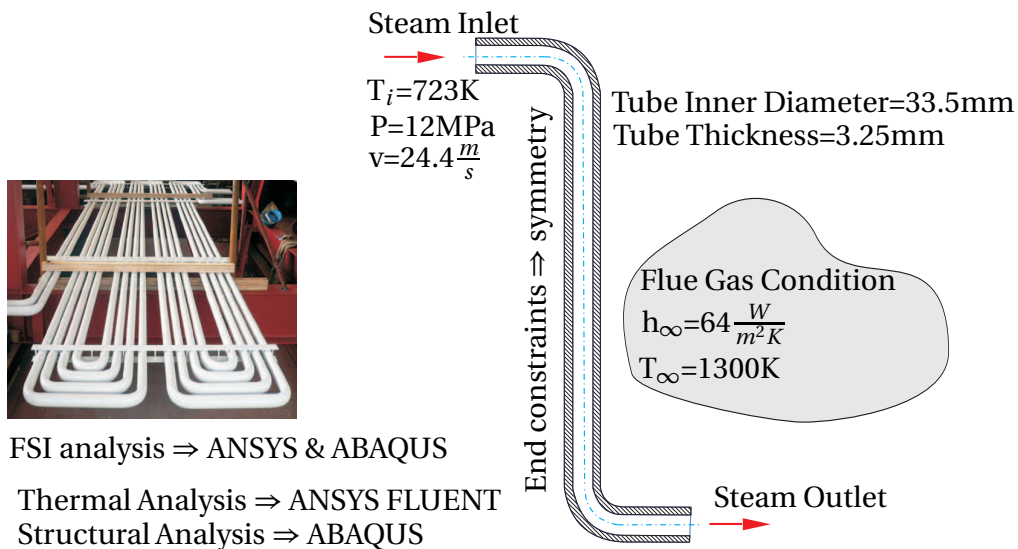
Figure 4.1 Superheater Tube and its Portion to be Modeled

In determining the velocity of the steam flow in the superheaters the

recommended values are given in table 4.1.

Table 4.1   Recommended Steam Mass Flows in Convective Superheater [90]

Steam Temperature, °C	Range of Mass Velocity in Convective Banks, $\frac{Kg}{m^2 s}$
370 –425	330–460
425–480	530–660
480–540	660–800
540–590	950 and above

To determine the heat transfer coefficient of the combustion gas flow over the outer surface of the superheater, it is better to decide the type of the super heater. There are different classifications of superheaters depending on design and flow arrangement criteria [90].

- Based on flow arrangement

  - Parallel flow,

  - Counter flow, and

  - Mixed.

- Based on type of dominant heat transfer

  - Radiant, and

  - Convective.

- Based on number of passes

  - Single-pass, and

  - Multiple-pass.

- Based on boiler layout

  - Vertical,

  - Horizontal, and

  - Combination.

The classification relevant here for the identification of heat transfer coefficient is radiant and convective type. The radiant superheaters are those found within the furnace (directly exposed to combustion area) and heat
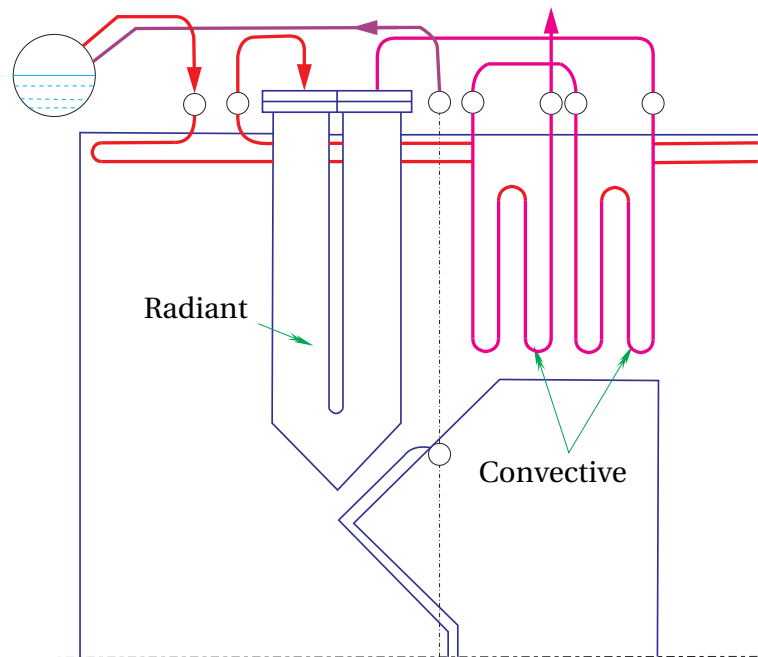
Figure 4.2   Typical Radiant and Convective Superheaters (after [90])

transfer here is predominantly by radiation, Fig. 4.2. In the case of convective superheaters, which are away from direct exposure to combustion area, the heat transfer is convection dominated. The convective superheater is selected for this simulation as determination of the heat transfer coefficient is more easier. The flue gas side heat transfer coefficients are approximately $64 \frac{W}{m^2 K}$ and $101 \frac{W}{m^2 K}$, respectively, for convective vertical and horizontal superheaters [96]. In general, the data used for the simulation are obtained by engineering assumptions from literature. This can be acceptable as the objective of this work is to test the implementation of the constitutive model for simulation of a practical problem. Exact data should be used when the result obtained from the simulation will be used for practical design. The other very important effect of heat transfer from material modeling point of view is the variation of temperature through the cross-section of the superheater tube. This results from variation of temperature on the surface of the tube due to cross-flow nature of the flue gas as shown in Fig. 4.3. The temperature variation in the circumferential, radial and axial directions (θ, r and z) results in thermal induced anisotropic behavior of the material which can make material modeling a bit tough and needs more future research effort for accurate prediction of the component life. The scope of the simulation is limited to the following points.
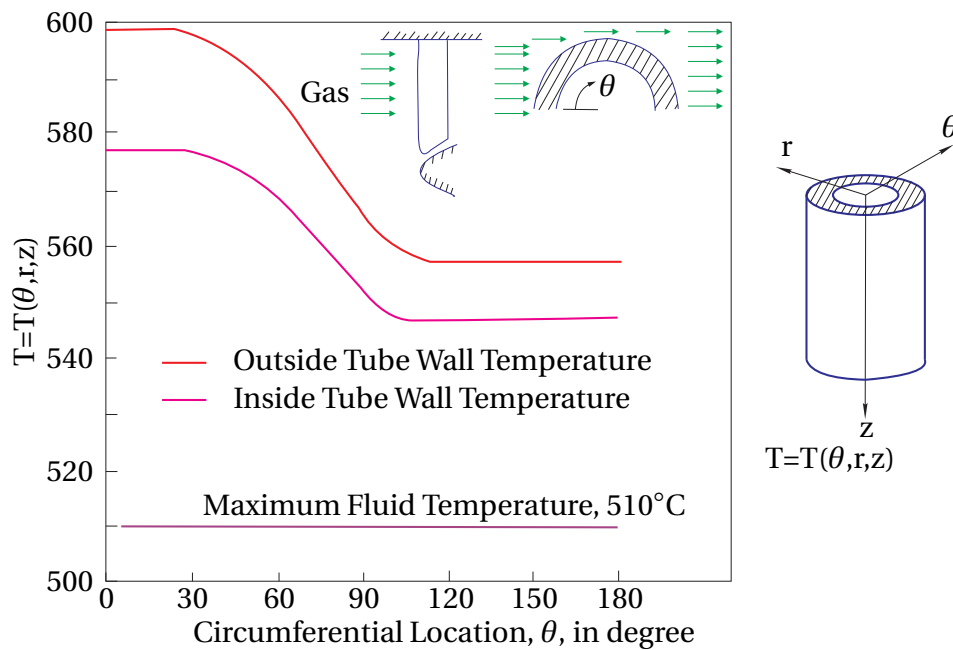
Figure 4.3 Wall Temperature Profile of Superheater Tube (after [53])

- Only one-way (sequential) fluid-structure interaction is considered.

- A part of the superheater geometry is modeled for simplicity.

Based on the scope, the flow and heat transfer analysis was first made in ANSYS FLUENT and then the structural analysis was made in ABAQUS applying structural constraints and thermal loads from FLUENT result.

4.2   Thermal Analysis

As explained in the problem statement section, the opertating pressure of the steam was taken to be 12MPa, which is the common operating pressure for many power plants.

4.2.1   Thermal Properties of Steam

Thermal properties of steam were collected at pressure of 12MPa and modeled to fit temperature variations [67]. The model is to be used in ANSYS FLUENT to simulate the flow in more realistic way. The thermal property variations are shown in Fig. 4.4.

$$\rho = a_\rho + b_\rho\,T + c_\rho\,T^2 + d_\rho\,T^3 + e_\rho\,T^4 + f_\rho\,T^5$$
$$c_P = a_c + b_c\,T + c_c\,T^2 + d_c\,T^3 + e_c\,T^4 + f_c\,T^5$$
$$\mu = a_\mu + b_\mu\,T$$
$$k = a_k + b_k\,T + c_k\,T^2 + d_k\,T^3 + e_k\,T^4 + f_k\,T^5$$
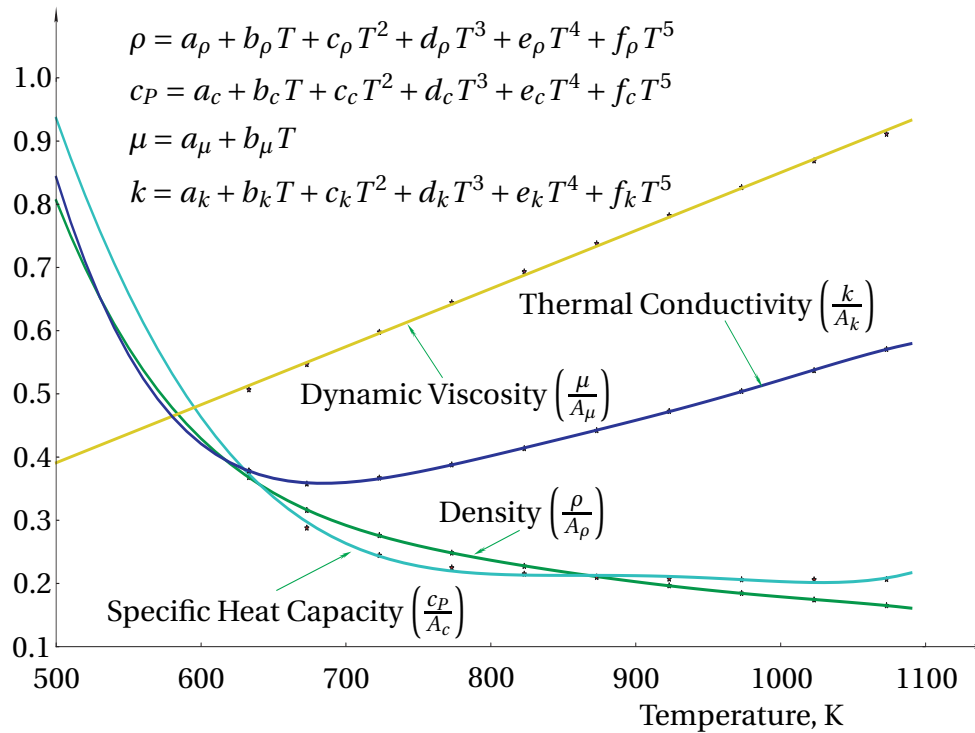
Figure 4.4   Normalized Thermal Properties of Steam at 12MPa (Data source: [67]) - The parameters are given in Appendix A

4.2.2   Superheater Materials

There are different materials used for constructing superheaters. These include carbon steels and advanced chromium steels, [43, 94, 19]. The most common ones are shown in Fig. 4.5. The modified 9Cr-1Mo-V (T91, named by ASTM [17] in 1983) steel has been used for this work mainly as it is widely used in constructing power plant tubes. T91 steel has the following advantages [98]:

- low linear thermal expansion,

- higher thermal conductivity,

- better mechanical properties, and

- a good resistance to creep and to swelling.

Depending on its manufacturers, T91 steel has different chemical compositions. Therefore, it is more convenient to give the ranges of its constituents as shown in table 4.2. Few of the effects of the constituents of steel on its properties are given in Table 4.3.
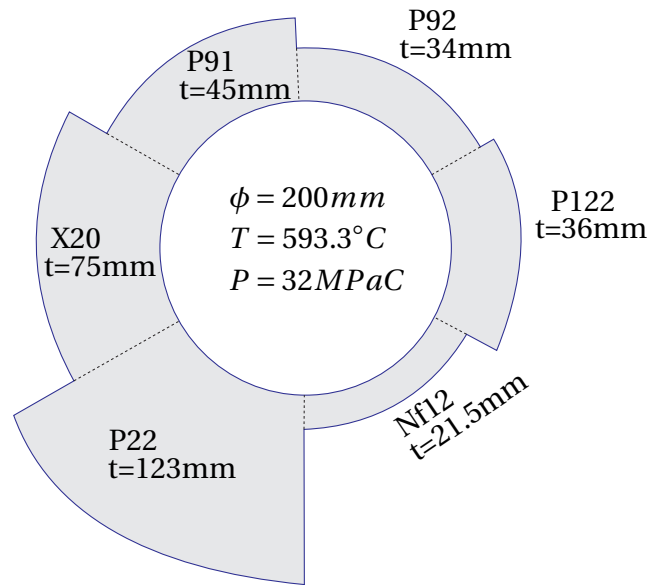
Figure 4.5   Tube Materials versus Tube Thickness (after [94])

Table 4.2   Chemical Composition of T91 Steel [46]

Elements	C	Mn	Si	Cr	Mo	Ni	Al	Nb	V	N
Min	0.08	0.3	0.2	8.0	0.85	-	-	0.06	0.18	0.03
Max	0.12	0.6	0.5	9.5	1.05	0.4	0.04	0.1	0.25	0.07

Table 4.3   Effect of Alloying Elements on Steel Properties [57, 89, 51, 61]

Elements	Effects
Carbon	Increases hardness, forms Nb, Cr and V carbides
Molybdenum	Adds corrosion resistance
Vanadium	Paired with Molybdenum improves creep resistance
Chromium	Raises yield strength and tensile strength
Niobium	Potent carbide former, especially good for creep
Silicon	More oxidation resistance
Nickel	Reduces thermal expansion
Manganese	Solid solution strengthening
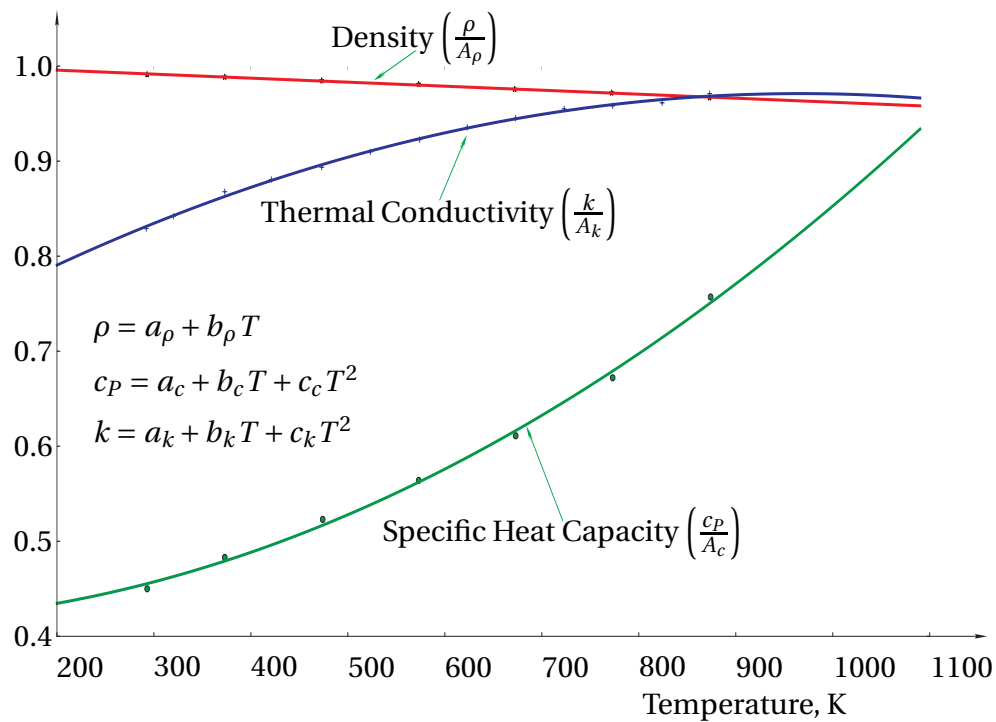
Figure 4.6 Normalized Thermal Properties of T91 Steel. (Data source: [14]) - The parameters are given in Appendix A

An increase in proportion of one constituent in favor of a specific property may ruin another property [2] and, therefore, there should always be a compromise that requires greater effort and research. So far the trend is to alloy new element to the steel or to modify the microstructure through special heat treatments to obtain a desired property.

4.2.3 Thermal Properties of T91 Steel

The thermal properties of T91 steel are also extremely temperature dependent as shown in Fig. 4.6. To get relatively simple model that can be easily implemented in ANSYS FLUENT for performing thermal analysis accounting for wide temperature range, these properties are modeled using a polynomial fit too.

4.2.4 Thermal Results

Applying the boundary conditions and the material properties given above, the thermal analysis has been performed. The temperature distribution result

Mesh

Temperature Distribution
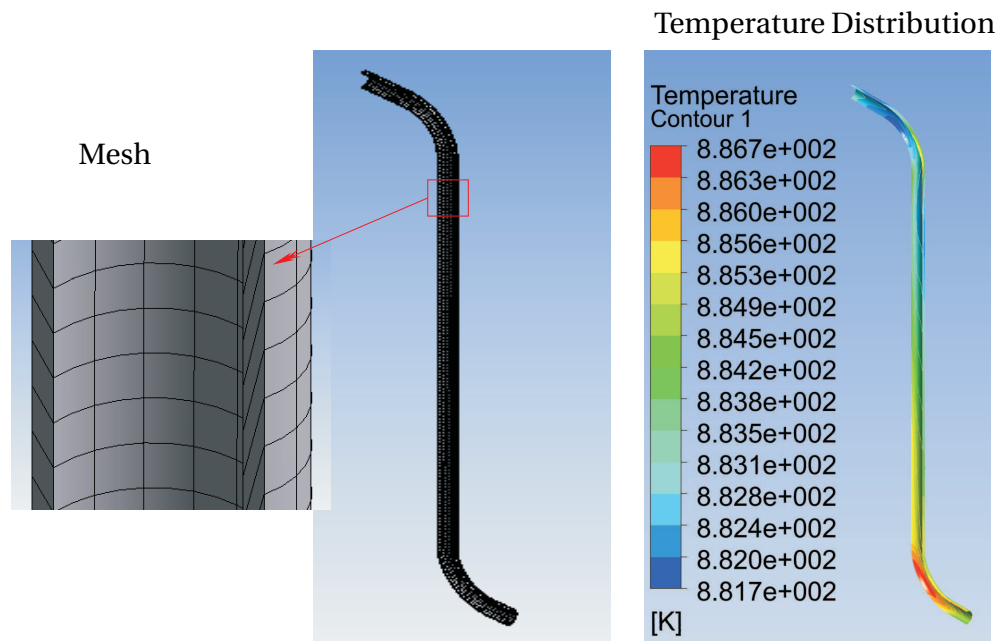
Figure 4.7 Temperature Distribution in the Superheater Body

in the superheater body from CFD Post (post processor of ANSYS CFD results) is shown in Fig. 4.7.

4.3 Structural Analysis

The main objective of the thermal analysis was to obtain more realistic boundary conditions to be used in the structural analysis. Temperature distribution result obtained from the thermal analysis performed in ANSYS FLUENT is to be imported in ABAQUS for structural analysis.

4.3.1 Mechanical Properties of T91 Steel

Like the thermal properties, the mechanical properties of T91 steel highly depend on temperature. To get more realistic simulation results, these properties should be modeled, as shown in Fig. 4.8, and incorporated in the computational software. Poisson's ratio of 0.3 was considered in the simulation.
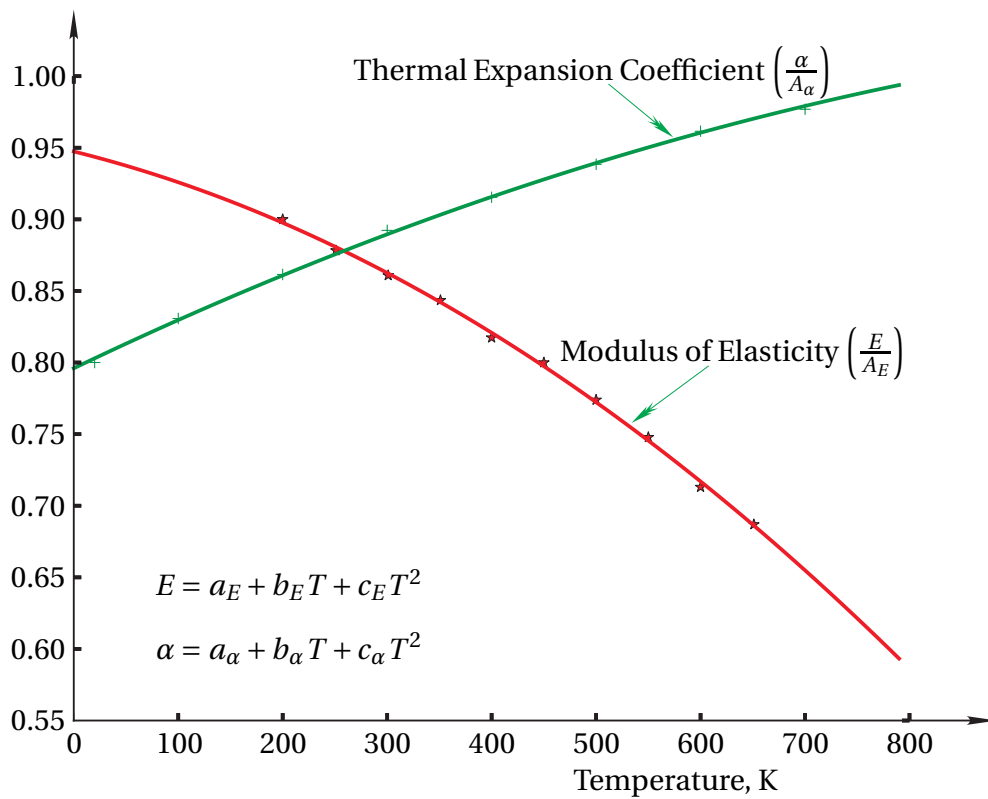
Figure 4.8 Normalized Mechanical Properties of T91 Steel. (Data source: [14]) - The parameters are given in Appendix A

Once all the material properties are modeled (or known) the next step is to implement both the constitutive and the mechanical properties models in to the computational software and perform the simulation. ABAQUS standard has been used in this work for simulating the structural part of the problem. The constitutive and the mechanical properties models were implemented in the software through the material user-subroutine, UMAT. The following are the general steps to be followed when implementing constitutive equations in ABAQUS via UMAT.

- Proper definition of constitutive model,

- Definition of dependence on time, temperature and state (evolution) variables,

- Definition of state variables,

- Transforming the constitutive equation that is in rate form in to incremental form by proper integration scheme,

- Calculation of the Jacobian, and

- Coding the UMAT following FORTRAN 77 or C conventions.

More details of these steps along with illustrative examples can be found in [34].

4.3.2 Structural Results

Representative results of the structural analysis are shown in Fig. 4.9. The distribution of stress before and after creeping of the component has been shown in Fig. 4.9 a) and b). The result shows a decrease in the maximum stress and an increase in the minimum stress with time. Here the fixed parameters are the loads (temperature and pressure), not stress. Therefore, the material undergoes stress redistribution, resulting in narrowing of stress range.

The corresponding strain of the superheater has been shown in Fig. 4.9 c) and d). The results show that creep strain obtained by implementing the constitutive model in ABAQUS is greater than static strain, as expected. In this chapter, the constitutive model has been successfully implemented in ABAQUS through the material user-subroutine UMAT. In addition to this, all the material properties were modeled to be used in the computational softwares ANSYS and ABAQUS in order to get a more realistic simulation results. For the purpose of comparison, both static and creep analysis were made. The creep analysis was made for 3.6×10^4 hours. The results show that the stress in the superheater decreases with time while the strain continues to increase(by about 0.19%). The result is for a small portion of a superheater, but as superheater is a very long component the cumulative strain will be much larger. This agrees, at least qualitatively, with expectations and indicates the successful implementation of the constitutive model in ABAQUS.
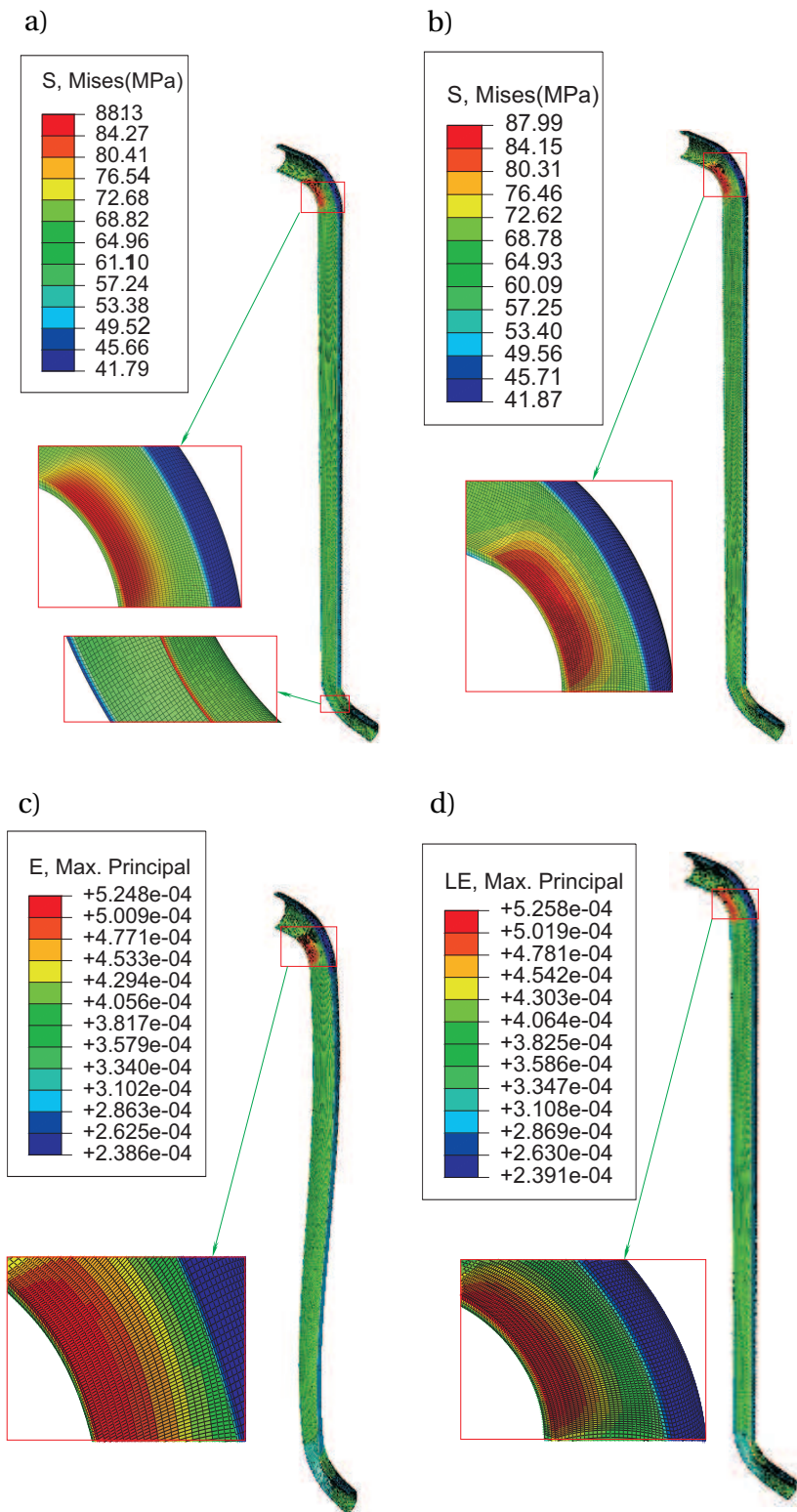
Figure 4.9 Temperature and Stress Distribution Results from ABAQUS: a) von Mises Stress Distribution (Time=0), b) von Mises Stress Distribution (Time=3.6×10^4h), c) Maximum Principal Strain Distribution (Time=0), d) Maximum Principal Strain Distribution (Time=3.6×10^4h).

5

Conclusion, Limitations and Outlook

In energy conversion processes involving fluid-structure-interactions, the following three points have been pointed out to be the very important areas of continuous attention:

1. Turbulent flow of fluids,

2. The challenges in computational formulation of the fluid-structure-interactions, and

3. The inelastic behavior of structures in response to loads from the interactions.

The main objective of this thesis was to deal with the third point above. The inelastic behavior of heat exchangers (superheaters) used in thermal power plants and face extremely high temperature and high pressure has been modeled. Specifically, the creep behavior of these heat exchangers was modeled considering both constant and cyclic loads. The mixture assumption based constitutive equation was used in the modeling. The modeling was done successfully by calibrating the material constants through optimization using available experimental data from literature. The results are very satisfactory as validations with experimental data and comparisons with results of other constitutive models show.

To test the applicability of the constitutive model, simulation of a superheater tube has been made for implementing the model in a computational software. The two important features of this part of the work were:

1. performing fluid-structure-interaction analysis of the superheater with the aim of loading of the component with realistic temperature and pressure distributions, and

2. utilization of material user-subroutine to implement the model in the structural simulation software, ABAQUS.

These two issues were also successfully done as the simulation results indicated.

Eventhough the results obtained are satisfactory for specific stresses and temperatures, there are limitations which can have negative effect on the utilization of the model or on its effective use for simulation.

- The data available in literature are of high limitations. It was not possible to get data over a wide range of stress and temperature. Therefore, the accuracy of the model is guaranteed only to those data range used for parameter determination.

- No effective single computational software was obtained for performing fully coupled fluid-structure-interaction analysis and addressing the inelastic behavior at the same time.

Being motivated by the impressive results and using the limitations as an opportunity for further work, the following points can be considered as an outlook.

- Performing creep test experiment for getting more realistic material parameters,

- Incorporating more state variables in the model to increase the accuracy of the model,

- Incorporating micromechanical phenomena to make the model more physical based,

- Adapting the model for materials used in different application areas like renewable energy technologies,

- Utilizing more accurate turbulence models to determine the thermal loads, and

- Working on the computational formulations the give more accurate fluid-structure-interaction modeling.

A

Parameters in the Curve-fit of Material Properties used in Simulation

1. Thermal properties of steam, Fig. 4.4

   a) Density, $\frac{Kg}{m^3}$

   $A_\rho = 150.0\frac{Kg}{m^3}$, $a_\rho = 3.66 \times 10^3\frac{Kg}{m^3}$, $b_\rho = -1.97 \times 10^1\frac{Kg}{m^3K}$, $c_\rho = 4.33 \times 10^{-2}\frac{Kg}{m^3K^2}$, $d_\rho = -4.78 \times 10^{-5}\frac{Kg}{m^3K^3}$, $e_\rho = 2.63 \times 10^{-8}\frac{Kg}{m^3K^4}$, $f_\rho = -5.80 \times 10^{-12}\frac{Kg}{m^3K^5}$

   b) Specific Heat Capacity, $\frac{kJ}{Kg.K}$

   $A_c = 12.0\frac{kJ}{Kg.K}$, $a_c = 9.78 \times 10^4\frac{kJ}{Kg.K}$, $b_c = -1.69 \times 10^2\frac{kJ}{Kg.K^2}$, $c_c = -4.19 \times 10^{-1}\frac{kJ}{Kg.K^3}$, $d_c = 1.33 \times 10^{-3}\frac{kJ}{Kg.K^4}$, $e_c = -1.21 \times 10^{-6}\frac{kJ}{Kg.K^5}$, $f_c = 3.67 \times 10^{-10}\frac{kJ}{Kg.K^6}$

   c) Thermal Conductivity, $\frac{W}{m.K}$

   $A_k = 0.2\frac{W}{m.K}$ $a_k = 7.98\frac{W}{m.K}$ $b_k = -4.50 \times 10^{-2}\frac{W}{m.K^2}$, $c_k = 1.02 \times 10^{-4}\frac{W}{m.K^3}$, $d_k = -1.14\times10^{-7}\frac{W}{m.K^4}$, $e_k = 6.38\times10^{-11}\frac{W}{m.K^5}$, $f_k = -1.42\times 10^{-14}\frac{W}{m.K^6}$

   d) Dynamic Viscosity, $10^{-5}Pa.s$

   $A_\mu = 4.5 \times 10^{-5}Pa.s$, $a_\mu = -3.07 \times 10^{-6}Pa.s$, $b_\mu = 4.13 \times 10^{-8}\frac{Pa.s}{K}$

2. Thermal Properties of T91 Steel, Fig. 4.6

   a) Density, $\frac{Kg}{m^3}$

   $A_\rho = 7800.0\frac{Kg}{m^3}$, $a_\rho = 7.83 \times 10^3\frac{Kg}{m^3}$, $b_\rho = -3.29 \times 10^{-1}\frac{Kg}{m^3K}$

   b) Specific Heat Capacity, $\frac{J}{Kg.K}$

   $A_c = 1000.\frac{J}{Kg.K}$, $a_c = 4.15 \times 10^2\frac{J}{Kg.K}$, $b_c = 1.47 \times 10^{-2}\frac{J}{Kg.K^2}$, $c_c = 4.23 \times 10^{-4}\frac{J}{Kg.K^3}$

c) Thermal Conductivity, $\frac{W}{m.K}$

$A_k = 31.0\frac{W}{m.K}$, $a_k = 7.98\frac{W}{m.K}$, $b_k = -4.50 \times 10^{-2}\frac{W}{m.K^2}$, $c_k = 1.02 \times 10^{-4}\frac{W}{m.K^3}$

3. Mechanical Properties of T91 Steel, Fig. 4.8

a) Young's Modulus, GPa

$A_E = 2.23 \times 10^2 GPa$, $a_E = 2.23 \times 10^2 GPa$, $b_E = 7.44 \times 10^{-4}\frac{GPa}{K}$, $c_E = -7.77 \times 10^{-5}\frac{GPa}{K^2}$

b) Thermal Expansion Coefficient, $10^{-6}\frac{1}{K}$

$A_\alpha = 8.86 \times 10^{-6}\frac{1}{K}$, $a_\alpha = 8.86 \times 10^{-6}\frac{1}{K}$, $b_\alpha = 5.89 \times 10^{-9}\frac{1}{K^2}$, $c_\alpha = -2.00 \times 10^{-12}\frac{1}{K^3}$

Bibliography

[1] F. Abe. Precipitate design for creep strengthening of 9% Cr tempered martensitic steel for ultra-supercritical power plants. *Science and Technology of Advanced Materials*, 9(1):013002, 2008.

[2] F. Abe. Strengthening mechanisms in creep of advanced ferritic power plant steels based on creep deformation analysis. pages 409–422, 2011.

[3] F. Abe, T. U. Kern, and R. Viswanathan. *Creep-Resistant Steels*. Series in Metals and Surface Engineering Series. Woodhead Publishing Ltd., Cambridge, 2008. ISBN 9781845691783. URL http://books.google.de/books?id=X6UCGgAACAAJ.

[4] H. Altenbach. Creep-damage behaviour of plates and shells. *Mechanics of Time-Dependent Materials*, 3(2):103–123, 1999.

[5] H. Altenbach. A nonclassical model for creep-damage processes. *Materials Physics and Mechanics*, 3:25–35, 2001.

[6] H. Altenbach, G. Kolarow, and K. Naumenko. Solution of creep-damage problems for beams and rectangular plates using the Ritz and finite element method. *Technische Mechanik*, 19:249–258, 1999.

[7] H. Altenbach, V. Kushnevsky, and K. Naumenko. On the use of solid- and shell-type finite elements in creep–damage predictions of thinwalled structures. *Archive of Applied Mechanics*, 71(2-3):164–181, 2001.

[8] H. Altenbach, G. A. Maugin, and V. Erofeev. *Mechanics of Generalized Continua*. Advanced Structured Materials.

Springer, Heidelberg, 2011. ISBN 9783642192197. URL
http://books.google.de/books?id=gdS2rXJaIO8C.

[9] A. Anandarajah. *Computational Methods in Elasticity and Plasticity: Solids and Porous Media.* Springer, New York, 2011. ISBN 9781441963796. URL http://books.google.de/books?id=Hsrj1snaYacC.

[10] B. Andersson. *Computational Fluid Dynamics for Engineers.* Cambridge University Press, Cambridge, 2012. ISBN 9781139505567. URL http://books.google.de/books?id=A_g5Ol6wS-0C.

[11] *ANSYS FLUENT 12.0/12.1 Documentation.* ANSYS, Inc., 2009.

[12] F. Ashby and D. R. H. Jones. *Engineering Materials 1: An Introduction to Properties, Applications and Design.* Butterworth-Heinemann, Oxford, 2012. ISBN 9780080966656. URL http://books.google.de/books?id=Dy5xbRrJpg8C.

[13] M. F. Ashby, H. Shercliff, and D. Cebon. *Materials: Engineering, Science, Processing and Design.* Elsevier Science, Oxford, 2009. ISBN 9780080961552. URL http://books.google.de/books?id=ZGexmdEqmYsC.

[14] M. Ashrafi-Nik. Thermo hydraulic optimisation of the EURISOL DS Target. Technical report, Paul Scherrer Institut, 2006.

[15] F. Axisa and J. Antunes. *Modelling of Mechanical Systems: Fluid-Structure Interaction.* Elsevier Ltd., Amsterdam, 2006. ISBN 9780080475400. URL http://books.google.de/books?id=NTu8dx7ce88C.

[16] K. J. Bathe. *Inelastic Analysis of Solids and Structures.* Computational Fluid and Solid Mechanics. Springer, 2006. ISBN 9783540265078. URL http://books.google.de/books?id=fDQlQyu-PgkC.

[17] A. A. Bazazi. *Evolution of Microstructure during Long-term Creep of a Tempered Martensite Ferritic Steel.* PhD thesis, Fakultät für Maschinenbau der Ruhr-Universität Bochum, 2009.

[18] A. Bejan and A. D. Kraus. *Heat Transfer Handbook.* Number v. 1. J. Wiley, California, 2003. ISBN 9780471390152. URL http://books.google.de/books?id=J91SAAAAMAAJ.

[19] H. Berns and W. Theisen. *Ferrous Materials: Steel and Cast Iron.* Springer, Berlin, 2008. ISBN 9783540718482. URL http://books.google.de/books?id=6ZgvRtOvMvUC.

[20] J. F. Besseling and E. Van Der Giessen. *Mathematical Modeling of Inelastic Deformation.* Applied Mathematics. Taylor & Francis, London, 1994. ISBN 9780412452802. URL http://books.google.de/books?id=IRRwxDHEDvIC.

[21] J. Betten. *Creep Mechanics.* Springer, Berlin, 2008. ISBN 9783540850519. URL http://books.google.de/books?id=vvq7Cg-5k1sC.

[22] R. I. Borja. *Plasticity: Modeling and Computation.* Springer, Berlin, 2013. ISBN 9783642385476. URL http://books.google.de/books?id=sWBEAAAAQBAJ.

[23] B. J. P. Buhre, R. Gupta, S. Richardson, A. Sharma, C. Spero, and T. Wall. PF-fired supercritical boilers. Technical Note 20, University of Newcastle, Callaghan, NSW 2308, March 2002.

[24] W. D. Callister. *Fundamentals of Materials Science and Engineering: An Interactive e.text.* John Wiley & Sons, Inc., New York, 2001.

[25] I. Celik. Introductory turbulence modeling. 1999.

[26] Y. A. Çengel and M. A. Boles. *Thermodynamics: An Engineering Approach.* McGraw-Hill Series in Mechanical and Aerospace Engineering. McGraw-Hill Higher Education, New York, 2008. ISBN 9780073305370. URL http://books.google.de/books?id=8G6NSQAACAAJ.

[27] E. Cerri, E. Evangelista, S. Spigarelli, and P. Bianchi. Evolution of microstructure in a modified 9Cr–1Mo steel during short term creep. *Materials Science and Engineering: A,* 245(2):285–292, 1998.

[28] J. L. Chaboche. Constitutive equations for cyclic plasticity and cyclic viscoplasticity. *International Journal of Plasticity,* 5(3):247 – 302, 1989. ISSN 0749-6419.

[29] J. Chakrabarty. *Theory of Plasticity.* Butterworth-Heinemann, Oxford, 2006. ISBN 9780080481364. URL http://books.google.de/books?id=uMcID-tu-8YC.

[30] J. Chakrabarty. *Applied Plasticity.* Mechanical Engineering Series. Springer, New York, 2010.

[31] W. F. Chen and D. J. Han. *Plasticity for Structural Engineers.* J. Ross Pub., New York, 2007. ISBN 9781932159752. URL `http://books.google.de/books?id=E8jptvNgADYC`.

[32] T. J. Chung. *Computational Fluid Dynamics.* Cambridge University Press, Cambridge, 2010. ISBN 9781139493291. URL `http://books.google.de/books?id=Cq6tqmMVJREC`.

[33] S. C. Cowin. *Continuum Mechanics of Anisotropic Materials.* Springer, New York, 2013.

[34] *Abaqus 6.10 Analysis User's Manual.* Dassault Systèmes, 2010.

[35] E. A. de Souza Neto, D. Peric, and D. R. J. Owen. *Computational Methods for Plasticity: Theory and Applications.* Wiley, Chichester, 2011. ISBN 9781119964544. URL `http://books.google.de/books?id=21QOoLGFZuoC`.

[36] N. E. Dowling, K. S. Prasad, and R. Narayanasamy. *Mechanical Behavior of Materials: Engineering Methods for Deformation, Fracture, and Fatigue.* Pearson Education, Limited, New Jersey, 2013. ISBN 9780273764557. URL `http://books.google.de/books?id=OrlxMAEACAAJ`.

[37] L. F. Drbal, P. Boston, and K. Westra. *Power Plant Engineering.* IFAC Proceedings Series. Springer, New York, 1996. ISBN 9780412064012. URL `http://books.google.de/books?id=4ewKE8MZAZIC`.

[38] F. Dunne and N. Petrinic. *Introduction to Computational Plasticity.* Oxford series on materials modelling. Oxford University Press, Oxford, 2005. ISBN 9780198568261. URL `http://books.google.de/books?id=jVxisjdpe8sC`.

[39] M. M. El-Wakil. *Power Plant Technology.* McGraw-Hill, New York, 1985. ISBN 9780070662742. URL `http://books.google.de/books?id=vw7QAAAACAAJ`.

[40] Y. Fung. *Foundations of Solid Mechanics.* Prentice-Hall international series in dynamics. Prentice-Hall, New Jersey, 1965. URL `http://books.google.de/books?id=P9AQAQAAIAAJ`.

[41] Y. Fung. *A First Course in Continuum Mechanics: For Physical and Biological Engineers and Scientists.* Tsinghua

University Press, Tsinghua, 1994. ISBN 9787302121381. URL http://books.google.de/books?id=C47upeFWcT4C.

[42] V. Gaffard. *Experimental Study and Modelling of High Temperature Creep Flow and Damage Behaviour of 9Cr1Mo-NbV Steel Weldments.* PhD thesis, École Nationale Supérieure des Mines de Paris (Mines ParisTech), 2004.

[43] V. Ganapathy. Superheaters: Design and performance, 2001. URL http://v_ganapathy.tripod.com/superhtr.pdf.

[44] Y. Gorash. *Development of a Creep-Damage Model for Non-Isothermal Long-Term Strength Analysis of High-Temperature Components Operating in a Wide Stress Range.* PhD thesis, Martin-Luther-Universität Halle-Wittenberg, July 2008.

[45] D. Y. Goswami and F. Kreith. *Handbook of Energy Efficiency and Renewable Energy.* Mechanical and Aerospace Engineering Series. Taylor & Francis, London, 2007. ISBN 9781420003482. URL http://books.google.de/books?id=OfiMKyFV8JIC.

[46] G. Guntz. *The T91 Book: Ferritic Tubes and Pipe for High Temperature Use in Boilers.* Vallourec Industries, Industrial Application Group, Power Generation Division, Boulogne-Billancourt, 1990. URL http://books.google.de/books?id=FrY6HwAACAAJ.

[47] W. Han and B. D. Reddy. *Plasticity: Mathematical Theory and Numerical Analysis.* Interdisciplinary Applied Mathematics. Springer, New York, 2012. ISBN 9781461459408. URL http://books.google.de/books?id=BTCgRiv1f-EC.

[48] E. M. Haney, F. Dalle, M. Sauzay, L. Vincent, I. Tournié, L. Allais, and B. Fournier. Macroscopic results of long-term creep on a modified 9Cr–1Mo steel (T91). *Materials Science and Engineering: A,* 510:99–103, 2009.

[49] O. M. Heeres, A. S. J Suiker, and R. de Borst. A comparison between the Perzyna viscoplastic model and the consistency viscoplastic model. *European Journal of Mechanics-A/Solids,* 21(1):1–12, 2002.

[50] J. P. Holman. *Heat Transfer (Si Units).* McGraw-Hill, New York, 2008. ISBN 9780070634510. URL http://books.google.de/books?id=1-qf1rzXgPgC.

[51] D. R. Jara. *9-12% Cr Heat Resistant Steels: Alloy Design, TEM Characterisation of Microstructure Evolution and Creep Response at 650°C.* PhD thesis, Ruhr-Universität Bochum, 2011.

[52] L. M. Kachanov. *Foundations of the Theory of Plasticity.* North-Holland series in applied mathematics and mechanics. North-Holland, Amsterdam, 1971. ISBN 9780720423631. URL http://books.google.de/books?id=b4PWKGA4U9oC.

[53] S. Kakaç. *Boilers, Evaporators, and Condensers.* John Wiley & Sons, Inc., New York, 1991. ISBN 9780471621706. URL http://books.google.de/books?id=M-FSAAAAMAAJ.

[54] M. E. Kassner. *Fundamentals of Creep in Metals and Alloys.* Elsevier Ltd., Amsterdam, 2008. ISBN 9780080914992. URL http://books.google.de/books?id=hJ3a-_1rtV0C.

[55] A. S. Khan and S. Huang. *Continuum Theory of Plasticity.* John Wiley & Sons, Inc., New York, 1995. ISBN 9780471310433. URL http://books.google.de/books?id=l1FPaaY355gC.

[56] B.-S. Kim, J.-C. Chang, Y.-K. Jung, and J.-J. Jung. Failure analysis of the superheater tubes of S-combined power plant. *Engineering Failure Analysis*, 2009.

[57] S. Kim, Y.-R. Im, S. Lee, H.-C. Lee, Y. J. Oh, and J. H. Hong. Effects of alloying elements on mechanical and fracture properties of base metals and simulated heat-affected zones of SA 508 steels. *Metallurgical and Materials Transactions A*, pages 903–911, 2001.

[58] W.-G. Kim, S.-H. Kim, and W.-S. Ryu. Creep characterization of type 316LN and HT-9 stainless steels by the KR creep damage model. *KSME International Journal*, 15(11):1463–1471, 2001.

[59] H. Kimura, K. amd Kushima and K. Sawada. Long-term creep deformation property of modified 9Cr–1Mo steel. *Materials Science and Engineering: A*, 510:58–63, 2009.

[60] K. Kimura, K. Sawada, and H. Kushima. Long-term creep strength of creep strength enhanced ferritic steels. In *Challenges of Power Engineering and Environment*, pages 1059–1065. Springer, 2007.

[61] R. L. Klueh. Elevated temperature ferritic and martensitic steels and their application to future nuclear reactors. *International Materials Reviews*, 50(5):287–310, 2005.

[62] A. S. Krausz and K. Krausz. *Unified Constitutive Laws of Plastic Deformation.* Elsevier Inc., California, 1996. ISBN 9780080543437. URL `http://books.google.de/books?id=OA9PxDRYpUoC`.

[63] E. Kuhl, S. Hulsho, and R. de Borst. An arbitrary Lagrangian Eulerian finite-element approach for fluidâ€"structure interaction phenomena. *International Journal for Numerical Methods in Engineering*, 57:117–142, 2003.

[64] L. Kunz and P. Lukáš. High temperature fatigue and cyclic creep of P91 steel. *European Structural Integrity Society*, 29:37–44, 2002.

[65] W. M. Lai, D. H. Rubin, D. Rubin, and E. Krempl. *Introduction to Continuum Mechanics.* Elsevier Inc., Amsterdam, 2009. ISBN 9780080942520. URL `http://books.google.de/books?id=lEhh-hjG6EgC`.

[66] J. Lemaitre and R. Desmorat. *Engineering Damage Mechanics: Ductile, Creep, Fatigue and Brittle Failures.* Springer, Berlin, 2006. ISBN 9783540272939. URL `http://books.google.de/books?id=SLyUINayQEoC`.

[67] Spirax-Sarco Limited. Steam Table: Superheated Steam Region, 2013. URL `http://www.spiraxsarco.com/esc/SH_Properties.aspx`.

[68] X. J. Liu, X. B. Kong, G. L. Hou, and J. H. Wang. Modeling of a 1000MW power plant ultra super-critical boiler system using fuzzy-neural network methods. *Energy Conversion and Management*, 65(0): 518 – 527, 2013. ISSN 0196-8904.

[69] A. Maczulak. *Renewable Energy: Sources and Methods.* Green technology. Infobase Publishing, New York, 2010. ISBN 9780816072033. URL `http://books.google.de/books?id=D8iIwdbUuTgC`.

[70] S. A. Maloy and M. R. James. The high temperature tensile properties of ferritic-martensitic and austenitic steels after irradiation in an 800 MEV Proton beam. In *Conference Proceedings of Seventh Information Exchange Meeting on Actinide and Fission Product Partitioning and Transmission*, pages 669–678, 14-16 Oct. 2002.

[71] G. E. Mase. *Theory and Problems of Continuum Mechanics.* Schaum's Outline Series in Engineering. McGraw-Hill, New York, 1970. URL http://books.google.de/books?id=atwuNAEACAAJ.

[72] G. T. Mase and G. E. Mase. *Continuum Mechanics for Engineers, Third Edition.* Computational Mechanics and Applied Analysis. Taylor & Francis, London, 2010. ISBN 9781439832578. URL http://books.google.de/books?id=uI1ll0A8B_UC.

[73] G. A. Maugin. *The Thermomechanics of Plasticity and Fracture.* Cambridge University Press, Cambridge, 1992. ISBN 9780521397803. URL http://books.google.de/books?id=NIT3FWwskKkC.

[74] G. A. Maugin. *Continuum Mechanics through the Twentieth Century.* Solid Mechanics and Its Applications. Springer, Dordrecht, 2013.

[75] J. D. McCalley. Energy conversion technologies, 2010.

[76] H. Mehrer. *Diffusion in Solids: Fundamentals, Methods, Materials, Diffusion-Controlled Processes.* Springer, 2007. ISBN 9783540714880. URL http://books.google.de/books?id=IUZVffQLFKQC.

[77] M. A. Meyers and K. K. Chawla. *Mechanical Behavior of Materials.* Cambridge University Press, Cambridge, 2009. ISBN 9780521866750. URL http://books.google.de/books?id=LXcjEAZ9tX4C.

[78] B. D. Middleton and J. Buongiorno. Supercritical water reactor cycle for medium power applications. Technical report, Nuclear Science and Engineering Department, Massachusetts Institute of Technology, Cambridge, April 2007.

[79] M. J. Moran. *Introduction to Thermal Systems Engineering: Thermodynamics, Fluid Mechanics, and Heat Transfer.* John Wiley & Sons, Inc., California, 2003. ISBN 9780471204909. URL http://books.google.de/books?id=G4woAQAAMAAJ.

[80] K. Naumenko and H. Altenbach. *Modeling of Creep for Structural Analysis.* Foundations of Engineering Mechanics. Springer, Berlin, 2007. ISBN 9783540708391. URL http://books.google.de/books?id=xxC0Syp0AhoC.

[81] K. Naumenko, H. Altenbach, and A. Kutschke. A combined model for hardening, softening, and damage processes in advanced heat resistant

steels at elevated temperature. *International Journal of Damage Mechanics*, 20(4):578–597, 2011.

[82] F. K. G. Odqvist. *Mathematical Theory of Creep and Creep Rupture.* Oxford Mathematical Monographs. Clarendon Press, Oxford, 1974. ISBN 9780198535225. URL `http://books.google.de/books?id=clh8AAAAIAAJ`.

[83] M. R. Patel. *Wind and Solar Power Systems: Design, Analysis, and Operation, Second Edition.* Taylor & Francis, London, 2012. ISBN 9781420039924. URL `http://books.google.de/books?id=8aQDw14fQnkC`.

[84] J. Pelleg. *Mechanical Properties of Materials.* Solid Mechanics and Its Applications. Springer, Dordrecht, 2012. ISBN 9789400743427. URL `http://books.google.de/books?id=2mGC832OcdoC`.

[85] D. R. Pitts and L. E. Sissom. *Theory and Problems of Heat Transfer.* Schaum's Outline Series. McGraw-Hill, New York, 1977. ISBN 9780070502031. URL `http://books.google.de/books?id=2IRUAAAAMAAJ`.

[86] S. B. Pope. *Turbulent Flows.* Cambridge University Press, Cambridge, 2000. ISBN 9780521598866. URL `http://books.google.de/books?id=HZsTw9SMx-0C`.

[87] V. Quaschning. Solar thermal power plants. *Renewable Energy World*, pages 109–113, 2003.

[88] A. K. Raja and A. P. Srivastava. *Power Plant Engineering.* New Age International, New Delhi, 2006. ISBN 9788122418316. URL `http://books.google.de/books?id=77wGPAKKilQC`.

[89] M. Rasul, editor. *Thermal Power Plants.* InTech, Rijeka, 2011.

[90] K. Rayaprolu. *Boilers for Power and Process.* Taylor & Francis, London, 2008. ISBN 9781420075373. URL `http://books.google.de/books?id=unGSfNa8wocC`.

[91] J. N. Reddy. *An Introduction to Continuum Mechanics.* Cambridge University Press, Cambridge, 2013. ISBN 9781107025431. URL `http://books.google.de/books?id=Rsj-Bwv5FP0C`.

[92] S. Rezvani, Y. Huang, D. McIlveen-Wright, N. Hewitt, and Y. Wang. Comparative assessment of sub-critical versus advanced super-critical oxyfuel fired PF boilers with CO_2 sequestration facilities. *Fuel*, 86(14): 2134 – 2143, 2007. ISSN 0016-2361.

[93] A. Rusinko and K. Rusinko. *Plasticity and Creep of Metals*. Springer, Berlin, 2011. ISBN 9783642212130. URL `http://books.google.de/books?id=TGKrn5o0aXkC`.

[94] I. A. Shibli and K. Coleman. Failure of P91 steel at the West Burton plant in England raise concerns about the long term behavior of the advanced steel. Technical report, European Technology Development.

[95] E. Stein, R. de Borst, and T. J. R. Hughes. *Encyclopedia of Computational Mechanics*. John Wiley, California, 2004. ISBN 9780470846995. URL `http://books.google.de/books?id=4YJUAAAAMAAJ`.

[96] P. M. V. Subbarao. Performance analysis of SG second pass. URL `http://web.iitd.ac.in/~pmvs/index.php?q=ppp`.

[97] Y. Takahashi. Study on creep–fatigue evaluation procedures for high chromium steels–part II: Sensitivity to calculated deformation. *International Journal of Pressure Vessels and Piping*, 85(6):423–440, 2008.

[98] A. Verleene, J.-B. Vogt, I. Serre, and A. Legris. Low cycle fatigue behaviour of T91 martensitic steel at 300°C in air and in liquid lead bismuth eutectic. *International Journal of Fatigue*, 28(8):843 – 851, 2006. ISSN 0142-1123.

[99] H. K. Versteeg and W. Malalasekera. *An Introduction to Computational Fluid Dynamics: The Finite Volume Method*. Pearson Education Ltd., Harlow, 2007. ISBN 9780131274983. URL `http://books.google.de/books?id=RvBZ-UMpGzIC`.

[100] R. L. Viana, S. R. Lopes, I. L. Caldas, J. D. Szezech, Z. Guimarães-Filho, G. Z. dos Santos Lima, P. P. Galuzio, A. M. Batista, Yu Kuznetsov, and I. C. Nascimento. Dynamical analysis of turbulence in fusion plasmas and nonlinear waves. *Communications in Nonlinear Science and Numerical Simulation*, 17(12):4690–4699, 2012.

[101] I. von Hagen and W. Bendick. Creep resistant ferritic steels for power plants. In *Proceedings of the International Symposium on Niobium*, pages 753–776, 2001.

[102] F. M. White. *Fluid Mechanics.* McGraw-Hill, New York, 2003. ISBN 9780072402179. URL `http://books.google.de/books?id=1DYtptq3OC4C`.

[103] D. C. Wilcox. *Turbulence Modeling for CFD: Text.* DCW Industries, Inc., California, 2006. ISBN 9781928729082. URL `http://books.google.de/books?id=tFNNPgAACAAJ`.

[104] H. C. Wu. *Continuum Mechanics and Plasticity.* Modern Mechanics and Mathematics Series. Taylor & Francis Group, London, 2005. ISBN 9781584883630. URL `http://books.google.de/books?id=OS4mICsHG3sC`.

[105] M. Yaguchi and Y. Takahashi. A viscoplastic constitutive model incorporating dynamic strain aging effect during cyclic deformation conditions. *International Journal of Plasticity*, 16(3):241–262, 2000.

[106] Q. Yang, X. Chen, and W.-Y. Zhou. Microplane-damage-based effective stress and invariants. *International Journal of Damage Mechanics*, 14 (2):179–191, 2005.

[107] M. Yu and J. C. Li. *Computational Plasticity: With Emphasis on the Application of the Unified Strength Theory.* Advanced Topics in Science and Technology in China. Springer, Heidelberg, 2012. ISBN 9783642245909. URL `http://books.google.de/books?id=V_WHBnP-sP8C`.

[108] A. H. Zerban and E. P. Nye. *Steam Power Plants.* International Textbooks in Mechanical Engineering. International Textbook Co., Chicago, 1952. URL `http://books.google.de/books?id=hifOAAAAMAAJ`.

[109] W. Zhang and Y. Cai. *Continuum Damage Mechanics and Numerical Applications.* Advanced Topics in Science and Technology in China. Springer, Heidelberg, 2010. ISBN 9783642047084. URL `http://books.google.de/books?id=h3K7NWTXIcAC`.

Biography

Personal Detail

Date of Birth	1977
Place of Birth	Bedele, Ethiopia
Marital Status	Married
Sex	Male
Nationality	Ethiopian

2010–2013	PhD Study, Otto-von-Guericke-Universität, Magdeburg, Germany.
2012	Training on IT Essentials: PC Hardware and Software, Cisco Networking Academy, Jimma University Branch.
2009	Training on Teaching Subject Related Didactics, Institut Technik und Bildung (Germany) and Engineering Capacity Building Program (Ethiopia), Addis Ababa.
2007–2010	Continuining and Distance Education Coordinator of College of Engineering and Technology, Jimma University, Jimma, Ethiopia.
2007	Training on Computational Mechanics, Martin Luther Universität Halle-Wittenberg, Germany.
	Training on Workshop Organization, InWent/PLANCO (Germany) and Ministry of Education (Ethiopia), Addis Ababa.
	Training on Entrepreneurship development, SAK Business and personal development, Addis Ababa, Ethiopia.
2006–Present	Lecturer, Jimma University, Jimma, Ethiopia.
2004–2006	MSc Study in Thermal Engineering, Addis Ababa University, Addis Ababa, Ethiopia.
2003–2004	Assistant Lecturer, Jimma University, Jimma, Ethiopia.
2002–2003	Graduate Assistant II, Jimma University, Jimma, Ethiopia.
1997–2002	BSc Study in Mechanical Engineering, Addis Ababa University, Addis Ababa, Ethiopia.